J. Phys. G: Nucl. Part. Phys. 19 (1993) 1069–1126. Printed in the UK

TOPICAL REVIEW

Prospects for measuring the B_s^0–$\bar{B}_s^0$ mixing ratio x_s

A Ali† and D London‡

† Deutsches Elektronen Synchrotron DESY, Hamburg, Federal Republic of Germany
‡ Laboratoire de physique nucléaire, Université de Montréal CP 6128, Montréal, Québec, Canada H3C 3J7

Received 22 June 1992, in final form 19 May 1993

Abstract. We review and update results bearing on the phenomenon of particle–antiparticle mixing in the neutral beauty meson sector. Our main focus is on the mixing ratio x_s, defined as $x_s = (\Delta M)/\Gamma$, relevant for B_s^0–$\bar{B}_s^0$ mixing. We present theoretical estimates of this quantity in the standard model (SM) and find that $x_s = O(10)$, which makes time-dependent oscillation measurements mandatory. We also discuss estimates of x_s in a number of extensions of the SM, some of which admit smaller values of x_s. Present and future experimental facilities where such measurements can be undertaken are reviewed on a case-to-case basis. These include the high luminosity LEP option, asymmetric threshold B-factories, the ep collider HERA, and hadron colliders, such as the Fermilab Tevatron, LHC and SSC.

1. Introduction

In the $SU(2) \times U(1)$ gauge theory of Glashow, Weinberg and Salam [1], now known as the standard model (SM), fermions get their masses through Yukawa couplings involving a Higgs doublet field. For the quarks, the gauge and mass eigenstates are not the same, leading to inter-generational couplings in the weak charged-current interactions. These flavour non-diagonal couplings are described by the unitary Cabibbo–Kobayashi–Maskawa (CKM) matrix [2]. The CKM matrix is one of the few aspects of the SM which remain to be fully tested. High-precision determinations of all CKM matrix elements may reveal some inconsistencies, and give us some clue as to the new physics which inevitably lies beyond the SM.

We recall here that the measurement of x_d by the ARGUS collaboration in 1987 giving $x_d \simeq 0.70$ was the first compelling hint that the top quark mass probably lies beyond 100 GeV. The measurement of x_d also provides, in principle, a determination of the CKM matrix element $|V_{td}|$. However, it is difficult to quantify it due to the (as yet) unknown top-quark mass and the attendant uncertainty in the hadronic matrix element. One ingredient which is very likely to aid in this programme is the measurement of B_s^0–$\bar{B}_s^0$ mixing, x_s. It is well appreciated that the ratio x_d/x_s is independent of the top-quark mass and the QCD corrections to the effective $|\Delta B| = 2$ Hamiltonian. However, it depends upon the ratio of the relevant hadronic matrix elements. A reliable theoretical estimate of the hadronic matrix elements would then provide a reliable determination of the CKM matrix element ratio $|V_{td}|/|V_{ts}|$. Hence, the interest in measuring x_s cannot be overemphasized.

In this paper, we will review the issues, both theoretical and experimental, involved in an eventual measurement of x_s. The present experimental information on the mixing probabilities, both in the B_d^0–$\bar{B}_d^0$ and B_s^0–$\bar{B}_s^0$ systems, is based on time-integrated measurements. Such methods are expected to work if the mixing ratio $x_i = O(1)$, as is

0954-3899/93/081069+58$07.50

the case for x_d. However, it is common knowledge that the expectation for x_s in the SM is more like O(10), which would necessitate time-dependent methods for its measurement. In anticipation of this, we have concentrated on time-dependent methods for determining x_s in a number of competing proposals.

We begin in section 2 by reviewing what is currently known about the CKM matrix. In section 3 we discuss how a measurement of x_s will help pin down the matrix elements, and give there predictions for x_s, both in and beyond the SM. After updating the time-integrated measurements of B^0–$\bar{B}^0$ mixing in section 4, in section 5 we discuss the general issues involved in a time-dependent measurement of x_s. In sections 6–9 we review in detail the experimental prospects for measuring x_s at LEP/SLC, at asymmetric B-factories, at HERA, and at hadron colliders, including, wherever possible, the results of detailed studies. We give a summary in section 10.

2. An update of the CKM matrix

2.1. The CKM matrix parameters

For three generations, the CKM matrix can be described by three angles and one complex phase. It was noticed some time ago by Wolfenstein [3] that the elements of this matrix exhibited a hierarchy in terms of λ, the Cabibbo angle. In this parametrization the CKM matrix can be written approximately as

$$V_{\rm CKM} \simeq \begin{pmatrix} 1-\frac{1}{2}\lambda^2 & \lambda & A\lambda^3(\rho-i\eta) \\ -\lambda & 1-\frac{1}{2}\lambda^2-iA^2\lambda^4\eta & A\lambda^2 \\ A\lambda^3(1-\rho-i\eta) & -A\lambda^2 & 1 \end{pmatrix}. \qquad (I)$$

What is known about the four CKM matrix parameters, λ, A, ρ, η? First of all, $|V_{us}|$ has been extracted with good accuracy from $K \to \pi e \nu$ and hyperon decays [4] to be

$$|V_{us}| = \lambda = 0.2205 \pm 0.0018. \qquad (2)$$

This agrees quite well with the determination of $V_{ud} \simeq 1 - \frac{1}{2}\lambda^2$ from β decay

$$|V_{ud}| = 0.9744 \pm 0.0010. \qquad (3)$$

The parameter A is related to the CKM matrix element V_{cb}, which can be obtained from semileptonic decays of B mesons. There are two classes of models which describe such decays. First of all, in the spectator quark model of Altarelli *et al* (ACCMM) [5], the semileptonic decay of a B meson is described at the quark level in a manner completely analogous to that of muon decay, with QCD and phase space effects taken into account. The main uncertainty is in the value of m_b, but this is reduced by constructing a bound-state model of the b-quark within the B meson. The crucial parameters for semileptonic B decays in this model are m_c, m_u (for $b \to u$ transitions) and p_F, the Fermi momentum of the b-quark. Although exclusive semileptonic branching ratios cannot be calculated, this model does predict the shape of the lepton spectrum.

The second class of models are form-factor models. In these models, the branching ratios for exclusive final states are predicted. In particular, for $b \to c$ transitions, the rates for $B \to D\ell\nu$ and $B \to D^*\ell\nu$ are given as functions of $|V_{cb}|^2$ with no parameters to vary. The model of Isgur *et al* (ISGW) [6] uses the quark potential model to calculate the

form factors, which gives the exclusive branching ratios. The inclusive lepton spectrum is obtained by summing over these exclusive modes, using only the lowest resonances. (As we will see when discussing $|V_{ub}/V_{cb}|$, this technique is somewhat doubtful.) In the models of Wirbel, Stech and Bauer (WBS) [7] and Körner and Schuler (KS) [8], the form factors are calculated using nearest-pole dominance. In these models only the exclusive rates are predicted.

One advantage of such form-factor models is that, in principle, $|V_{cb}|$ is best extracted from the branching ratio for $B \to D\ell\nu$, since this decay can be described by one form factor. Ultimately, with more data, it should be possible to distinguish between various form-factor models, and obtain $|V_{cb}|$ much more precisely than through the ACCMM model. Even now, the value of $|V_{cb}|$ obtained from $B \to D\ell\nu$ is rather insensitive to the model used.

Recently, there has been a further development in such models. By taking the formal limit of infinite quark masses, one obtains what is known as the heavy-quark effective theory (HQET). In this limit it has been observed that all hadronic form factors can be expressed in terms of a single function, the Isgur–Wise function [9]. Interestingly, in contrast to the above comments, it has been shown that this analysis works best for $B \to D^*\ell\nu$ decays, since these decays are unaffected by $1/m_b$ corrections [10–12]. On the other hand, $B \to D\ell\nu$ decays *are* affected, and the corrections can only be calculated in a model-dependent way.

Following [13], the 1990 Particle Data Group [4] gives the following value for $|V_{cb}|$:

$$|V_{cb}| = 0.044 \pm 0.009. \tag{4}$$

This value has been obtained using only the exclusive decay $B \to D\ell\nu$ (as discussed above) and the model of WBS. The error includes the model dependence of the form factors. Note that the B lifetime

$$\tau_B = (1.15 \pm 0.14) \times 10^{-12}\ \text{s} \tag{5}$$

has been used in extracting this value of $|V_{cb}|$. In fact, the 1990 Particle Data Group [4] itself updates τ_B (without updating the above $|V_{cb}|$) to

$$\tau_B\ (1990) = (1.18 \pm 0.11) \times 10^{-12}\ \text{s}. \tag{6}$$

Since then, the ARGUS and CLEO groups have updated their analyses. Furthermore, we now have additional information from LEP. The average B hadron lifetime measured at LEP [14] is

$$\tau_B = (1.28 \pm 0.06) \times 10^{-12}\ \text{s}. \tag{7}$$

This is somewhat larger than (though within errors consistent with) the 1990 Particle Data Group value (equation (6)). Since the essential difference between the two sets of measurement lies in the production of the B_s^0-mesons and Λ_b-baryons at LEP, it is conceivable that the lifetimes and the semileptonic branching ratios for the various B hadrons are, in fact, different. Precision measurements in future from the $\Upsilon(4S)$ and Z^0 decays should be watched carefully to discern a significant deviation. In particular, measurements of the individual lifetimes of the B hadrons will clarify this point. We note parenthetically that the recent τ_B measurements in a non e^+e^- experiment giving [15]

$$\begin{aligned} \tau_{B^0} &= (0.6^{+0.23}_{-0.15}) \times 10^{-12}\ \text{s} \\ \tau_{B^-} &= (2.4^{+1.5}_{-0.8}) \times 10^{-12}\ \text{s} \end{aligned} \tag{8}$$

while statistically not persuasive, are tantalizingly different! On the other hand, ALEPH has reported the first measurements of the individual B^0, B^- lifetimes, giving a ratio

$$\tau_{B^+}/\tau_{B^0} = 0.96^{+0.69}_{-0.44} \tag{9}$$

which is consistent with 1, though the present errors are still quite large. We shall, however, continue using the simplifying assumption that all the B hadron lifetimes as well as their semileptonic branching ratios are equal. Therefore, averaging the LEP B-lifetime with that of the 1990 Particle Data Group, we obtain

$$\tau_B = (1.23 \pm 0.06) \times 10^{-12} \text{ s}. \tag{10}$$

In order to update $|V_{cb}|$ (and hence A) we shall use the exclusive decays. This is done both by following the lead of the Particle Data Group in which a value of $|V_{cb}|$ is extracted from exclusive $B \to D\ell\nu$ decays using the WBS model, and by using the HQET [9] to extract the same quantity from the exclusive $B \to D^*\ell\nu$ decays, as has been done by the CLEO collaboration.

Let us first consider the exclusive decay $B \to D\ell\nu$. Although experiments at LEP have measured the inclusive semileptonic branching ratio, they have not yet been able to measure exclusive decay modes. Therefore we shall use the latest ARGUS and CLEO results, adjusting them to take account of the new value for τ_B. Using the old (1990) value for τ_B, CLEO [16] gives

$$\begin{aligned} |V_{cb}| &= 0.043 \pm 0.006 \text{ (WBS, KS)} \\ |V_{cb}| &= 0.037 \pm 0.005 \text{ (ISGW)}. \end{aligned} \tag{11}$$

ARGUS [17] gives very similar results:

$$\begin{aligned} |V_{cb}| &= 0.044 \pm 0.007 \text{ (WBS, KS)} \\ |V_{cb}| &= 0.038 \pm 0.006 \text{ (ISGW)}. \end{aligned} \tag{12}$$

Updating these numbers to take equation (10) into account, we find, for the WBS model,

$$|V_{cb}| = 0.043 \pm 0.005. \tag{13}$$

It is clear that the model dependence is becoming larger than the experimental error. Hopefully, with more data, we will be able to rule out certain of these models. (In fact, in comparing with experiment, there seem to be some problems with the ISGW model, as detailed in [16].)

Alternatively, one could use the (less model-dependent) HQET approach to the exclusive $B(v) \to D^*(v')\ell\nu$ decay, in which case the decay at the symmetry point $v \cdot v' = 1$ is governed by the Isgur–Wise function $\xi(v \cdot v')$, having the normalization $\xi(v \cdot v' = 1) = 1$ (here v and v' are the four-velocities as indicated). Since $O(1/m_Q)$ corrections to the Isgur–Wise function $\xi_{A_1}(v \cdot v' = 1)$ determining the rate for the decay $B \to D^*\ell\nu_\ell$ at the symmetry point are absent, any deviation from the relation $\xi_{A_1}(v \cdot v' = 1) = 1$ is dominantly of perturbative QCD origin. The differential decay rate is given by

$$\lim_{v\cdot v' \to 1} \frac{1}{\sqrt{(v \cdot v')^2 - 1}} \frac{d\Gamma(B \to D^*\ell\nu_\ell)}{d(v \cdot v')} = \frac{{G_F}^2}{4\pi^3} M_{D^*}^3 (M_B - M_{D^*}) |V_{cb}|^2 \eta_{QCD}^2. \tag{14}$$

The QCD-correction factor turns out to be essentially 1, namely $\eta_{QCD} \simeq 0.99$, leading to the very interesting result that the rate for this decay at the symmetry point remains practically unrenormalized from its Isgur–Wise value [12]. To obtain useful phenomenology from this work, one has to extrapolate the data to the point $y = v \cdot v' = 1$, for which one needs an ansatz for the Isgur–Wise function $\xi(y)$, which is a model-dependent enterprise. To extract V_{cb} from data, the following parametrization was employed [12]

$$\xi(y) = \frac{2}{1+y} \exp\left\{-(2y_0^2 - 1)\frac{y-1}{y+1}\right\}. \tag{15}$$

A fit of the data on $B \to D^* \ell \nu_\ell$ was then attempted in terms of the parameters, y_0 and $|V_{cb}|$, getting

$$|V_{cb}| \left(\frac{\tau_{B^0}}{1.18 \text{ ps}}\right)^{1/2} = 0.045 \pm 0.007 \qquad y_0 = 1.19 \pm 0.25. \tag{16}$$

These numbers were obtained using the leading log result $\eta_{QCD} = 0.95$. Updating it for $\eta_{QCD} = 0.99$ and the new average for τ_B, one gets

$$|V_{cb}| \left(\frac{\tau_{B^0}}{1.23 \text{ ps}}\right)^{1/2} = 0.044 \pm 0.006. \tag{17}$$

With the perturbative corrections being at the level of 1%, the dominant theoretical uncertainty lies in extrapolation of the data. To get an idea of the uncertainty from this source, Mannel [18] has recently studied the parametrization dependence of the Isgur–Wise function for $v \cdot v' \neq 1$ by fitting simultaneously four inputs from the $B \to (D, D^*)\ell\nu$ data in the HQET approach, namely the D*-energy spectrum, the total branching ratio, the ratio Γ_{D^*}/Γ_D and the polarization variable $\alpha = 2\Gamma_L/\Gamma_T - 1$. For this purpose three different parametrizations have been fitted to the data. The first,

$$\xi(v \cdot v') = 1 + \tfrac{1}{4} a (v - v')^2 (v + v')^2 \tag{18}$$

is best fit to the CLEO data with $a = 0.53$. If instead only the lepton energy spectrum from $B \to D^* \ell \nu_\ell$ is used the best fit is $a = 0.54$. The second parametrization due to Rosner [19],

$$\xi(v \cdot v') = \frac{1}{1 - (v - v')^2/\omega_0^2} \tag{19}$$

is fitted again to the four inputs, giving $1/\omega_0^2 = 1.27 \pm 0.06$. A third parametrization, which is very similar to the one used by Neubert and Rieckert [12],

$$\xi(v \cdot v') = \exp\{b(v - v')^2\} \tag{20}$$

gives $b = 0.91 \pm 0.03$ [18]. Concentrating on the decay width $\Gamma(B^0 \to D^{*+} \ell^- \nu_\ell)$ and the polarization parameter α as benchmarks, Mannel has found $\pm 7\%$ dependence of these quantities on the parametrizations. This, in our opinion, is a fair estimate of the residual model dependence of the CKM matrix element $|V_{bc}|^2$ in the HQET approach. Based on the various methods presented here, we conclude that the CKM matrix element V_{cb} has been determined by the present ARGUS and CLEO data to an accuracy of $\pm 13\%$. Also, there is remarkable consistency between the extracted value of $|V_{cb}|$ from the two approaches.

For the purposes of the fit which follows, we shall use the value of the CKM parameter A obtained from the HQET

$$A = 0.90 \pm 0.12. \tag{21}$$

The other two CKM parameters ρ and η are constrained by the measurements of $|V_{ub}/V_{cb}|$, $|\epsilon|$ (the *CP*-violating parameter in the kaon system), x_d (B_d^0–$\bar{B}_d^0$ mixing) and (in principle) ϵ'/ϵ ($\Delta S = 1$ *CP* violation in the kaon system). After discussing each of these in turn, we will present a fit in which the allowed region of ρ and η is shown.

First of all, $|V_{ub}/V_{cb}|$ can be obtained by looking at the endpoint of the inclusive lepton spectrum in semileptonic B decays. The earlier values for the ARGUS and CLEO results are found in table 1. It should be noted that the apparently strong model dependence of $|V_{ub}/V_{cb}|$ obtained in this way essentially disappears if one ignores the ISGW model. In fact, it has been argued [20] that, by using only the lowest resonances of the quark potential, the ISGW model does not accurately reproduce the lepton spectrum. It therefore seems reasonable to exclude the ISGW model when discussing the extraction of $|V_{ub}/V_{cb}|$ from the inclusive lepton spectrum. The results of table 1 then give

$$|V_{ub}/V_{cb}| = 0.12 \pm 0.02. \tag{22}$$

Table 1. Values of V_{ub}/V_{cb} for different theoretical models, from [21].

	ARGUS data	CLEO data
Method	$p_e > 2.3$ GeV	$p_e > 2.4$ GeV
ACCMM [5]	0.11 ± 0.01	0.12 ± 0.02
ISGW [6]	0.20 ± 0.02	0.19 ± 0.03
WBS [7]	0.13 ± 0.02	0.13 ± 0.02
KS [8]	0.11 ± 0.01	0.11 ± 0.01

The ARGUS collaboration has presented evidence for the exclusive decay $B \to \rho \ell \nu_\ell$ [22]. The ratio $|V_{ub}/V_{cb}|$ extracted is quite model-dependent:

$$\left|\frac{V_{ub}}{V_{cb}}\right| = \begin{cases} 0.17 \pm 0.03 & \text{WBS [7]} \\ 0.30 \pm 0.06 & \text{ISGW [6]} \\ 0.15 \pm 0.03 & \text{KS [8].} \end{cases} \tag{23}$$

Obviously, $|V_{ub}/V_{cb}|$ as obtained from this exclusive decay is larger (for the ISGW model, very much larger) than that found in inclusive semileptonic B decays.

It is clear that, although there is quite good evidence for a non-zero $|V_{ub}/V_{cb}|$, its value is quite uncertain. Very recently, the CLEO collaboration has reported a significant decrease in the value of $|V_{ub}/V_{cb}|$. The new results are consistent with the value

$$|V_{ub}/V_{cb}| = 0.08 \pm 0.02. \tag{24}$$

This gives

$$\sqrt{\rho^2 + \eta^2} = 0.36 \pm 0.09. \tag{25}$$

The experimental value of $|\epsilon|$ is [4]

$$|\epsilon| = (2.26 \pm 0.02) \times 10^{-3}. \tag{26}$$

Theoretically, $|\epsilon|$ is essentially proportional to the imaginary part of the box diagram for K^0–$\bar{K}^0$ mixing (figure 1), and is given by [23]

$$|\epsilon| = \frac{G_F^2 f_K^2 M_K M_W^2}{6\sqrt{2}\pi^2 \Delta M_K} B_K \left(A^2\lambda^6\eta\right)\left(y_c\{\eta_{ct} f_3(y_c, y_t) - \eta_{cc}\} + \eta_{tt} y_t f_2(y_t) A^2\lambda^4(1-\rho)\right). \tag{27}$$

Here, the η_i are QCD correction factors, $\eta_{cc} \simeq 0.82$, $\eta_{tt} \simeq 0.62$, $\eta_{ct} \simeq 0.35$ for $\Lambda_{QCD} = 200$ MeV [24], $y_i \equiv m_i^2/M_W^2$, and the functions f_2 and f_3 are given by

$$f_2(x) = \frac{1}{4} + \frac{9}{4}\frac{1}{(1-x)} - \frac{3}{2}\frac{1}{(1-x)^2} - \frac{3}{2}\frac{x^2 \ln x}{(1-x)^3}$$

$$f_3(x, y) = \ln\frac{y}{x} - \frac{3y}{4(1-y)}\left(1 + \frac{y}{1-y}\ln y\right). \tag{28}$$

(The above form for $f_3(x, y)$ is an approximation, obtained in the limit $x \ll y$. For the exact expression, see [25].)

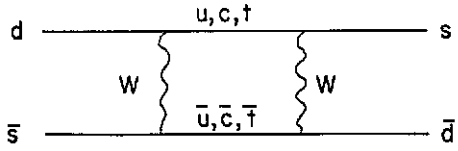

Figure 1. Box diagram for K^0–$\bar{K}^0$ mixing. There is another diagram in which the internal quark and W lines are interchanged.

One of the unknowns in equation (27) is the top-quark mass. The most model-independent lower bound comes from LEP [26],

$$m_t > 45 \text{ GeV}. \tag{29}$$

There is a stronger lower limit (95% CL) of

$$m_t > 89 \text{ GeV} \tag{30}$$

from CDF [27], but this limit may be weakened in the presence of certain types of physics beyond the SM (e.g. charged Higgses). Radiative corrections in the electroweak sector have been used to determine a range for m_t. While the exact range of m_t depends on a number of details, a range $m_t = 140 \pm 35$ GeV has been obtained by Altarelli [28]. In the same vein Ellis *et al* obtain $m_t = 120 + 27 - 28$ GeV at 68% CL [29], whereas an upper limit (95% CL) of

$$m_t < 182 \text{ GeV} \tag{31}$$

comes from similar considerations in [30].

Table 2. Values of B_K using different methods of calculation.

Method	Value of B_K
Vacuum insertion	1
Hadronic sum rules	0.33 ± 0.09 [31]
	0.39 ± 0.10 [32]
Chiral symmetry	0.33 ± 0.2 [33]
QCD Sum rules	0.50 ± 0.22 [34]
	0.58 ± 0.16 [35]
	0.84 ± 0.08 [36]
	0.74 ± 0.17 [37]
1/N	0.66 ± 0.10 [38]
Lattice theories	0.87 ± 0.20 [39]
	1.03 ± 0.07 [40]
	0.94 ± 0.01 [41]
	0.77 ± 0.07 [41]
	0.92 ± 0.03 [42]

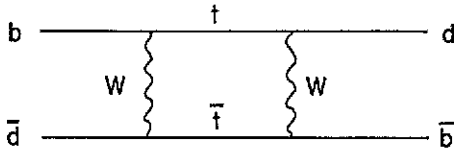

Figure 2. Box diagram for B_d^0–$\bar{B}_d^0$ mixing. There is another diagram in which the internal t-quark and W lines are interchanged.

The final parameter in the expression for $|\epsilon|$ is B_K, which represents our ignorance of the matrix element $\langle K^0|(\bar{d}\gamma^\mu(1-\gamma_5)s)^2|\bar{K}^0\rangle$. The evaluation of this matrix element has been the subject of much work. The results are summarized in table 2. Although the entire range of B_K is $1/3 \leqslant B_K \leqslant 1$, the $1/N$ and lattice approaches are generally considered more reliable. For this reason, in what follows we shall take

$$B_K = 0.8 \pm 0.2. \tag{32}$$

We now turn to B_d^0–$\bar{B}_d^0$ mixing. The latest value of x_d, which is a measure of this mixing, is [43]

$$x_d = 0.67 \pm 0.10. \tag{33}$$

The mixing parameter x_d is calculated from the B_d^0–$\bar{B}_d^0$ box diagram (figure 2). Unlike the kaon system, where the contributions of both the c- and t-quarks in the loop were important, this diagram is dominated by t-quark exchange

$$x_d \equiv \frac{(\Delta M)_B}{\Gamma} = \tau_B \frac{G_F^2}{6\pi^2} M_W^2 M_B \left(f_{B_d}^2 B_{B_d}\right) \eta_B y_t f_2(y_t) |V_{td}^* V_{tb}|^2 \tag{34}$$

where, using equation (1), $|V_{td}^* V_{tb}|^2 = A^2\lambda^6\left[(1-\rho)^2+\eta^2\right]$. Here, η_B is the QCD correction. In [44], this correction is analysed in great detail, including the effects of a heavy t-quark. They find that η_B depends sensitively on the definition of the t-quark mass, and that, strictly speaking, only the product $\eta_B(y_t)f_2(y_t)$ is free of this dependence. For this reason we will use the value, $\eta_B = 0.55$, advocated in [44].

For the B system, the hadronic uncertainty is given by $f_{B_d}^2 B_{B_d}$, analogous to B_K in the kaon system, except that in this case, neither is f_{B_d} measured. And, just like B_K, the evaluation of $f_{B_d}^2 B_{B_d}$ has been the subject of much work, summarized in table 3. (Note that the results in table 3 are mainly for f_{B_d}, and not B_{B_d}. This is because, due to the heavy b-quark mass, it is expected that $B_{B_d} = 1$.) Until very recently, the scaling law,

$$f_B(m_B)\sqrt{m_B} = \text{constant} \tag{35}$$

was thought to be valid for the B system. This led to rather small values for $f_{B_d}^2 B_{B_d}$ (above the line in table 3), in the range

$$100 \text{ MeV} \leqslant f_{B_d}\sqrt{B_{B_d}} \leqslant 170 \text{ MeV}. \tag{36}$$

However, recent lattice calculations have indicated that there are scaling violations. These have led to larger estimates for $f_{B_d}^2 B_{B_d}$ (below the line in table 3), roughly in the range

$$200 \text{ MeV} \leqslant f_{B_d}\sqrt{B_{B_d}} \leqslant 300 \text{ MeV}. \tag{37}$$

We will therefore consider two ranges for $f_{B_d}^2 B_{B_d}$, corresponding approximately to the ranges in equations (36) and (37):

$$\begin{aligned} &\text{(old)} : f_{B_d}\sqrt{B_{B_d}} = 135 \pm 25 \text{ MeV} \\ &\text{(new)} : f_{B_d}\sqrt{B_{B_d}} = 200 \pm 30 \text{ MeV}. \end{aligned} \tag{38}$$

Table 3. Values of f_{B_d} and $f_{B_d}\sqrt{B_{B_d}}$ using different methods of calculation. For the entries marked with an asterisk, which have been calculated in the static limit, it is estimated that the $1/m_b$ corrections will reduce these values by about 25% [54].

Method	
QCD sum rules	$f_{B_d} = 115 \pm 15$ MeV [45]
	$f_{B_d} = 129 \pm 13$ MeV [46]
	$f_{B_d} = 170 \pm 20$ MeV [47]
	$f_{B_d} = 100$–126 MeV[48]
	$f_{B_d}\sqrt{B_{B_d}} = 165 \pm 25$ MeV [49]
	$f_{B_d}\sqrt{B_{B_d}} = 130 \pm 50$ MeV [50]
Potential models	$f_{B_d} = 155 \pm 15$ MeV [51]
Lattice theories (1)	$f_{B_d} \sim 120$ MeV [52]
	$f_{B_d} = 105 \pm 17 \pm 30$ MeV [53]
Lattice theories (2)	$f_{B_d} = 310 \pm 25 \pm 50$ MeV* [54]
	$f_{B_d} = 320 \pm 20$ MeV* [55]
	$f_{B_d} = 188$–246 MeV [56]

We now turn to the final piece of information which can give constraints on ρ and η, ϵ'/ϵ. In the kaon system, $|\epsilon|$ reflects the (indirect) *CP* violation in the mixing. However, in the SM, there is also (direct) *CP* violation in the decays of kaons, conventionally denoted by ϵ'/ϵ. There are two experiments which have results for ϵ'/ϵ. Unfortunately, they are not in agreement:

$$\begin{aligned} &\text{NA31[59]} : \quad \epsilon'/\epsilon = (2.3 \pm 0.7) \times 10^{-3} \\ &\text{E731[60]} : \quad \epsilon'/\epsilon = (6.0 \pm 6.9) \times 10^{-4}. \end{aligned} \tag{39}$$

On the theoretical side, direct *CP* violation in the kaon system is usually described by so-called penguin diagrams. However, the value of ϵ'/ϵ obtained in such calculations has large uncertainties. First of all, for a heavy t-quark mass, $m_t \simeq 200$ GeV, it has been noticed [61] that there can be cancellations among the various contributions, giving $\epsilon'/\epsilon \simeq 0$, while for a small t-quark mass, $m_t \simeq 100$ GeV, one finds $\epsilon'/\epsilon \sim O(10^{-3})$. On the other hand, recent calculations [62] indicate that these cancellations are avoided when two loop effects are included. Even apart from this strong dependence on m_t, there are large theoretical uncertainties due to hadronic matrix elements (the equivalent of B_K and $f_{B_d}^2 B_{B_d}$) and the s-quark mass. Because both the experimental and theoretical results are not yet well established, we will not include ϵ'/ϵ in constraining ρ and η.

2.2. *The unitarity triangle*

The information regarding the allowed region in ρ–η space can be displayed quite elegantly using the so-called unitarity triangle. This is constructed as follows. Because the CKM matrix is unitary, one has the following relation

$$V_{ud}V_{ub}^* + V_{cd}V_{cb}^* + V_{td}V_{tb}^* = 0. \tag{40}$$

Using the form of the CKM matrix in equation (1), this can be recast as

$$\frac{V_{ub}^*}{\lambda V_{cb}} + \frac{V_{td}}{\lambda V_{cb}} = 1 \tag{41}$$

that is a triangle relation in the complex plane (i.e. ρ–η space). This is illustrated in figure 3. Thus, allowed values of ρ and η translate into allowed shapes of the unitarity triangle.

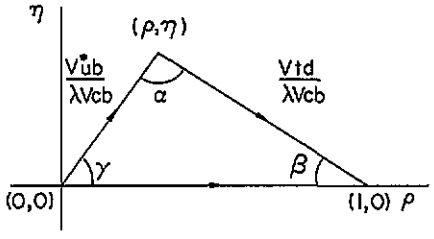

Figure 3. The unitarity triangle. The angles α, β and γ can be measured via *CP* violation in the B system.

In order to find the allowed unitarity triangles, we use the computer program MINUIT to fit the CKM parameters A, ρ and η to the experimental values of $|V_{cb}|$, $|V_{ub}/V_{cb}|$, $|\epsilon|$ and x_d. For m_t, we take three different values: $m_t = 100,\ 140,\ 180$ GeV. For the uncertainties in the hadronic matrix elements, we use the ranges for B_K and $f_{B_d}^2 B_{B_d}$ defined in equations (32) and (38). (Note that, strictly speaking, this is not correct—theoretical 'errors' are not Gaussian. However, this is the best we can do.)

The results are shown in figures 4 and 5. Figures 4(*a*)–(*c*) have $f_{B_d}\sqrt{B_{B_d}} = 135 \pm 25$ MeV, with $m_t = 100$, 140 and 180 GeV, respectively, while for figures 5(*a*)–(*c*) we take $f_{B_d}\sqrt{B_{B_d}} = 200 \pm 30$ MeV, with $m_t = 100$, 140 and 180 GeV, respectively. Note that the graph for $f_{B_d}\sqrt{B_{B_d}} = 135 \pm 25$ MeV and $m_t = 100$ GeV is a bad fit of the data ($\chi^2/d.o.f. = 1.97$). In all these graphs, the full curve has $\chi^2 = \chi^2_{\min} + 1$. *Note*

that, although many authors use this curve to represent '1σ', it is, in fact, only a 39% CL region [4]! For comparison, we include the broken curve, which is the 90% CL region ($\chi^2 = \chi^2_{\min} + 4.6$). It is clear that, as we pass from figure 4(a) to figure 5(c), the 'most likely' unitarity triangles become more and more acute, as has already been pointed out [63]. However, it is also clear that there is an enormous overlap between the 90% CL regions of $f_{B_d}\sqrt{B_{B_d}} = 135 \pm 25$ MeV and those with $f_{B_d}\sqrt{B_{B_d}} = 200 \pm 30$ MeV, so that it will take a great deal of new experimental evidence to tell us which of the 'old' or 'new' values of $f^2_{B_d} B_{B_d}$ in equation (38) is correct.

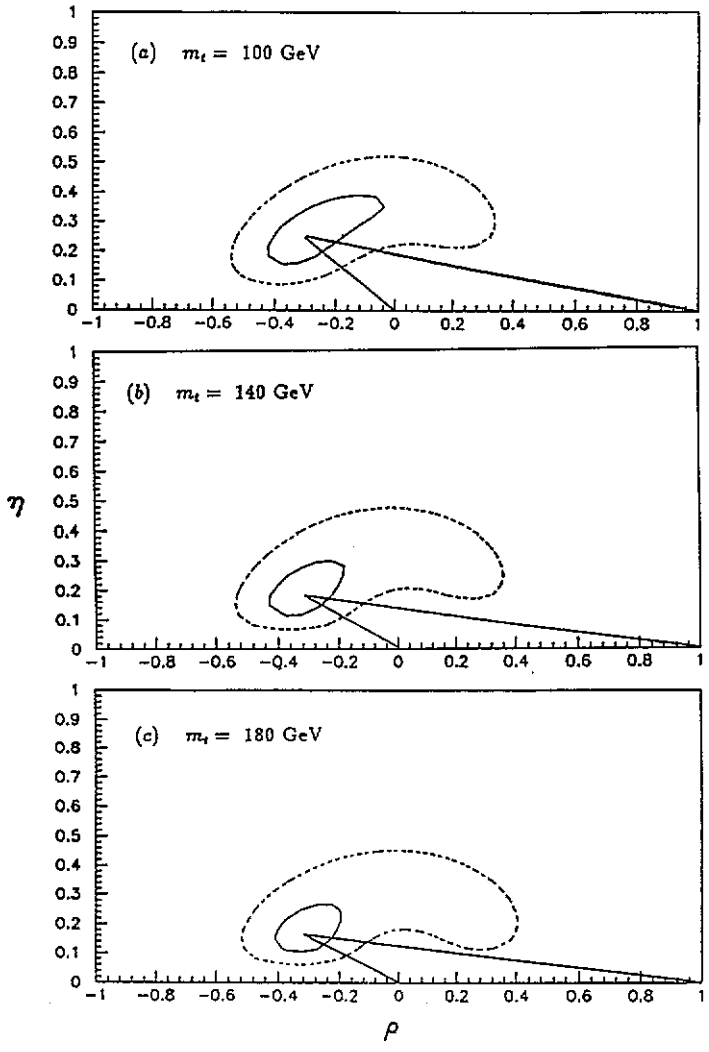

Figure 4. Allowed region in ρ–η space for different values of the SM parameters. (a)–(c) have $f_{B_d}\sqrt{B_{B_d}} = 135 \pm 25$ MeV, with $m_t = 100$, 140 and 180 GeV, respectively. The full curve represents the region with $\chi^2 = \chi^2_{\min} + 1$; the broken curve denotes the 90% CL region. The triangles show the best fit.

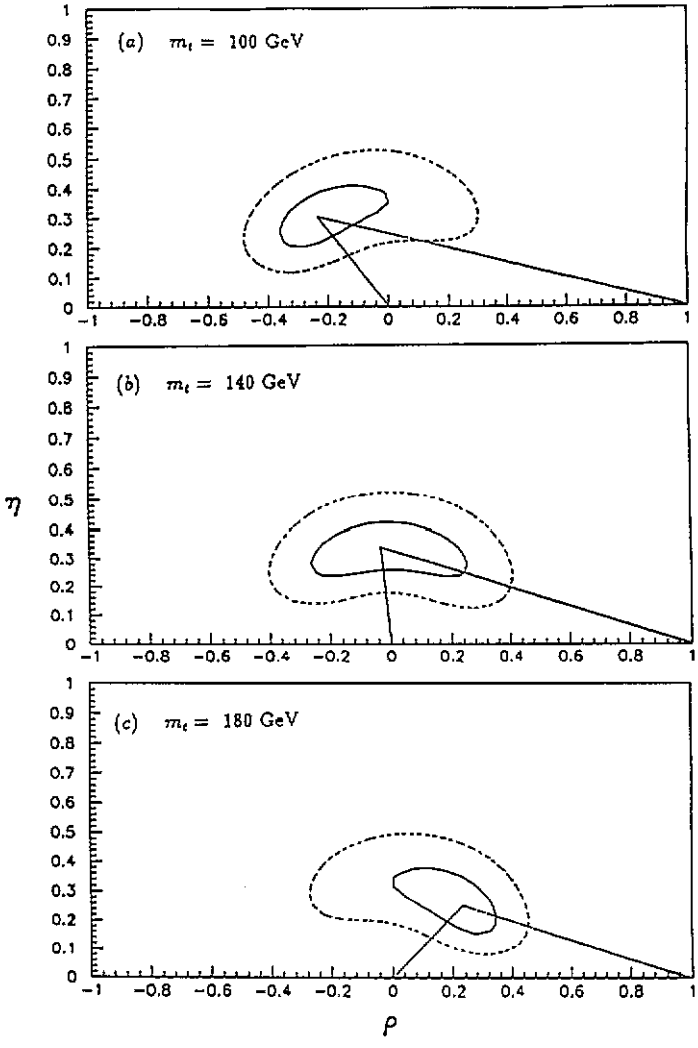

Figure 5. Allowed region in ρ–η space for different values of the SM parameters. (*a*)–(*c*) have $f_{B_d}\sqrt{B_{B_d}} = 200 \pm 30$ MeV, with $m_t = 100$, 140 and 180 GeV, respectively. The full curve represents the region with $\chi^2 = \chi^2_{min} + 1$; the broken curve denotes the 90% CL region. The triangles show the best fit.

3. B_s^0–$\bar{B}_s^0$ mixing

It is evident from figures 4 and 5 that there is, at present, much uncertainty in the shape of the unitarity triangle. If we wish to test the CKM matrix as the explanation for *CP* violation, we will need much more information. Ideally, we should measure enough angles and sides to overconstrain the unitarity triangle of figure 3. How can we do this? First of all, the angles α, β and γ can be measured via *CP* violating rate asymmetries in the B system [64]. The angle $\sin 2\alpha$ is measured in the decays $B_d^0(\bar{B}_d^0) \to \pi^+\pi^-$, $\sin 2\beta$ is measured through $B_d^0(\bar{B}_d^0) \to \Psi K_S$, and $\sin 2\gamma$ is measured in $B_s^0(\bar{B}_s^0) \to \rho K_S$ [65]. Obviously, if all three angles were obtained in this way with enough accuracy, this would suffice to ascertain whether or not the unitarity triangle closes, i.e. whether or not *CP* violation can

be explained via the CKM matrix. However, it appears to be extremely difficult, at least for the first generation of B-factories, to measure the angle γ. It is therefore necessary to combine the measurements of α and β with a measurement of one of the sides ($|V_{ub}/\lambda V_{cb}|$ or $|V_{td}/\lambda V_{cb}|$). Unfortunately, it is evident from equation (24) that there is an enormous uncertainty, mostly theoretical, in $|V_{ub}/\lambda V_{cb}|$. Furthermore, although one can extract a value of $|V_{td}|$ from a measurement of x_d, the unknown t-quark mass and the enormous uncertainty in $f_{B_d}^2 B_{B_d}$ (equations (36) and(37)) will lead to an extremely imprecise value for this quantity.

There are several possible resolutions to this problem. First of all, it may be possible to measure the parameter f_{B_d} directly via the decay $B^+ \to \tau\nu_\tau$. Second, the error on $|V_{ub}/\lambda V_{cb}|$ could perhaps be reduced by experimentally ruling out certain models. A third, perhaps more interesting, possibility is to use rare B decays involving the transitions $b \to s$ and $b \to d$. Of these, the CKM-suppressed radiative decays $B \to X_d + \gamma$ (and $B \to \rho + \gamma, \ldots$), as well as the FCNC semileptonic decays $B \to X_d + (\ell^+\ell^-)$ (and $B \to (\pi, \rho, A_1, \ldots)(\ell^+\ell^-)$) are particularly useful since they all measure the CKM matrix element $|V_{td}|$. The inclusive rates depend only on m_t while the exclusive rates also depend on form factors. However, it can be shown that the relative rates satisfy the following relations (up to small $SU(3)$-breaking effects denoted by δ_i) [66]:

$$\Gamma(b \to d + \gamma)/\Gamma(b \to s + \gamma) = \frac{|V_{td}|^2}{|V_{ts}|^2}(1 + \delta_1) \tag{42}$$

$$\Gamma(b \to d + \ell\bar{\ell})/\Gamma(b \to s + \ell\bar{\ell}) = \frac{|V_{td}|^2}{|V_{ts}|^2}(1 + \delta_2). \tag{43}$$

Similar relations also apply to the ratios of the exclusive rare decays, for example, $\Gamma(B \to \rho + \gamma)/\Gamma(B \to K^* + \gamma)$ and $\Gamma(B \to \rho + \ell\bar{\ell})/\Gamma(B \to K^* + \ell\bar{\ell})$ ($\ell = e, \mu, \tau, \nu$). The estimated rates are such that some should be measurable in a first-generation B-factory with $O(10^7)$ events [66].

Another possibility, which is the one we will emphasize, is to use the information from x_s, the B_s^0–$\bar{B}_s^0$ mixing parameter.

3.1. x_s and the unitarity triangle

Mixing in the B_s^0–$\bar{B}_s^0$ system follows quite closely that of the B_d^0–$\bar{B}_d^0$ system. The B_s^0–$\bar{B}_s^0$ box diagram (figure 6) is again dominated by t-quark exchange, and the mixing parameter x_s is given by a formula analogous to that of equation (34)

$$x_s \equiv \frac{(\Delta M)_{B_s}}{\Gamma_{B_s}} = \tau_{B_s}\frac{G_F^2}{6\pi^2}M_W^2 M_{B_s}\left(f_{B_s}^2 B_{B_s}\right)\eta_{B_s} y_t f_2(y_t)|V_{ts}^* V_{tb}|^2. \tag{44}$$

Using the fact that $V_{cb} = V_{ts}$ (equation (1)), it is clear that one of the sides of the unitarity triangle, $|V_{td}/\lambda V_{cb}|$, can be obtained from the ratio of x_d and x_s

$$\frac{x_d}{x_s} = \frac{\tau_{B_d}\eta_{B_d} M_{B_d}\left(f_{B_d}^2 B_{B_d}\right)}{\tau_{B_s}\eta_{B_s} M_{B_s}\left(f_{B_s}^2 B_{B_s}\right)}\left|\frac{V_{td}}{V_{ts}}\right|^2. \tag{45}$$

All dependence on the t-quark mass drops out, and we are left with the square of the ratio of CKM matrix elements, multiplied by a factor which reflects $SU(3)_{\text{flavour}}$-breaking effects. The only uncertainty in this factor is the ratio of hadronic uncertainties—the other quantities

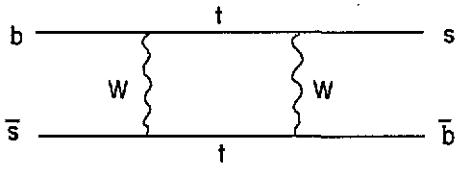

Figure 6. Box diagram for B_s^0–$\bar{B}_s^0$ mixing. There is another diagram in which the internal t-quark and W lines are interchanged.

Table 4. Values of f_{B_s} using different methods of calculation.

Method	
Potential models	$f_{B_s} = 210 \pm 20$ MeV [51]
Lattice theories (I)	$f_{B_s} \sim 150$ MeV [52]
	$f_{B_s} = 155 \pm 31 \pm 48$ MeV [53]
Lattice theories (2)	$f_{B_s} = 204$–241 MeV [56]

will be either calculated or measured. Whether or not x_s can be used to help constrain the unitarity triangle will depend crucially on the theoretical status of the ratio $f_{B_d}^2 B_{B_d}/f_{B_s}^2 B_{B_s}$.

Until recently, it was generally thought that f_{B_s} is roughly 35% larger than f_{B_d} (see table 4). In addition, lattice calculations indicated that the ratio f_{B_d}/f_{B_s} could be calculated much more accurately than either of f_{B_d} or f_{B_s}, due to the cancellation of some systematic uncertainties. For example, in their 1988 calculations, Bernard *et al* give [53]

$$f_{B_d} = 105 \pm 17 \pm 30 \text{ MeV}$$

$$f_{B_s} = 155 \pm 31 \pm 48 \text{ MeV} \tag{46}$$

with

$$f_{B_s}/f_{B_d} = 1.47 \pm 0.07 \pm 0.30. \tag{47}$$

However, recent lattice calculations do not seem to support the hypothesis that f_{B_s} is significantly larger than f_{B_d}: [56] gives

$$f_{B_d} = 188\text{–}246 \text{ MeV}$$

$$f_{B_s} = 204\text{–}241 \text{ MeV}. \tag{48}$$

Along the same lines, Abada *et al* [57] quote $f_{B_s}/f_{B_d} = 1.06 \pm 0.04$; a recent average over a number of lattice calculations gives $f_{B_s}/f_{B_d} = 1.08 \pm 0.06$ [58]. It is not clear whether the error on this ratio would eventually be smaller than the error on either f_{B_s} or f_{B_d}. This is the crucial point—if f_{B_d} can be calculated as accurately as f_{B_s}/f_{B_d}, then the measurement of x_s will not help in extracting the CKM matrix element V_{td} with more precision, assuming that the t-quark mass is known. On the other hand, if the calculation of f_{B_s}/f_{B_d} is more accurate than that of f_{B_d}, or if the t-quark mass is still unknown (which seems unlikely), then a measurement of B_s^0–$\bar{B}_s^0$ mixing will allow a more accurate measurement of $|V_{td}/\lambda V_{cb}|$, and will be an important further test of the unitarity triangle. (It should be noted that, even if it turns out that x_s is not as useful as is hoped for constraining the unitarity triangle in the above manner, its value is, in any case, necessary to obtain the angle γ via *CP* violation in B_s decays.)

Having motivated the necessity for measuring x_s, we will now turn to an estimate of its size in the SM, and in models beyond the SM.

3.2. SM prediction for x_s

The SM expression for x_s is given in equation (44). Using equation (1) to substitute for $V_{ts}^* V_{tb}$, we obtain

$$x_s = \tau_{B_s} \frac{G_F^2}{6\pi^2} M_W^2 M_{B_s} \left(f_{B_s}^2 B_{B_s}\right) \eta_{B_s} A^2 \lambda^4 y_t f_2(y_t). \tag{49}$$

Although the main uncertainties in this equation are the t-quark mass and $f_{B_s}^2 B_{B_s}$, the mass and lifetime of the B_s meson are also unknown. We will assume that the lifetime is the same as that of the other B hadrons (equation (10)), and that the B_d–B_s mass difference is 100 MeV [67]. We will also take the QCD correction η_{B_s} to be equal to its B_d counterpart, i.e. $\eta_{B_s} = 0.55$. Using the value for A, equation (21), we obtain

$$x_s = (153 \pm 26) \frac{f_{B_s}^2 B_{B_s}}{(1\ \text{GeV})^2} y_t f_2(y_t). \tag{50}$$

For $89 \leqslant m_t \leqslant 182$ GeV, the function $y_t f_2(y_t)$ is in the range 0.88–2.72, and is equal to 2.03 for the value of $m_t = 150$ GeV. As for $f_{B_s}^2 B_{B_s}$, as mentioned above, there is some controversy regarding its value. We will therefore consider two ranges for $f_{B_s}^2 B_{B_s}$:

$$\begin{aligned} &\text{(old)}: \qquad f_{B_s}\sqrt{B_{B_s}} = 180 \pm 35\ \text{MeV} \\ &\text{(new)}: \qquad f_{B_s}\sqrt{B_{B_s}} = 225 \pm 25\ \text{MeV}. \end{aligned} \tag{51}$$

This leads to

$$\begin{aligned} &\text{(old)}: \qquad x_s = (5.0 \pm 1.6)\, y_t f_2(y_t) \\ &\text{(new)}: \qquad x_s = (7.8 \pm 1.8)\, y_t f_2(y_t) \end{aligned} \tag{52}$$

which gives '1σ' lower limits

$$\begin{aligned} &\text{(old)}: \qquad x_s > 3.0 \\ &\text{(new)}: \qquad x_s > 5.2. \end{aligned} \tag{52}$$

The 'central values' (taking $m_t = 150$ GeV) are

$$\begin{aligned} &\text{(old)}: \qquad x_s = 10.0 \\ &\text{(new)}: \qquad x_s = 15.8. \end{aligned} \tag{54}$$

The SM therefore predicts extremely large values for x_s. This is to be expected since, from equation (45), one has $x_s \sim 20 x_d$, apart from $SU(3)_{\text{flavour}}$-breaking effects. Due to these large values, time-dependent measurements are necessary to obtain x_s.

3.3. Estimates of x_s beyond the SM

In the SM, we have seen that the diagram of figure 6 yields very large values of x_s. It is therefore of interest to see whether there exist models beyond the SM which predict a smaller value of x_s than in the SM. This can happen if such models of new physics significantly alter the SM prediction or if there are new contributions which destructively interfere with the SM contribution. We will see that there are some models which can give small values of x_s.

3.3.1. Four generations. Although LEP has ruled out the existence of four light neutrinos, it is still possible to have four generations if the extra neutrino is heavy. The CKM matrix is then a 4×4 unitary matrix. In this case there are additional contributions to B_s^0–$\bar{B}_s^0$ mixing, which come by replacing one or both of the t-quarks in figure 6 by t′-quarks. The complete expression for x_s then becomes

$$x_s = \tau_{B_s} \frac{G_F^2}{6\pi^2} M_W^2 M_{B_s} \left(f_{B_s}^2 B_{B_s}\right) \left\{ |V_{ts}^* V_{tb}|^2 \eta_{B_s} y_t f_2(y_t) + |V_{t's}^* V_{t'b}|^2 \eta_{t't'} y_{t'} f_2(y_{t'}) \right.$$
$$\left. + 2 V_{ts}^* V_{tb} V_{t's}^* V_{t'b} \eta_{tt'} y_t y_{t'} g_3(y_t, y_{t'}) \right\} \tag{55}$$

where the ηs are QCD corrections, and

$$g_3(y_i, y_j) = \left[\frac{1}{4} + \frac{3}{2} \frac{1}{(1-y_j)} - \frac{3}{4} \frac{1}{(1-y_j)^2} \right] \frac{\ln y_j}{y_j - y_i} + (y_i \leftrightarrow y_j) - \frac{3}{4} \frac{1}{(1-y_i)(1-y_j)}. \tag{56}$$

It is possible to find CKM matrix elements and t- and t′-masses such that the three contributions above result in a small value of x_s [68]. It should be noted, however, that this happens only in a small region of parameter space—most of the parameter space yields large values of x_s.

3.3.2. Supersymmetry. In supersymmetric (SUSY) models, there exist flavour changing gluino–squark–quark ($\tilde{g}$–$\tilde{q}_i$–q_j) couplings. This implies that there are new contributions to the B_d^0–$\bar{B}_d^0$ and B_s^0–$\bar{B}_s^0$ mixings via intermediate gluinos and squarks (figure 7). Whether or not the effects of such diagrams are important depends on whether they arise in the context of minimal SUSY models or in non-minimal SUSY models.

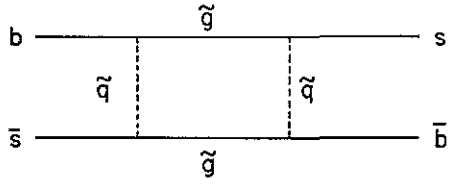

Figure 7. Additional box diagram contributing to B_s^0–$\bar{B}_s^0$ mixing in supersymmetric theories. There is another diagram in which the internal gluino and squark lines are interchanged.

In minimal SUSY models, the $\tilde{g}$–$\tilde{q}_i$–q_j couplings arise mainly in the left-handed sector (i.e. $\tilde{g}$–$\tilde{q}_{iL}$–q_{jL}). Furthermore, these couplings are proportional to the CKM matrix element V_{ij}. The contribution of figure 7 is then [69]

$$x_s^{\tilde{g}} = \frac{\alpha_s^2}{54 m_{\tilde{g}}^2} \tau_{B_s} f_{B_s}^2 B_{B_s} M_{B_s} |V_{ts}^* V_{tb}|^2 \Delta S_t(m_{\tilde{s}}, m_{\tilde{b}}, m_{\tilde{g}}) \tag{57}$$

where

$$\Delta S_t = S(w_3, w_3) + S(w_2, w_2) - 2S(w_2, w_3) \tag{58}$$

$$S(x, y) = 11 g(x, y) + 4 h(x, y) \tag{59}$$

$$g(x, y) = \frac{1}{x-y} \left[\frac{x^2 \ln x}{(x-1)^2} - \frac{1}{x-1} - (x \leftrightarrow y) \right] \tag{60}$$

$$h(x, y) = \frac{1}{x-y} \left[\frac{x \ln x}{(x-1)^2} - \frac{1}{x-1} - (x \leftrightarrow y) \right] \tag{61}$$

with $w_i = m_{\tilde{d}_i}^2/m_{\tilde{g}}^2$ ($\tilde{d}_i = \tilde{d}, \tilde{s}, \tilde{b}$). For reasonable values of masses for the supersymmetric particles ($m_{\tilde{d}_i}, m_{\tilde{g}} \geqslant$ 100–300 GeV), it is found that, although the SUSY contributions to B_s^0–$\bar{B}_s^0$ mixing are not negligible, x_s is still dominated by the SM box diagram [69]. In this context the values of $\Delta M(B_d)$ and $\Delta M(B_s)$ in the minimal supersymmetric model with electroweak radiative breaking (RMSSM) have been calculated in [70]. Their results for the ratio $\Delta M(B_d)_{SUSY}/\Delta M(B_d)_{SM}$ and $\Delta M(B_s)_{SUSY}/\Delta M(B_s)_{SM}$ are plotted in figure 8. This figure shows that the inclusion of SUSY particles leads to no more than 30% enhancement over the SM predictions. Moreover, for all the parametric values SUSY contributions add a positive contribution to $\Delta M(B_d)$ and $\Delta M(B_s)$. Therefore, it is not possible to obtain small values of x_s in minimal SUSY models.

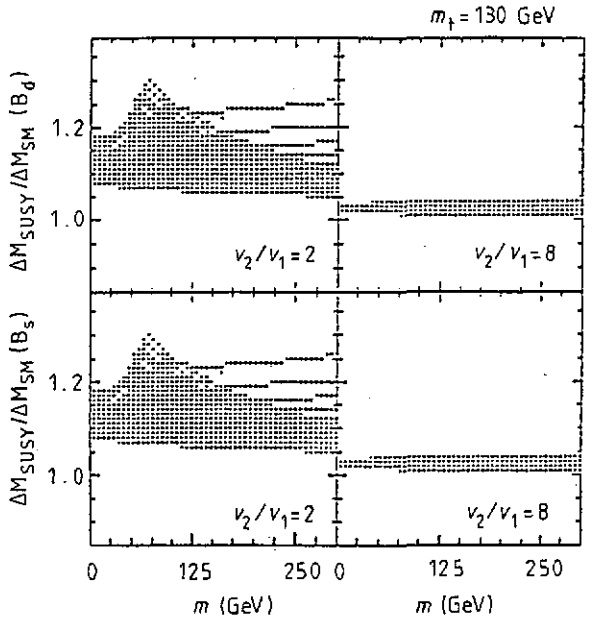

Figure 8. The ratio of the mimimal supersymmetric model contribution to $\Delta M(B_q)$ (q = d, s) over the corresponding SM prediction is shown for m_t = 130 GeV and $\tan\beta$ = 2, 8, as a function of the soft supersymmetry breaking mass m (from [70]).

In non-minimal models, on the other hand, the flavour changing $\tilde{g}$–$\tilde{q}_i$-q_j couplings are no longer dominated by the left-handed sector—the box diagrams with right-handed squarks are now also important. Furthermore, the $\tilde{g}$–$\tilde{q}_i$R–q_jR couplings are not related at all to V_{ij}. In this case, for certain values of the right-handed $\tilde{g}$–$\tilde{q}_i$–q_j couplings, it is possible to get cancellations between the SM and SUSY contributions to B_s^0–$\bar{B}_s^0$ mixing [71]. Therefore, it is possible to obtain small values of x_s in non-minimal SUSY models.

3.3.3. Multi-Higgs doublets with natural flavour conservation (NFC). In multi-Higgs doublet models, there are physical charged Higgses ($\phi^{\pm}$). These can contribute to B_s^0–$\bar{B}_s^0$ mixing through box diagrams such as those of figure 6 in which one or both of the $W^{\pm}$s is replaced by a $\phi^{\pm}$. In a general n-doublet model with NFC, the couplings of the ϕ^+ to quarks is given by [72]

$$\mathcal{L} = \sum_{k=2}^{n} \frac{g_2 \phi_k^+}{2\sqrt{2}M_W} \bar{U} \left[-\left(\frac{Y_{1k}}{Y_{11}}\right) M_u V_{CKM}(1-\gamma_5) + \frac{Y_{2k}}{Y_{21}} M_d V_{CKM}(1+\gamma_5) \right] D + \text{HC.} \qquad (62)$$

Here, Y is the matrix which rotates the mass eigenstate charged scalars to the interaction basis. In general, Y is unrelated to V_{CKM}. However, for B_s^0–$\bar{B}_s^0$ mixing, the leading contribution comes from the term proportional to m_t. This gives $(Y_{1k}V_{td})(Y_{1k}V_{td})^*$, and thus the new contributions from charged Higgs exchange simply add to that of the SM. A simple (but approximate) expression for x_s in the multi-Higgs model can be written as [73]

$$x_s = (x_s)_{SM}\left[1 + \frac{1}{4}\left(\frac{Y_{1k}}{Y_{11}}\right)^4 \frac{m_t^2}{m_H^2}\right]. \tag{63}$$

Therefore small x_s is not possible in multi-Higgs doublet models with NFC. (If NFC is abandoned, then constraints from flavour changing neutral currents require the masses of the charged Higgses to be extremely large, so that the new contributions to B_s^0–$\bar{B}_s^0$ mixing are negligible, and x_s remains as in the SM.)

3.3.4. Left–right symmetric models. In left–right (LR) symmetric models, the gauge sector is extended to $SU(2)_L \times SU(2)_R \times U(1)$. Minimal LR models include spontaneous *CP* violation, in which case the right-handed CKM matrix is identical to, or the complex conjugate of, the left-handed CKM matrix. In this case, there are rather strong lower limits on the mass of the W_R, $M_R > 1.5$–2.5 TeV, arising from the requirement that the short-distance contribution to the K_L–K_S mass difference not exceed the experimental value. New contributions to B_s^0–$\bar{B}_s^0$ mixing can come from diagrams such as figure 6 but with one or both Ws replaced by a right-handed W_R [74,75]. Including W and W_R exchange, the expression for x_s is

$$x_s^{TOT} = x_s^{SM}\left\{1 + \frac{3}{2}\frac{M_W^2}{M_R^2}\left(\frac{M_{B_s}^2}{(m_b + m_s)^2} + \frac{1}{6}\right)\frac{1}{\eta_{B_s}}\frac{1}{f_2(y_t)} \times \left[\eta_1^{LR}\left(\frac{4 - y_t}{1 - y_t} + \frac{4 - 2y_t + y_t^2}{(1 - y_t)^2}\ln y_t\right) + \eta_2^{LR}\ln\frac{M_W^2}{M_R^2}\right]\right\} \tag{64}$$

where M_R is the mass of the W_R, and $\eta_1^{LR} \simeq \eta_2^{LR} \simeq 1.8$ are QCD corrections. Altarelli and Franzini [69] have noted that, although the inclusion of the effects of the W_R acts to decrease the total amount of B_s^0–$\bar{B}_s^0$ mixing, the very stringent constraints on M_R make these effects rather small. Thus the SM prediction is essentially unaltered in minimal LR models.

If spontaneous *CP* violation is abandoned, then the right-handed CKM matrix is completely arbitrary. Langacker and Sanker [76] have analysed limits on M_R in this case. They find that bounds on M_R from ΔM_K can be evaded if right-handed CKM matrix takes one of the two following forms:

$$(A): \begin{pmatrix} 1 & * & * \\ * & \cos\phi & \sin\phi \\ * & -\sin\phi & \cos\phi \end{pmatrix} \qquad (B): \begin{pmatrix} * & 1 & * \\ \cos\phi & * & \sin\phi \\ -\sin\phi & * & \cos\phi \end{pmatrix}. \tag{65}$$

(The asterisks represent elements of $O(10^{-2})$, and phases have been ignored.) In these cases, the W_R can be as light as several hundred GeV, depending on the nature of the right-handed neutrino. However, a further analysis by London and Wyler [77] points out that, except in some exceedingly fine-tuned cases, bounds from ϵ then force M_R to be greater than ~ 30 TeV when phases are taken into account. Therefore, even if one does not implement spontaneous *CP* violation, the effects of the W_R on B^0–$\bar{B}^0$ mixing are, in general, small, and x_s remains large. (However, as pointed out in [77], fine-tuned solutions do exist which evade bounds from ϵ, and which can lead to small values of x_s through cancellations of the SM contributions.)

3.3.5. Z-mediated flavour changing neutral currents (FCNC). In these models [78], an $SU(2)_L$-singlet quark of charge $-1/3$ is added and allowed to mix with ordinary quarks. In this case, the CKM matrix is no longer unitary. In the basis in which the up-quark mass matrix is diagonal, the CKM matrix is the upper 3×4 submatrix of the 4×4 down-quark mass matrix. This leads to Z-mediated FCNC. There are two consequences of this. First of all, the constraints from unitarity on V_{ts} and V_{tb} are relaxed—V_{ts} and V_{tb} can be smaller than in the SM. Secondly, B_s^0–$\bar{B}_s^0$ mixing can come about directly through Z exchange (figure 9). There is a region of parameter space in which there is a cancellation between these new diagrams and those of the SM. Therefore it is possible to obtain small x_s in models with Z-mediated FCNC.

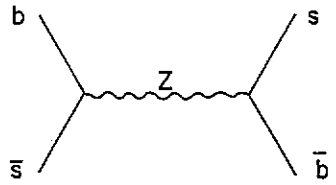

Figure 9. The additional diagram contributing to B_s^0–$\bar{B}_s^0$ mixing in models with Z-mediated flavour-changing neutral currents.

To summarize, the SM predicts x_s to be of O(10), with a value less than about 5 extremely improbable. Small values for x_s are possible in some models beyond the SM. Although x_s is always large in minimal supersymmetric models, multi-Higgs doublet models, and minimal left–right symmetric models, small values for x_s can be found in models with four generations, non-minimal supersymmetric models, non-minimal left–right symmetric models, and models with Z-mediated flavour-changing neutral currents. (However, for models with four generations and for non-minimal left–right symmetric models, it should be noted that this happens in a very small region of parameter space.) As we shall see, large x_s can be measured only via time-dependent techniques; time-integrated measurements are sensitive only to small values of x_s which, however, would point directly to physics beyond the SM. We turn to a discussion of both methods of measurement in the following sections.

4. Time-integrated measurements of B^0–$\bar{B}^0$ mixing—an update

We briefly discuss the present (time-integrated) measurements of B_d^0–$\bar{B}_d^0$ and B_s^0–$\bar{B}_s^0$ mixing. The data in the continuum have been analysed in terms of the time-integrated quantity χ, defined as

$$\chi = P_d \chi_d + P_s \chi_s \tag{66}$$

where P_d and P_s represent the probabilities $P(b \to B_d)$ and $P(b \to B_s)$, respectively, and χ_d and χ_s are the B_d^0–$\bar{B}_d^0$ and B_s^0–$\bar{B}_s^0$ mixing parameters, defined in terms of the time-integrated probabilities

$$\chi_{d,s} = \frac{P(B_{d,s} \to \bar{B}^0_{d,s})}{P(B_{d,s} \to B_{d,s}) + P(B_{d,s} \to \bar{B}^0_{d,s})}. \tag{67}$$

Note that $\chi_{d,s}$ is related to $x_{d,s}$ via

$$\chi_{d,s} = \frac{x_{d,s}^2}{2(1+x_{d,s}^2)}. \tag{68}$$

The quantity χ has been measured at LEP using the semileptonic decays of the B hadrons, giving rise to the dilepton final states. It is easy to show that the following relation holds

$$\frac{\Gamma(Z^0 \to b\bar{b} \to \ell^\pm\ell^\pm X)}{\Gamma(Z^0 \to b\bar{b} \to \ell^+\ell^- X)} = \frac{2\chi(1-\chi)}{(1-\chi)^2+\chi^2}. \tag{69}$$

The updated LEP average is [14,26]

$$\chi = 0.131 \pm 0.010. \tag{70}$$

This can be combined with the measurements at the $p\bar{p}$ colliders at CERN and Fermilab [79,80]

$$\chi = 0.145 \pm 0.038 \qquad \text{(UA1)}$$
$$\chi = 0.176 \pm 0.050 \qquad \text{(CDF)} \tag{71}$$

which gives the present world average for χ, $\chi = 0.133 \pm 0.0095$. Since the quantity χ_d has been measured by the ARGUS and CLEO collaborations using $\Upsilon(4S)$ decays, with the present average [43]

$$\chi_d = 0.155 \pm 0.031 \tag{72}$$

(corresponding to the value $x_d = 0.67 \pm 0.10$), one could use this as an input and extract χ_s from χ, assuming the specific probabilities P_d and P_s introduced earlier in the defining equation for χ. This gives

$$\chi_s = \frac{0.133 \pm 0.0095 - P_d(0.155 \pm 0.031)}{P_s}. \tag{73}$$

Using the folklore values $P_d = 0.35 \pm 0.05$ and $P_s = 0.20 \pm 0.07$ for the probability $b \to B_d X$ and $b \to B_s X$ in the continuum, respectively [79–81], one gets

$$\chi_s = 0.43 \pm 0.17 \tag{74}$$

in agreement with the large (almost complete) mixing anticipated for the B_s^0–$\bar{B}_s^0$ case in the SM, $\chi_s \simeq 0.50$. The present measurements of χ_d and χ_s are summarized in figure 10, which also shows the allowed region in the SM following from the unitarity constraints on the CKM matrix.

There exists a cross check on the determination of χ from the dilepton final state at LEP and SLC through the measurement of the forward–backward (FB) charge asymmetry in $Z^0 \to b\bar{b}$. It has been known for some time that B^0–$\bar{B}^0$ mixing reduces the time-integrated FB charge asymmetry $A_{FB}^{b\bar{b}}$(obs.) by an amount $(1-2\chi)$ [83]:

$$A_{FB}^{b\bar{b}} = \frac{A_{FB}^{b\bar{b}}(\text{obs.})}{(1-2\chi)}. \tag{75}$$

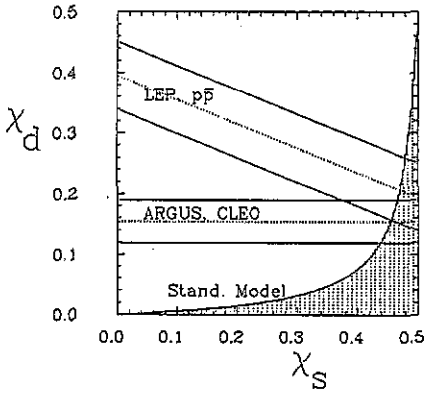

Figure 10. Present experimental measurements of χ_d and χ_s. The hatched region is the allowed range following from the CKM unitarity limit $|V_{td}|^2/|V_{ts}|^2 < 0.21$ (from [82]).

The measured value of χ at LEP (equation (70)) and the FB asymmetry $A_{FB}^{b\bar{b}}$(obs.) give $A_{FB}^{b\bar{b}} = 0.126 \pm 0.022$, which translates into the following determination of the weak mixing angle [26]

$$\sin^2 \bar{\theta}_W = 0.226 \pm 0.005 \tag{76}$$

to be compared with the other independent measurements of the same quantity at LEP [26]

$$\sin^2 \bar{\theta}_W = 0.233 \pm 0.001. \tag{77}$$

More data at LEP would reduce the indicated errors on the quantities χ and $A_{FB}^{b\bar{b}}$, enabling a more precise determination of the weak angle by this method. However, the extraction of χ_s from such measurements is intrinsically model-dependent. It is therefore important to think about measurements which could reduce this model dependence. The first qualitative improvement at LEP is expected to come through time-integrated measurements of the final states in the decays $Z^0 \to b\bar{b}$, in which the quantity χ_s would be measured by invoking the characteristic flavour correlations due to $B_s^0/\bar{B}_s^0$ production and decay AB. A point in question is the measurement of the dilepton final state $Z^0 \to b\bar{b} \to \ell^{\pm}\ell^{\pm}X$, where now X includes a tagged D_s meson. Since this ratio involves a different weighting of the quantities χ_d and χ_s, compared with the dilepton ratio χ without flavour tagging, defined earlier, the two measurements can be combined to extract χ_s. Since the detection of the D_s mesons in the decays of the B_s mesons is anticipated to play a central role in the measurement of both the time-integrated quantity χ_s, as well as the mixing ratio x_s, we shall discuss this point at some length below.

5. Time-dependent measurements of x_s: preliminaries

In this section we review the prospects for determining x_s by measuring the oscillation lengths due to B_s^0–$\bar{B}_s^0$ mixing. The oscillation period, defined as $T_{osc} \equiv 2\pi\tau_B/x_s$, and the oscillation length, $L_{osc} = \beta\gamma c T_{osc}$, are both inversely proportional to x_s. Hence, measuring the oscillation length allows the extraction of x_s, given the Lorentz boost factor $\beta\gamma$ (which is related to the energy of the B_s-meson) and the B hadron lifetime, τ_B. The precision

with which x_s can be measured then depends on two factors—the error on the tracklength measurement, $\Delta L/L$, and the error on the energy, $\Delta E/E$, where the energy is related to $\beta\gamma$. In order to have a hope of measuring x_s, it is at least necessary that there be a large decay length. This points to five possible experimental facilities where measurements of x_s could be undertaken:

(i) at LEP and SLC, $\sqrt{s} = m_Z \simeq 90$ GeV;
(ii) at an asymmetric B-factory, $\sqrt{s} = 10$–12 GeV;
(iii) at HERA, $\sqrt{s}(\mathrm{ep}) \simeq 310$ GeV;
(iv) at the TEVATRON, $\sqrt{s}(\mathrm{p\bar{p}}) = 1.8$ TeV;
(vi) at the LHC (pp, $\sqrt{s} = 16$ TeV) and SSC (pp, $\sqrt{s} = 40$ TeV).

In addition, x_s measurements are also feasible in experiments at fixed-target hadron machines.

Note that for B_s^0 production at a symmetric B-factory in the process $\Upsilon(5S) \to B_s^0\bar{B}_s^0, \ldots$, the average Lorentz boost factor $\langle\beta\gamma\rangle$ is only $O(10^{-2})$, and this therefore speaks against the feasibility of x_s measurements in a symmetric threshold B facility. On the other hand, for an asymmetric threshold machine of the type being actively entertained in a number of project studies [85–88], $\langle\beta\gamma\rangle \simeq O(1)$, and since the B_s energy is very precisely known in a threshold production process, the error $\Delta\langle\beta\gamma\rangle$ would be small. Hence, the error on the proper time Δt would be dominated by the tracklength measurement errors. In order to reduce the error on $\Delta L/L$, a large decay length is preferred. This, in turn, implies a more asymmetric B-machine.

We shall take up possible measurements of x_s at each of the above facilities in the subsequent sections. In the following subsection, we first review the time evolution of the various states taking into account the quantum mechanical restrictions when the B-meson pair is produced in a quantum state with well defined charge conjugation and angular momentum properties.

5.1. Time-dependent B_s^0–$\bar{B}_s^0$ oscillations: formalism

The time dependence of an initially pure B^0 state to be observed as a B^0 or $\bar{B}^0$ is determined by the averaged decay width, Γ, the oscillation frequency proportional to the mixing parameter $x = \Delta M/\Gamma$, and the lifetime difference $y = (\Gamma_1 - \Gamma_2)/\Gamma$. Here, Γ_1 and Γ_2 refer to the decay widths of the mass eigenstates B_1 and B_2, respectively, whose mass difference is denoted by ΔM. However, for both neutral B-meson systems being discussed it is expected that $y \ll 1$ and hence the dependence of the oscillation pattern on y will be discarded. Concentrating on the B_s^0–$\bar{B}_s^0$ system, the modulated time dependence of the single-meson state $\langle B_s^0 \to B_s^0; t|$ and the charged conjugate state produced due to mixing $\langle B_s^0 \to \bar{B}_s^0; t|$ are given by

$$|B_s^0(t)\rangle = e^{-t/\tau_B}\cos^2(x_s t/2\tau_B)|B_s^0; t = 0\rangle$$
$$|\bar{B}_s^0(t)\rangle = e^{-t/\tau_B}\sin^2(x_s t/2\tau_B)|B_s^0; t = 0\rangle. \tag{78}$$

These equations are to be interpreted as probabilities (at time t) of observing the decays of a B_s^0 or $\bar{B}_s^0$ meson, respectively, which was initially produced as a B_s^0 meson (at $t = 0$). It is known that, due to *CP* violation, there exists a small asymmetry in the time evolution of an initially produced B_s^0 and $\bar{B}_s^0$ state. However, in view of the expected tiny asymmetry in the B_s^0–$\bar{B}_s^0$ system in the SM, we shall ignore this difference altogether. In addition, it is obvious from the above evolution equations that to observe an oscillation one will have to detect the decays of the B_s^0 and $\bar{B}_s^0$ in final states which are *not* flavour neutral. Otherwise, the time

modulation due to mixing will disappear. As an example, the decays $(B_s^0, \bar{B}_s^0) \to J/\psi\phi$ are no good for this purpose but the decays $(B_s^0, \bar{B}_s^0) \to (D_s^- \pi^+, D_s^+ \pi^-)$ are.

In continuum production processes, such as is the case in all experimental facilities mentioned above except the B-factory, one can treat the time evolution of a single B^0 or $\bar{B}^0$ state independently of the other. The reason for this is that the final state containing the B hadron is the superposition of a large number of angular momentum states and hence, on average, there are no constraints from angular momentum selection rules.

In contrast, for the process $e^+e^- \to \Upsilon(5S) \to B_s^0\bar{B}_s^0$, the angular momentum constraints lead to very specific restrictions on the time evolution of the B_s^0–$\bar{B}_s^0$ state produced at time $t = 0$. The time evolution of the final state depends on the charge conjugation properties of the $B\bar{B}$ pair. (Note that, in fact, the $B\bar{B}$ pair can be either $B_d^0\bar{B}_d^0$ or $B_s^0\bar{B}_s^0$ since both can be produced in the decay of the $\Upsilon(5S)$.) A $B\bar{B}$ pair which is produced directly or through the decay of the excited state $B^*\bar{B}^*$ will have $C = -1$, whereas a $B\bar{B}$ pair which comes from $B^*\bar{B}$ or $B\bar{B}^*$ has $C = +1$. For the $C = -1$ states the opposite-sign and like-sign states have the following differential (in time) probabilities:

$$P(B^0\bar{B}^0; t_1, t_2) = \exp(-(t_1 + t_2)/\tau_B) \cos^2(x(t_1 - t_2)/2\tau_B)$$
$$P(B^0B^0; t_1, t_2) = \exp(-(t_1 + t_2)/\tau_B) \sin^2(x(t_1 - t_2)/2\tau_B). \tag{79}$$

For the $C = +1$ states, the corresponding time evolution is given by

$$P(B^0\bar{B}^0; t_1, t_2) = \exp(-(t_1 + t_2)/\tau_B) \cos^2(x(t_1 + t_2)/2\tau_B)$$
$$P(B^0B^0; t_1, t_2) = \exp(-(t_1 + t_2)/\tau_B) \sin^2(x(t_1 + t_2)/2\tau_B). \tag{80}$$

Since the beam interaction point in the beam direction is not known accurately, t_1 and t_2 cannot be determined individually. However, the proper-time difference $|t_1 - t_2|$ can be measured. Integrating over the variable $t_1 + t_2$, one gets the following distribution in the time difference interval $\delta t = |t_1 - t_2|$ [89]:

$$P(B^0\bar{B}^0; \delta t) = \exp(-\delta t/\tau_B) \cos^2(\tfrac{1}{2}x\delta t/\tau_B) \qquad C = -1$$

$$P(B^0B^0 + \bar{B}^0\bar{B}^0; \delta t) = \exp(-\delta t/\tau_B) \sin^2(\tfrac{1}{2}x\delta t/\tau_B) \qquad C = -1$$

$$P(B^0\bar{B}^0; \delta t) = \frac{1}{2}\frac{1}{1+x^2} \exp\left(-\frac{\delta t}{\tau_B}\right)\left\{2\cos^2\left(\frac{x}{2}\frac{\delta t}{\tau_B}\right) + x^2 - x\sin\left(x\frac{\delta t}{\tau_B}\right)\right\}$$
$$C = +1$$

$$P(B^0B^0 + \bar{B}^0\bar{B}^0; \delta t) = \frac{1}{2}\frac{1}{1+x^2} \exp\left(\frac{-\delta t}{\tau_B}\right)\left\{2\sin^2\left(\frac{x}{2}\frac{\delta t}{\tau_B}\right) + x^2 + x\sin\left(x\frac{\delta t}{\tau_B}\right)\right\}$$
$$C = +1. \tag{81}$$

We shall denote these δt-dependent probabilities as: $f_{\text{odd}}^{+-}(x_i, \delta t)$, $f_{\text{odd}}^{\pm\pm}(x_i, \delta t)$, $f_{\text{even}}^{+-}(x_i, \delta t)$, $f_{\text{even}}^{\pm\pm}(x_i, \delta t)$, respectively, where $x_i = x_d, x_s$. Note that for the $C = -1$ states, the angular momentum constraint does not change the modulated form of time evolution. The relevant equations for the time evolution of a single B^0-meson state given in equation (78) and those for the evolution of a pair of B mesons with odd charge conjugation, $f_{\text{odd}}^{+-}(x_i, \delta t)$, $f_{\text{odd}}^{\pm\pm}(x_i, \delta t)$, are identical if one substitutes t by δt. Consequently, the oscillations in the $C = -1$ B-meson states are very pronounced. On the other hand, oscillations in the even

charge conjugation parity states have a more complicated δt dependence and are, in general, much less pronounced due to the $(1 + x^2)$ suppression. This is the reason why the issue of the accessibility of the vector meson pair states in the decay $\Upsilon(5S) \to B_s^{0*}\bar{B}_s^{0*}$, which are produced in the $C = -1$ state, is such an important matter for the observability of B_s^0–$\bar{B}_s^0$ mixing in threshold B-factories. In addition, the amplitude of oscillation is much more pronounced in the same sign states (i.e. B^0B^0 and $\bar{B}^0\bar{B}^0$, which may be tagged as the *same-sign dilepton states due to the semileptonic decays of the two B mesons).*

5.2. Sources of measurement error

We now discuss the relation between the measurement errors and the accessible x_s range. The decay proper time, t, is measured with a certain given accuracy, Δt, and the observed time evolution is a convolution of the expression for $|B_s^0(t)\rangle$ and $|\bar{B}_s^0(t)\rangle$ given above with a Gaussian distribution. This would reduce the oscillation amplitude by an amount D [92]

$$D = e^{-(x_s^2/2)(\Delta t/\tau_B)^2}. \tag{82}$$

For example, the oscillation amplitude is reduced to 10% of its initial value for $x_s \Delta t/\tau_B = 2.1$. The accessible x_s range depends on the proper-time resolution $\Delta t/\tau_B$. Thus, there are two parameters that determine the measureability of x_s: the efficiency of tagging the $B_s^0/\bar{B}_s^0$ at $t = 0$; and the proper-time resolution.

Concerning the latter, we recall that since the proper time is defined as $t = L/(c\beta\gamma)$, where L is the decay length, the global error on the proper time can be estimated by the quadratic addition of errors

$$\left(\frac{\Delta t}{\tau_B}\right)^2 = \left(\frac{\Delta L}{L_0}\right)^2 + \left(\frac{t}{\tau_B}\frac{\Delta E_B}{E_B}\right)^2 \tag{83}$$

where $L_0 = c\beta\gamma\tau_B$. The first term on the right-hand side is determined by the resolution of the decay vertex position. The second term in equation (83) is determined by the accuracy on the B_s^0-hadron energy measurements. Measuring E_B in a fully reconstructed B_s^0 would provide the required accuracy of a few per cent on $(\Delta E_B/E_B)$. This would, however, demand a very large number of B hadrons due to the very small B_s^0 reconstruction efficiency, as has been argued by Krawczyk *et al* [89].

Finally, a reduction in the oscillation amplitude is caused if one misidentifies the particle/antiparticle nature of the $B_s^0/\bar{B}_s^0$ at $t = 0$. Since the B_s^0 and $\bar{B}_s^0$ oscillate with opposite phases one loses the signal not only due to the efficiency of the tagging but also due to the fact that an equal amount of the oscillation signal vanishes. Defining A_0 as the *amplitude for perfect tagging, the actual observed signal A(obs.) becomes diluted by the* wrong tag at $t = 0$. The observed signal A(obs.) is given by

$$A(\text{obs.}) = A_0 \frac{N_{\text{good tag}} - N_{\text{bad tag}}}{N_{\text{good tag}} + N_{\text{bad tag}}}. \tag{84}$$

In the following subsection, we shall estimate A(obs.) for definite final states in which a B_s^0 meson has been flavour-tagged.

5.3. Flavour-tagging the B_s^0 meson

One of the principal issues is to tag the B_s^0 and $\bar{B}_s^0$ mesons, which can be done by observing an exclusive or semi-inclusive decay involving, for example, a $D_s^\pm$ meson in the semileptonic decays $\bar{B}_s^0 \to D_s^+ \ell^- \nu_\ell$, or a completely constrained event satisfying the B_s^0 meson mass constraint, for example in $\bar{B}_s^0 \to D_s^+ \rho^-$. In time-dependent measurements, one should, in addition, know the particle–antiparticle nature of the B_s^0 at the time of production, since otherwise the oscillations will be 'flavour bleached' and washed away! Since the B hadrons are pair-produced in flavour-neutral production processes, such as $e^+e^- \to B\bar{B}X$ and $p\bar{p} \to B\bar{B}X$, flavour-tagging the B hadron recoiling against the B hadron being probed will also determine the particle–antiparticle nature of the probed hadron at the time $t = 0$. As the B_s^0 is expected to mix essentially completely, it is not a good particle to tag in the recoiling hadron sample. Likewise, B_d, due to the observed mixing, has a chance of 1:3 of being wrongly identified. One has to take this into account if B_d mesons are used for tagging. The hadrons $B_u^\pm$, $B_c^\pm$, and Λ_b on the recoil side are good flavour tags at $t = 0$. Insisting on a complete reconstruction of these hadrons is not necessary. It is sufficient to establish one of the two properties:

(i) that the overall charge of the tracks initiating from the B-decay vertex sums up to ± 1. (This, for example, would be the case for the $B_u^\pm$ and $B_c^\pm$ decays); and

(ii) that characteristic flavour correlations in Λ_b decays are used.

In this context it is worth noting that the characteristic semileptonic decays of the Λ_b, namely $\Lambda_b \to \Lambda_c \ell^- \nu_\ell$, with the subsequent decay $\Lambda_c \to \Lambda X$, giving $(\Lambda \ell^- X)$ as opposed to the $(\Lambda \ell^+ X)$, have been measured at a statistically significant level at LEP. An excess of 53 ± 13 events corresponding to the product branching ratio $BR(\Lambda_b \to \Lambda \ell^- X) BR(b \to \Lambda_b) = (0.95 \pm 0.22(\text{stat}) \pm 0.21(\text{syst}))\%$ has been established by the ALEPH collaboration at LEP [90]. Of course, the lepton charge in the decays $B \to X, \ell^+ \nu_\ell$ also tags the b-quark, modulo mixing corrections. Flavour-tagging the recoiling b-quark by these methods can already help the ongoing experiments at LEP and CDF to determine χ_s. For example, with a tagged $\bar{b}$-quark on the recoil side, the decay products of a b-quark jet satisfy the following relation

$$\frac{b \to D_s^- \ell^+ \nu_\ell}{b \to D_s^+ \ell^- \nu_\ell} = \frac{\chi_s}{1 - \chi_s} \tag{85}$$

which is independent of the parameters P_d and P_s.

Another method to determine the particle/antiparticle nature of the B_s^0 and $\bar{B}_s^0$ mesons at $t = 0$ was proposed some time ago in [84]. One starts from the observation that in sufficiently inelastic production processes, such as $e^+e^- \to B\bar{B}X$ at LEP, the B hadron and $\bar{B}$-hadron are expected to be well separated topologically. Using some jet criterion such as the Sterman–Weinberg definition of jets [91], for example, it is easy to show that the probability of having a b-quark and a $\bar{b}$-quark in a single jet, having the jet size (ϵ, δ), and recoiling against a gluon jet in an e^+e^- annihilation process is given by $(\alpha_S/\pi) f(\epsilon, \delta)$, where $f(\epsilon, \delta) \sim O(\epsilon, \delta)$ and hence negligible for sufficiently small ϵ, δ. B_s^0 production in a b-quark jet comes via the excitation of an $s\bar{s}$ pair from the vacuum, forming a $\bar{B}_s^0$-hadron and the subsequent fragmentation process initiated from the leftover s-quark: $b \to (b\bar{s}) + s$. It is an experimental fact that the probability of producing an $s\bar{s}$ quark pair from the vacuum is markedly lower than its $SU(3)$-symmetric value, with the present data being consistent with $P_s = 0.1$–0.15. Hence, it makes sense to use P_s as an order parameter, implying that multiple $s\bar{s}$ pair-production in a jet is suppressed by powers of P_s. Concentrating on the

leading contribution, since an s-quark will dominantly lead to a prompt K^- as opposed to a prompt K^+ in the process of fragmentation, it follows that the production of the $B_s^0/\bar{B}_s^0$ meson in a jet is correlated with the sign of the prompt charged kaon, $K^\pm$ at the instant of production, $t = 0$. Thus, one expects that final states with the 'right-sign K' such as $\bar{B}_s^0 K^-$ and $B_s^0 K^+$ will be much more abundant in jets than the 'wrong-sign K', $\bar{B}_s^0 K^+$ and $B_s^0 K^-$, with the parameter P_s providing a quantitative measure. A typical situation in a b-quark jet is shown in figure 11, where the prompt kaon is labelled as 'Kmora', borrowing the fishing terminology used in [92]. Likewise, an s-quark will lead to a Λ-baryon more often than to $\bar{\Lambda}$-baryon. In the present context, this will then give rise to final states in jets such as $\bar{B}_s^0 \Lambda$ and not $\bar{B}_s^0 \bar{\Lambda}$.

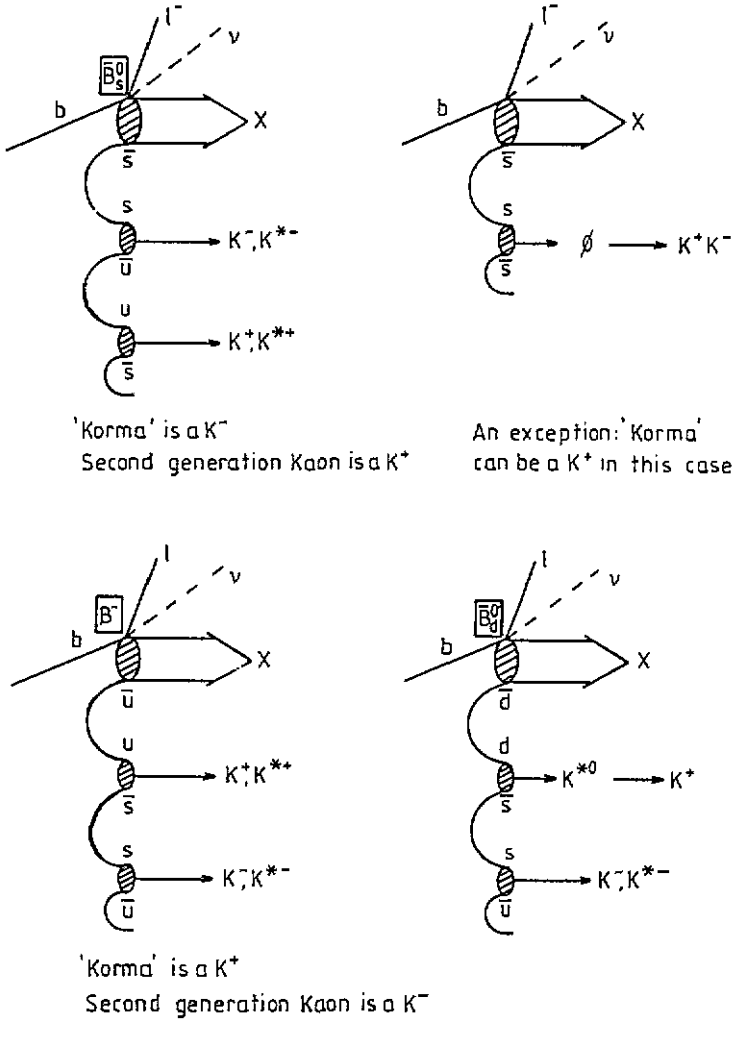

Figure 11. Production of B hadron and charged kaons $K^\pm, K^{*\pm}$ in the fragmentation of a b-quark jet. The associated $K^\pm$ is being called here a 'Kmora' (from [92]).

It is clear that B_s^0–$\bar{B}_s^0$ mixing will wash out the correlation stemming from the fragmentation process just discussed. In fact, it is easy to show that in the leading order in

the parameter $P_s = f(s\bar{s})$, B_s^0–$\bar{B}_s^0$ mixing will lead to the relation

$$\frac{P(b \to B_s^0 K^-)}{P(b \to B_s^0 K^-) + P(b \to \bar{B}_s^0 K^-)} = \chi_s. \tag{86}$$

For complete mixing, $\chi_s \simeq 0.5$. Measuring the ratio on the left-hand side in the above equation then provides a measurement of χ_s. This ratio is independent of the quantitities P_s and P_d, as opposed to the dilepton ratio or the FB asymmetry, $A_{FB}^{b\bar{b}}$, discussed previously. Given large statistics and good particle identification, it should be possible to construct the B_s^0 and $\bar{B}_s^0$ hadrons, either non-leptonically, as in $\bar{B}_s^0 \to (D_s^-, D_s^{*-})\pi^+$, or semileptonically, through $\bar{B}_s^0 \to (D_s^-, D_s^{*-})\ell^+\nu_\ell$. One could also use the characteristic charged lepton–kaon states in the decays of the B_s, $\bar{B}_s \to \ell^+ K^- \nu_\ell X$, and measure the final state $\ell^+K^-K^-X$ as a reliable estimator of the state $B_s^0 K^- X$ (and likewise the charge conjugate state for the decay of $\bar{B}_s^0$). In that case, one could interpret the above relation as follows [84]

$$\frac{P(b \to \ell^+ K^- K^-)}{P(b \to \ell^+ K^- K^-) + P(b \to \ell^- K^+ K^-)} = \chi_s. \tag{87}$$

There are corrections to this relation due to the quadratic (and higher) terms in P_s, and from the Cabibbo-suppressed B decays producing the 'wrong sign' $K^\pm$-mesons. They have been estimated for LEP in [84], and these estimates can now be put on firmer grounds by using the measured probability of the Cabibbo-suppressed B decays, thanks to the recent ARGUS data on the charged lepton–kaon states in B^+/B^0 decays [93]. The charged lepton–kaon correlation can be simply understood in terms of the b-quark decay, $\bar{b} \to \bar{c}\ell^+\nu_\ell$, followed by the decay $\bar{c} \to \bar{s}X$, giving rise to the dominant (Cabibbo-allowed) decays $B^+/B^0 \to \ell^+\nu_\ell K^+ X$, having the same-sign lepton and kaon. The opposite-sign lepton–kaon state in the decays $B^+/B^0 \to \ell^+\nu_\ell K^- X$ is Cabibbo-suppressed. The branching ratios $BR(B^+/B^0 \to \ell^+\nu_\ell(K^\pm, K_s^0)X)$ and $BR(B^+/B^0 \to (K^\pm, K_s^0)X)$ from the ARGUS data are shown in table 5. It follows from table 5 that the branching ratio of the opposite-sign lepton–kaon state in B^+/B^0 decays is indeed $O(\sin^2\theta_C)$. This measurement establishes that there is no spurious enhancement of the Cabibbo-suppressed inclusive decay modes in B^+/B^0, and that the opposite-sign lepton–kaon charge correlations are potentially very useful in tagging the B_s mesons, since one expects the decays $B_s^0 \to \ell^+ K^- \nu_\ell X$ to have no such Cabibbo-suppression.

Table 5. Mean kaon multiplicities and branching ratios of B-meson decays, where ℓ^+ represents an e^+ or μ^+. The non-semileptonic numbers include production through mixing (from [93]).

Decay modes	$BR(B \to \ell^+\nu_\ell KX)/BR(b \to \ell^+\nu_\ell X)$
$B^+/B^0 \to \ell^+\nu_\ell K^+ X$	$0.536 \pm 0.021 \pm 0.075$
$B^+/B^0 \to \ell^+\nu_\ell K^- X$	$0.077 \pm 0.011 \pm 0.045$
$B^+/B^0 \to \ell^+\nu_\ell K_s^0 X$	$0.187 \pm 0.018 \pm 0.023$
Decay modes	$BR(B \to KX)$
$B^+/B^0 \to K^+ X$	$0.557 \pm 0.016 \pm 0.050$
$B^+/B^0 \to K^- X$	$0.160 \pm 0.010 \pm 0.038$
$B^+/B^0 \to K_s^0 X$	$0.283 \pm 0.007 \pm 0.020$

The associated production $b \to \bar{B}_s^0 K^+ X$ and the charge conjugate process have been taken up in a number of subsequent studies for LEP and SLC [92, 94, 95]. There are two

characteristics of the $K^{\pm}$ mesons so produced, namely that they will follow the direction of the $B_s^0/\bar{B}_s^0$, and that they will have a higher momentum than other kaons from the secondary stages of fragmentation. These features have been evaluated in a number of Monte Carlo studies. A representative Dalitz distribution of the momentum and direction of the $K^{\pm}$ (measured with respect to the b-jet axis), as well as the $K^{\pm}$-energy and angular distributions from these simulations are shown in figure 12.

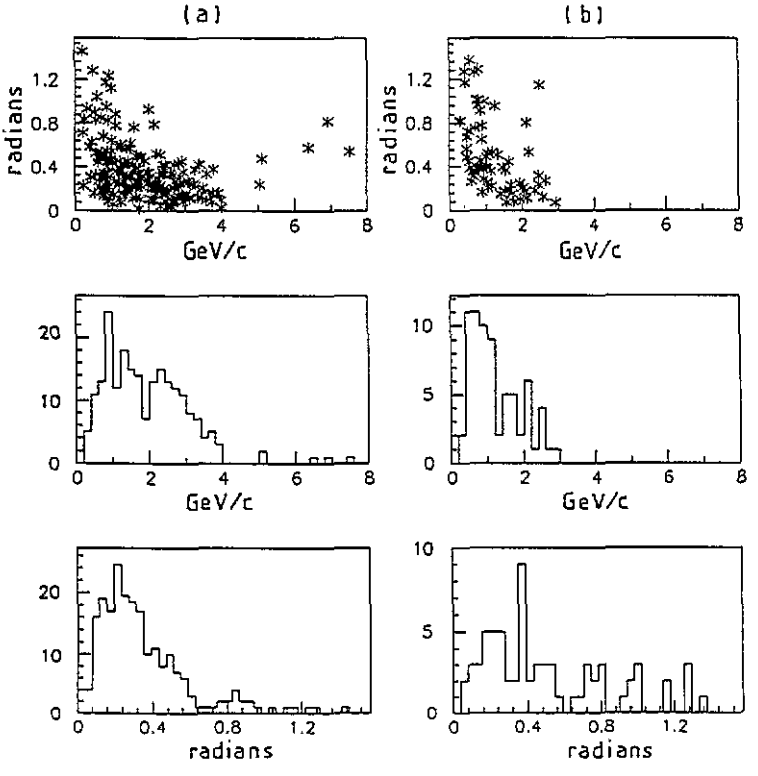

Figure 12. A Monte Carlo study of the correlation between the momentum and the direction of the charged kaons produced at the primary vertex in association with a B_s^0 meson at LEP: (*a*) $\bar{B}_s^0K^-$ and $B_s^0K^+$ events; (*b*) $\bar{B}_s^0K^+$ and $B_s^0K^-$ events (from [92]).

The potential power of the $K^{\pm}$-tagging method can be illustrated by the following numerical estimate [96,97]. Suppose that one has already a B_s^0-tagging technique that results in a sample of 1000 $B_s^0/\bar{B}_s^0$ mesons and 1000 B_u/B_d mesons. Assume that this technique does not distinguish between the particle/antiparticle nature of the $B_s^0/\bar{B}_s^0$ meson at time $t = 0$. The result of applying the $K^{\pm}$-tag in Z^0 decays is summarized in table 6. After the associated $K^{\pm}$-tag has been applied to the sample of 2000 B hadrons, the ability to tag the particle/antiparticle nature of the $B_s^0/\bar{B}_s^0$ at its production is now $345/49 \simeq 7$. The ability to reject B_u and B_d is now $394/142 = 2.8$. Results obtained in [92,94] are also very similar. The $K^{\pm}$-tag method requires good particle identification and vertex reconstruction capabilities to separate the 'Kmora-kaons' from the B-decay kaons, otherwise the efficiency of this method will be greatly reduced. Assuming that these capabilities are at hand, which is the case for most of the LEP/SLC detectors, a ratio of better than 5:1 for the correct/incorrect identity of the $B_s^0/\bar{B}_s^0$ can be achieved. The price to pay is that only (roughly) half of the

$B_s^0/\bar{B}_s^0$ events would survive this tag. Again, such estimates can now be put on a firm experimental footing due to the lepton–kaon charge correlation measured by ARGUS.

Table 6. Summary of results after applying fragmentation $K^{\pm}$ technique (from [96]).

Cut applied	B_s Correct $t = 0$ tag	B_s Incorrect $t = 0$ tag	B_s Total	$B_u + B_d$ Total
No $K^{\pm}$ tag	500	500	1000	1000
Highest momentum $K^{\pm}$	412	83	495	242
$\sin\theta_{BK^{\pm}} < 0.5$	345	49	394	142

6. Prospects for x_s measurements at LEP and SLC

Having discussed the main points involved in the measurement of x_s generally, including methods of tagging and B_s^0 enrichment, we review in this section the prospects for such measurements at LEP (and SLC). In doing this we draw heavily from the studies in [92, 94].

Apart from a good quality particle/antiparticle tag, one needs a reliable E_B (or t) estimator, so that unconstrained events (such as, for example, the semileptonic decays $B_s^0 \to D_s^{\pm}\ell\nu_\ell$) can also be included. We refer the reader to the studies in [94] on this point, where the information contained in the tracking results, particle identification and jet-axis (B-direction) measurements have been used to obtain reliable E_B estimators in a typical LEP environment. We show the conclusions based on this study at the end of this section. However, we first discuss the end result of a Monte Carlo based study undertaken in [92] using the above-mentioned B_s^0 semileptonic decays.

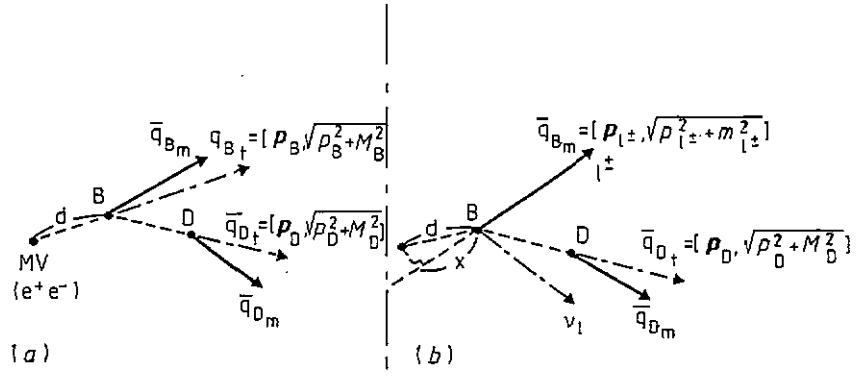

Figure 13. Decay vertices and momenta used in estimating the B momentum (and proper time) for (*a*) hadronic modes and (*b*) semileptonic modes in the Monte Carlo study of x_s measurements at LEP (from [94]).

Recapitulating briefly, let us concentrate on the semileptonic decay $B_s^0 \to D_s^- \ell^+ \nu_\ell X$, where the B_s^0 is produced as a result of the decay $Z^0 \to b\bar{b}$. For this case, the B_s^0 decay vertex should be situated on the lepton track, which is the closest distance from the reconstructed $D_s^{\pm}$ trajectory (impact parameter), as shown in figure 13. Since the neutrino is missing,

to obtain a zero constraint kinematics, one has to measure the B_s^0 direction and assume that the B_s^0 mass is known. The B_s^0 direction can be estimated from the b-jet direction, which can be measured to an accuracy of ~50 mrad. This method, called the signed impact parameter technique, has been successfully used to measure the B hadron lifetime at LEP using semileptonic B-decays [14], showing that the b-jet axis is a reliable estimator of the B-direction. This strengthens the conclusion arrived at in [92], that an accuracy $\Delta E_B/E_B \sim 0.1$ on the B_s^0 energy can be achieved, if one retains events having a visible B_s^0 mass in excess of 4 GeV. This last result also depends somewhat on the assumption of an end-point peaked $b \to B_s^0$ fragmentation function. Specifically, a Peterson *et al* type fragmentation function [98] with $\epsilon_B = 0.008$, giving $\langle x_B \equiv E_B/E_{beam} \rangle = 0.71$, has been used in the analysis of [94]. The energy fraction $\langle x_B \rangle$ has now been measured at LEP: $\langle x_B \rangle = 0.699 \pm 0.011$ [99]. Though the measured value of $\langle x_B \rangle$ is slightly lower than that assumed in the Monte Carlo study of [92], the resulting effect on the resolution of B_s^0 energy is not important. A representative estimate of the error on the proper-time measurements from semileptonic decays at LEP/SLC is [92]

$$(\Delta t/\tau_B)^2 = 4.4 \times 10^{-3} + 1.2 \times 10^{-2}\ (t/\tau_B)^2 \tag{88}$$

where the second term, due to the B_s^0 energy resolution, clearly dominates. The above expression also underlines the importance of measuring the oscillations at small decay proper time, $t/\tau_B < 2$, as can be seen from figure 14, where the dilution factor D, defined earlier, is plotted for the various choices of x_s.

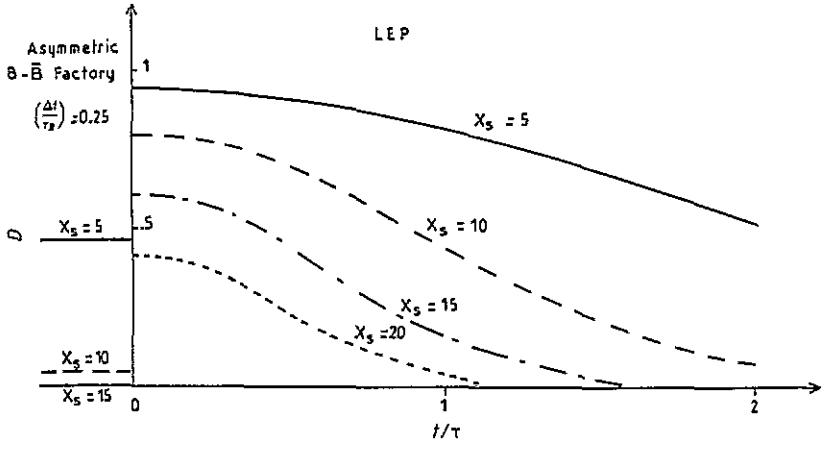

Figure 14. Dilution factor D defined in the text for the B_s^0 oscillations due to the experimental resolution on the decay proper time at LEP. The assumed value of x_s is indicated on the curves (from [92]).

Next we discuss the point concerning the quality of particle/antiparticle tags. The results of a Monte Carlo based study undertaken for the DELPHI detector at LEP to estimate $N_{\text{good tag}}$ and $N_{\text{bad tag}}$, using the $\bar{B}_s^0 K^-$ and $B_s^0 K^+$ final states are given in table 7 [92]. This gives $A(\text{obs.}) = 0.74$. A study done for the SLD detector at SLC also leads to very similar results [96, 97]. Knowing the dilution factor D, the tagging efficiency at $t = 0$, $A(\text{obs.})$, the $B_s^0/\bar{B}_s^0$ decay reconstruction efficiency, ϵ_s, and the purity of the B hadron sample in

Table 9. Efficiency of right B_s^0 identification and tagging (referring to the total number of $B_s^0(\rightarrow \geqslant 3$ charged particles + $D_s(\rightarrow \geqslant 3$ charged particles)) and $B_s^0 \rightarrow \ell^{\pm}\nu_{\ell} + D_s^{\mp}(\rightarrow \geqslant 3$ charged particles) and the final oscillation signal emerging from an assumed sample of 10^8 Z^0 in the DELPHI detector (from [94]).

	Hadr. (Eff.)	Hadr. (Tags)	Semilept. (Eff.)	Semilept. (Tags)
$K^{\pm}/B_s^0$ tagging	0.04	4045 ± 1170	0.033	3370 ± 1070
$(B_u, B_d)/B_s^0$ tagging	0.042	1810 ± 510	0.06	$2,600 \pm 610$
Total	0.082	5850 ± 1270	0.093	5970 ± 1230
Grand total	$11\,800 \pm 1800$			

$B_s^0/\bar{B}_s^0$ mesons, P, the number of Z^0 bosons to measure a given x_s with an error Δx_s can be estimated from the expression [92]

$$N(Z^0) = \left(\frac{x_s}{\Delta x_s}\right)^2 \frac{1}{8PD^2A(\text{obs.})^2\epsilon_s}. \tag{89}$$

Assuming $\Delta x_s/x_s = 0.1$, the required number of Z^0s for the DELPHI detector at LEP, for various values of x_s, is given in table 8. The study in [92] leads to the conclusion that, given the above assumed efficiencies, one would need 1.3×10^7 Z^0 events to measure $x_s \simeq 10$ with a 10% error.

Table 7. $N_{\text{good tag}}$ and $N_{\text{bad tag}}$ estimated for the DELPHI detector at LEP using the $K^{\pm}$-tagging (from [92]).

	Good sign K(%)	Wrong sign K(%)
B_s^0	20	3
Background	5.4	9.4

Table 8. Required number of Z^0 to measure x_s estimated for the DELPHI detector at LEP (from [92]).

x_s	5	10	15
$N_Z(\times 10^6 \text{events})$	5	13	55

Very similar conclusions have been reached in [94] in the context of the feasibility of x_s measurements at a high luminosity LEP. As opposed to the study of Roudeau discussed above, which concentrates on the semileptonic decays of the $B_s^0/\bar{B}_s^0$, the analysis of Defoix [94] makes use of both the semileptonic and non-leptonic decays of the $B_s^0/\bar{B}_s^0$. In addition, $B_s^0/\bar{B}_s^0$ identification at time $t = 0$ is done both by tagging the B_u, B_d meson in the recoil jet, and the associated $K^-B_s^0$ and $K^+\bar{B}_s^0$ signal in the same jet, discussed above. The efficiencies of the two methods are found to be comparable, given the assumed $K^{\pm}$-tagging capability, as shown in table 9. Also shown in this table are the number of tagged and flavour identified $B_s^0/\bar{B}_s^0$ events at LEP for an assumed 10^8 Z^0 events. The overall $B_s^0/\bar{B}_s^0$-detection efficiency has been estimated as $\sim 1.2 \times 10^{-4}$ for the combined (semileptonic and non-leptonic) sample, and $\sim 0.6 \times 10^{-4}$ for the semileptonic decays alone. The latter estimate is in agreement with the one due to Roudeau [92].

The number of the Z^0 decays needed to measure x_s, assuming a certain resolution on the proper time $\Delta t/\tau_B$, is shown as a function of x_s in figure 15. Also shown in this figure is the number of tagged $B_s^0/\bar{B}_s^0$ mesons needed to measure x_s, at 99% CL and 26% purity (the quantity P defined above). For an assumed precision on the proper-time measurements, $\Delta t/\tau_B = 0.1$, which is attainable at LEP, measurements of $x_s \sim 10$ would require $O(10^7)$ Z^0 events.

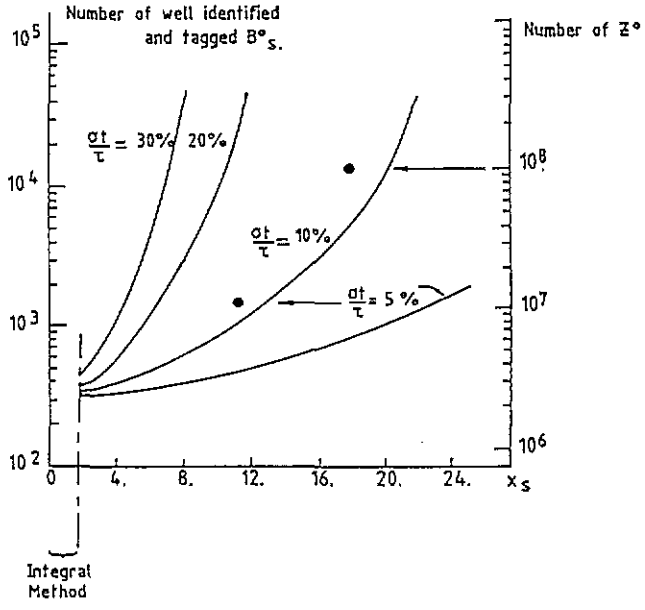

Figure 15. Estimates of the required number of Z^0s to measure x_s at LEP. The assumed value of the proper-time resolution is indicated on the curves. Also shown are estimates of the corresponding number of well identified and tagged B_s^0 for the DELPHI detector (from [94]).

7. Prospects for x_s measurements at asymmetric B-factories

In this section, we study the prospects for a time-dependent measurement of B^0–$\bar{B}^0$ mixing in the decay of a resonance of the Υ series and concentrate on the decays of the $\Upsilon(5S)$. This state, which has $(J)^{PC} = (1)^{--}$, has been seen as a resonance in e^+e^- annihilation having a production cross section $\sigma(e^+e^- \to \Upsilon(5S)) = 0.27$ nb, mass $M_{\Upsilon(5S)} = 10.865 \pm 0.008$ GeV and width $\Gamma(\Upsilon(5S)) = 110 \pm 13$ MeV [4]. It is widely believed that the $\Upsilon(5S)$ lies above the $B_s^0\bar{B}_s^0$ and $B_s^0\bar{B}_s^{0*}$ pair-production threshold, and perhaps also above that of the $B_s^{0*}\bar{B}_s^{0*}$ [100, 101]. On the other hand, the states B_s^0 and B_s^{0*} have not yet been seen directly, though their observation is probably imminent, in particular in LEP experiments. In the present context, the issue of whether or not the state $B_s^{0*}\bar{B}_s^{0*}$ is available in the decays of $\Upsilon(5S)$ is a very important one. As shown earlier, since $B_s^{0*}\bar{B}_s^{0*}$ is a $C = -1$ state, the modulation of its time evolution due to B^0–$\bar{B}^0$ mixing is markedly more pronounced than that of the even-charge conjugation states such as $B_s^0\bar{B}_s^{0*}$. In a number of studies, which we review in this report, the assumption of a large branching ratio for the decay of the $\Upsilon(5S)$ into the $B_s^{0*}\bar{B}_s^{0*}$ state has been made. This is worth pointing out at the very outset, since, in the

absence of this decay mode, the required luminosity for an x_s measurement in a B-factory will be significantly higher than what is being presented. Hopefully, this issue will be settled in the ongoing experiments at CESR in favour of a significant branching ratio for the decay $\Upsilon(5S) \to B_s^{0*}\bar{B}_s^{0*}$.

7.1. Time evolution of odd- and even-charge conjugation states in $\Upsilon(5S)$ decays

As mentioned in the previous section, the beam spot in the asymmetric B-machine is too long to allow the measurements of the decay lengths of the two B mesons individually. Instead, the difference in the decay length of the two mesons projected along the beam direction, $\delta z = z_1 - z_2$, can be measured with an accuracy $\Delta(\delta z)$. The two decaying B mesons can be tagged in same-sign (BB) or opposite-sign ($B\bar{B}$) events, using dileptons for example. The measurement of x_s is derived from the event distributions with respect to δz. However, since the B-mesons have a non-zero momentum in the $\Upsilon(5S)$ rest frame, the difference in length δz cannot be identified directly with $\delta t = t_1 - t_2$. For the asymmetric machine, which has a boost factor $\beta\gamma$ from the centre-of-mass to the laboratory frame, one has instead the relation [89]

$$\frac{\delta t}{\tau} = \frac{\delta z}{\beta\gamma\gamma_{cm}c\tau} - \frac{\beta_{cm}}{\beta\tau}(t_1 + t_2)\cos\theta \tag{90}$$

where β_{cm} and γ_{cm} give the boost from the $\Upsilon(5S)$ frame to the B-meson frame, and θ is the angle between the z direction and the B momentum in the $\Upsilon(5S)$ rest frame. In general, since the masses of the various B-meson species produced in $\Upsilon(5S)$ decays are different, one should put a subscript on β_{cm} and γ_{cm} corresponding to each of them. The error in the first term is essentially determined by the resolution $\Delta(\delta z)$. For a given value of $\Delta(\delta z)$, a larger machine boost $\beta\gamma$ reduces this error. The second term gives a systematic uncertainty in δt. The average value of this term is zero, and its standard deviation can be obtained from the average value of $|\cos\theta|$

$$\left(\frac{\Delta(\delta t)}{\tau}\right)_{syst} \simeq 2\langle|\cos\theta|\rangle\frac{\beta_{cm}}{\beta}. \tag{91}$$

The average value $\langle|\cos\theta|\rangle$ depends on the production process; it has been estimated that its value lies somewhere between $2/\pi$ and $1/2$ [85]. To minimize this error one needs a large value of the machine boost β and a small value of β_{cm}.

To get the signal in the same-sign and opposite-sign dilepton states, one has to assume the decay branching ratio of the $\Upsilon(5S)$ into $(C = +1)$ and $(C = -1)$ final states with definite flavours. There could be as many as nine different final states in the decays $\Upsilon(5S) \to B_1\bar{B}_2$, including the 0^- and 1^- B mesons but not entertaining the possibility of additional pion production. Since estimating the branching ratio is a model-dependent enterprise and many parameters are needed, it is difficult to get a sharp profile of the oscillation patterns in the decays of $\Upsilon(5S)$. However, it is not essential to know all these branching ratios individually. The point is that, as far as the time-evolution of the final states is concerned, one needs only the charge-conjugation quantum number ($C = +1$ or -1), and the same-sign (BB) or opposite-sign ($B\bar{B}$) nature of the final states. Following Le Diberder [102], we write this evolution as

$$F_n^C(t_1, t_2) = \frac{1}{N_n^C}e^{-(t_1+t_2)}(1 + n\cos[x(t_1 + Ct_2)] \tag{92}$$

where the normalization N_n^C depends on x, n and C, and is given by

$$N_n^C = 1 + n(1 - x^2C)/(1 + x)^2. \tag{93}$$

With the convention $n = -1(+1)$ for the $B\bar{B}(B\bar{B})$ state, one has $N_{-1}^{\pm 1} = 0$ and $N_{+1}^{\pm 1} = 1$ for the $B_u^+B_u^-$ final state. This implies that, concentrating on the same-sign states ($B\bar{B}$ and $\bar{B}\bar{B}$), only the following cross sections are needed to determine the range of x_s that can be measured at an asymmetric B-factory:

(i) $N_{-1}^{-1}(x_d)$: cross section for $e^+e^- \to \Upsilon(5S) \to B_d^0X$ $(C = -1)$
(ii) $N_{-1}^{+1}(x_d)$: cross section for $e^+e^- \to \Upsilon(5S) \to B_d^0X$ $(C = +1)$
(iii) $N_{-1}^{-1}(x_s)$: cross section for $e^+e^- \to \Upsilon(5S) \to B_s^0X$ $(C = -1)$
(iv) $N_{-1}^{+1}(x_s)$: cross section for $e^+e^- \to \Upsilon(5S) \to B_s^0X$ $(C = +1)$.

The measurements of these four cross sections must precede x_s measurements and should be the first order in priority after the masses for the B_s-mesons have been determined. In addition to the above cross sections and x_d (equation (33)), one needs to know $\Delta(\delta z)$, which depends on the vertex detector resolution, the Lorentz boost factor $\beta\gamma$ (i.e. the choice of beam energies), and the B-meson boost parameters, $(\beta\gamma)_{cm}$. Knowing (or assuming) these quantities, one could determine the needed luminosity for a given x_s and the precision on this quantitity $\Delta x_s/x_s$. In the rest of this section we show the results of Monte Carlo studies, taken from the KEK B-Physics Task Force report [87], the CESR B-factory proposal [85], the SLAC asymmetric B-factory report [86] and the DESY asymmetric B-factory report [88], reflecting their assumptions about the cross sections, proper-time resolution, and the possible choices of the asymmetric beam energies to estimate the luminosity required for measuring x_s with the error $\Delta x_s/x_s$. We also show the results of a semi-analytic analysis by Le Diberder [102].

7.2. The KEK simulation for the measurements of x_s in $\Upsilon(5S)$ decays

The KEK study is based on an analysis of same-sign dilepton events, assuming an integrated luminosity of 10 fb^{-1}, corresponding to $N = 2.7 \times 10^6$ $\Upsilon(5S)$ events, and a vertex resolution $\sqrt{\langle\sigma^2\rangle} \simeq 73$ μm. For this study two choices of the asymmetric beam energies have been made (2.5×11.8 and 3.7×8.0 GeV). Moreover, it was determined that the background to the same-sign dilepton state from the e^+e^- continuum is negligible and about 10% from the secondary decays $B \to D \to \ell$, if the lepton energy is taken to be in excess of 1.5 GeV in the $\Upsilon(5S)$ rest frame. In view of this, only the four final states discussed above were generated. The branching ratios for the decays of $\Upsilon(5S)$ in the required final states were taken from [101]. This then leads to the theoretical distribution

$$f(\delta t) = 0.28 f_{odd}^{\pm\pm}(x_d, \delta t) + 0.22 f_{even}^{\pm\pm}(x_d, \delta t) + 0.47 f_{odd}^{\pm\pm}(x_s, \delta t) + 0.03 f_{even}^{\pm\pm}(x_s, \delta t). \tag{94}$$

The functions defined as $f_{odd}^{\pm\pm}(x_i, \delta t)$ and $f_{even}^{\pm\pm}(x_i, \delta t)$ in the KEK study are related to the functions $F_{n=-1}^{C=\pm 1}$, defined earlier, after the required integration. The simulated δt distribution has been fitted to a function which was obtained by convoluting the $f(\delta t)$ distribution with an assumed resolution function for the vertex measurements. To take into account the non-Gaussian tail of the vertex resolution, two Gaussian functions with different widths were used:

$$F(\delta t, \sigma_1, \sigma_2) = \int \left(a \exp\left(-\frac{(\delta t - \delta t')^2}{2\sigma_1^2} \right) + b \exp\left(-\frac{(\delta t - \delta t')^2}{2\sigma_2^2} \right) \right) f(\delta t')\, d(\delta t'). \tag{95}$$

A maximum likelihood analysis was then made of the above function with x_s as a free parameter, taken to be $x_s = 2, 3, 4, 6, 8$. The result of this fitting procedure is shown in figure 16, where the performance of the x_s measurements for the two assumed beam energy options is shown. In this figure, the x_s value from the fit is plotted against the input x_s value in the event generator and the errors shown correspond to 90% CL. It can be seen that, given the parameters of the KEK study, x_s can be determined up to $\sim$ 3–4 for the (3.7×8.0) GeV option, and up to $\sim$ 6–7 for the more asymmetric beam choice (2.5×11.8) GeV. We remark that the first of the accessible x_s values in the KEK study is close to the lower bound obtained by the presently available time integrated measurements, from which one obtains $x_s/x_d > 5$ at 90% CL, giving $x_s > 3.4$ for $x_d = 0.67$ [43]. However, as discussed earlier, this lower bound on x_s is not model independent. With the increase in the LEP luminosity, and making use of the flavour correlation due to the production and decays of the $B_s^0/\bar{B}_s^0$ mesons discussed in the previous section, one expects that LEP experiments can determine the time-integrated measure χ_s in a much less model-dependent way. This would allow a sensitivity up to about $x_s = 4$. With $O(10^7)$ Z^0 decays, expected to be accumulated in the not too distant future, the experiments at LEP are well poised to reach the x_s values in the higher x_s accessible range in the KEK study. In order to gain sensitivity for larger values of x_s, one will have to improve the vertex detector resolution, as well as aim for a much higher integrated luminosity. This is quantified below based on the simulations of the DESY and SLAC groups and the analysis in [102].

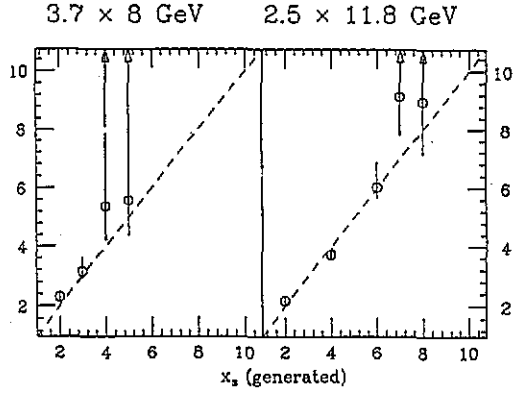

Figure 16. The relation between the input x_s value in the event generator and the x_s value obtained from the fit in the KEK study for an asymmetric B-factory at $\Upsilon(5S)$. The assumed beam energies are indicated and other parameters are discussed in the text (from [87]).

7.3. The Cornell simulation for the measurements of x_s in $\Upsilon(5S)$ decays

The Cornell Monte Carlo study in the context of an asymmetric B-factory [85] follows closely the analysis reported above for the KEK case, in which the distribution in δz using dileptons was simulated. Based on an earlier CUSB study [101], the following branching ratios were assumed:

$$\begin{aligned} &BR(\Upsilon(5S) \to B_s X(C = -1)) = 31\% \\ &BR(\Upsilon(5S) \to B_d X(C = -1)) = 18\% \\ &BR(\Upsilon(5S) \to B_s X(C = +1)) = BR(\Upsilon(5S) \to B_d X(C = +1)) = 17\%. \end{aligned} \tag{96}$$

A b cross section of 0.27 nb, an (e+μ) semileptonic branching ratio of 20%, an acceptance of 22%, and $x_d = 0.7$ were used to construct the time evolution of like-sign dileptons. The p_T^ℓ cutoff was taken to be 1.4 GeV to remove the $b \to c \to \ell^\pm + X$ secondaries. The resulting distribution was convoluted with an (assumed) Gaussian function with a time width corresponding to 80 μm in δz, for a (3.7 × 8.0) GeV collider. The 80 μm was the resolution obtained from an analysis in which the response of a detector with 2 cm radius beam pipe was simulated. To convert this function into a histogram for fitting, the bin width was taken to be one-fourth of the resolution and an additional smearing randomized the bin heights according to the Poisson error of the central value for that bin. This led to the conclusion that the maximum x_s obtainable with these parameters and an integrated luminosity of 30 fb^{-1} is around $x_s^{max} = 5$–6, in line with the KEK study conclusions. The same-sign dilepton plots for $x_s = 5$ from this study, assuming a resolution of $\delta z = 80$ μm and $\delta z = 20$ μm (corresponding to a perfect spatial resolution detector) are shown in figure 17. It has been argued that, in order to be sensitive to values up to $x_s = 10$, one needs [85]

$$(\Delta(\delta z))^2 \leqslant (\beta\gamma(390\ \mu\text{m}))^2 \left(\left(\frac{2\pi}{30} \right)^2 - \left(\frac{0.09}{\beta} \right)^2 \right) \tag{97}$$

giving an approximate relationship between the boost and the spatial resolution needed to measure $x_s = 10$ with a 4σ precision. Using $E_{high} = 10$ GeV gives $\beta = 0.54$ and $\beta\gamma = 0.64$, which implies a resolution of 32 μm on δz. For a more realistic resolution, one would have to have an asymmetric B-factory with $E_{high} = 14$ GeV.

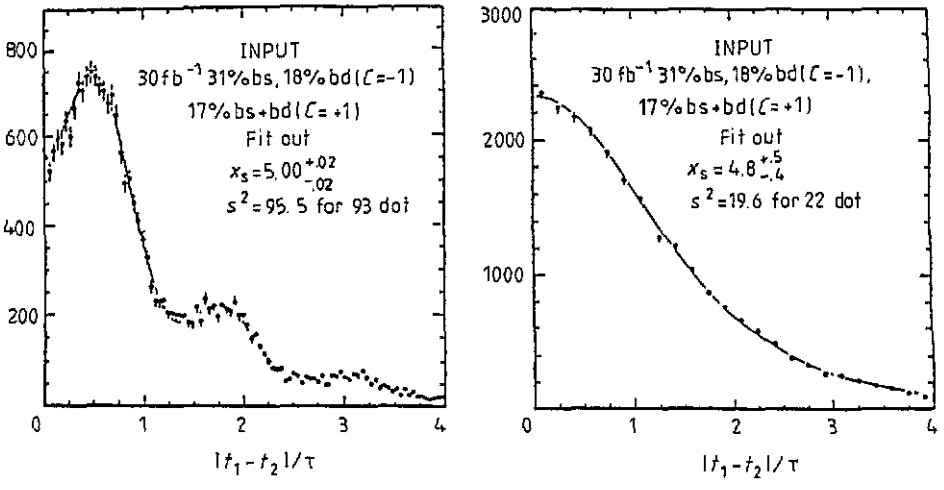

Figure 17. Like-sign lepton time evolution (B_s plus background). (*a*) Time evolution for mixture of B_s and B_d states assumed in the Cornell study with $x_s = 5$ and smeared with a Gaussian error of $\Delta(\delta z) = 20$ μm. Points are simulated data corresponding to a luminosity of 30 fb^{-1}, and the full curve is a fit to the data. (*b*) Same as (*a*) but for $\Delta(\delta z) = 80$ μm (from [85]).

7.4. The SLAC analysis for the measurements of x_s in $\Upsilon(5S)$ decays

The final state used in the SLAC analysis for x_s measurements at an asymmetric B-factory is again inclusive dileptons, with emphasis on the same-sign events, resulting from the decay of the $\Upsilon(5S)$ into $C = -1$ $B_s^0\bar{B}_s^0$ and $B_s^{0*}\bar{B}_s^{0*}$ states, mixing, and subsequent semileptonic decays. The decay rates of all the B mesons are assumed to have the same value, giving a lifetime 1.1 ps. The efficiency and semileptonic branching ratios assumed dictate that about 1% of the $\Upsilon(5S)$ decays will be available for further analysis. The branching ratios of the $\Upsilon(5S)$ decays into the various neutral $B\bar{B}$ states assumed in the SLAC analysis are given in table 10, where the branching ratios in the charged $B_u^+B_u^-$ states have been taken to be equal to their $B_d^0\bar{B}_d^0$ counterparts.

Table 10. Assumed branching fraction of $\Upsilon(5S)$ to neutral B-pairs for the SLAC asymmetric B-factory study.

Decay	Fraction	Mixing	C parity
$B_d^{0*}\bar{B}_d^{0*}$	0.11	x_d	1
$B_s^{0*}\bar{B}_s^{0*}$	0.26	x_s	1
$B_d^0\bar{B}_d^{0*}$	0.15	x_d	+1
$B_s^0\bar{B}_s^{0*}$	0.02	x_s	+1
$B_u^0\bar{B}_d^0$	0.07	x_d	1
$B_s^0\bar{B}_s^0$	0.05	x_s	1

Having fixed the branching ratios, the SLAC study aimed at determining the maximum value of x_s measurable, x_s^{max}, assuming a definite luminosity on the $\Upsilon(5S)$ resonance for a given accuracy on the vertex resolution $\Delta(\delta z)/\langle\delta z\rangle$. Seven values were chosen in their study: 0.667, 0.444, 0.333, 0.250, 0.182, 0.143, and 0.125. The assumed resolutions can be converted as requirements on the Lorentz boost factors $\beta\gamma$ (i.e. beam energies) and the vertex resolution. For example, to achieve $\Delta(\delta z)/\langle\delta z\rangle = 0.125$, a high boost machine (2.2 × 12.5) GeV and a vertex resolution of 40 μm are needed. In the analysis, no Monte Carlo simulation was undertaken. Instead, the expected theoretical distributions were smeared with a Gaussian having a definite resolution and the background was assumed to be exponentially distributed in time. The resulting estimates of x_s^{max} as a function of $\delta z/\Delta(\delta z)$ for an assumed luminosity 3 fb^{-1} are shown in figure 18, and for an integrated luminosity of 30 fb^{-1} in figure 19. The figures also show a least-squares fit to a straight line. The fitted functions for x_s^{max} and their χ^2 for five degrees of freedom were determined to be [86]:

$$L = 3 \text{ fb}^{-1}: \qquad x_s^{max} = 0.06 + 2.29\frac{\langle\delta z\rangle}{\Delta(\delta z)} \qquad \chi^2 = 2.8$$

$$L = 30 \text{ fb}^{-1}: \qquad x_s^{max} = 0.08 + 3.00\frac{\langle\delta z\rangle}{\Delta(\delta z)} \qquad \chi^2 = 3.3. \tag{98}$$

This gives a linear dependence of x_s^{max} on $\langle\delta z\rangle/\Delta(\delta z)$. Increasing the luminosity increases the slope of the relation between these two quantities but the intercept is almost independent of this. The origin of the constant term can be traced back to the systematic error discussed earlier.

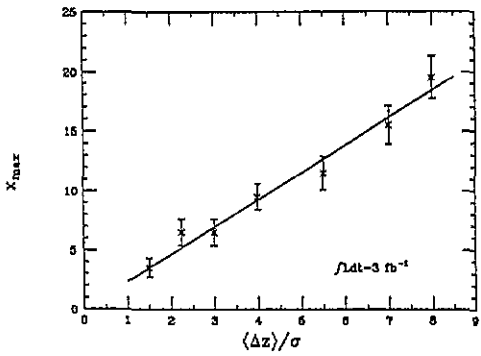

Figure 18. The maximum value of x_s reachable in the SLAC study as a function of the vertex resolution parameter, $\langle \delta z \rangle / \Delta(\delta z)$. The error bars correspond to an assumed integrated luminosity of 3 fb^{-1}, and the straight line corresponds to the minimum χ^2 fit described in the text (from [86]).

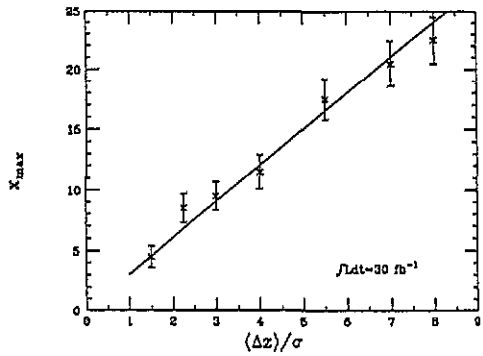

Figure 19. Same as figure 18 but for an assumed 30 fb^{-1} integrated luminosity (from [86]).

7.5. The DESY simulation for the measurements of x_s in $\Upsilon(5S)$ decays

The simulation for the accessibility of x_s at the DESY asymmetric B-factory proposal is also based on an analysis of same-sign dilepton events in the decay $\Upsilon(5S) \to B^0\bar{B}^0 \to \ell^\pm\ell^\pm X$. However, in this study a broader range of the beam energy options (and hence $\beta\gamma$ values) has been entertained, namely $\beta\gamma = 0.6, 0.8, 1.0$ and 1.2. For a given value of the $\beta\gamma$, one can determine the two beam energies, E_{low} and E_{high}, from the following formulae:

$$E_{low} = M/2\left(\sqrt{1+(\beta\gamma)^2} - \beta\gamma\right)$$
$$E_{high} = \beta\gamma M + E_{low} \tag{99}$$

where $M = M(\Upsilon(5S)) = 10.860$ GeV. With the assumed values of $\beta\gamma$, the energies E_{low} and E_{high} are given in table 11. The masses for the B_s^0 and B_s^{0*} were taken to be $m(B_s^0) = 5.377$ GeV and $m(B_s^{0*}) = 5.427$ GeV. The branching ratios for the decays of the $\Upsilon(5S)$ to pairs of neutral B mesons were taken from Byers and Huang [100]. The relative rates for the neutral B mesons are given in table 12. The absolute branching ratios were obtained by using the value $BR(\Upsilon(5S) \to B_s^*\bar{B}_s^*) = 0.15$. Moreover, a 100% branching ratio for the decay $B_s^* \to B_s + \gamma$ and a semileptonic branching ratio $BR(B_s^0 \to \ell^\pm X) = 0.12$ were assumed. The resolution in the distance on the z-axis was determined to be $\Delta(\delta z) = 70$ μm, using the intercept of one lepton track on the z-axis. This resolution was found to be considerably improved if an angular acceptance cut on each lepton in the range $30° < \theta < 150°$ was applied, yielding $\Delta(\delta z) = 38$ μm. This is approximately a factor of two better than the resolution assumed in the KEK and Cornell studies. In addition, three data sets with integrated luminosities of 5, 20, and 200 fb^{-1} were assumed to estimate the accessible x_s^{max}.

The x_s analysis for the DESY proposal follows very similar lines to those described earlier for the KEK study, except that the theoretical distribution $f(\delta t)$ in the DESY study has been convoluted with a single Gaussian with the width $\Delta(\delta t)/\tau_B = 0.1$. This will not reproduce the non-Gaussian width of the δt resolution; however, except for very large x_s

Table 11. Assumed values of $\beta\gamma$ and beam energies for the asymmetric B-factory study at DESY (from [88]).

$\beta\gamma$	E_{low}	E_{high}
0.6	3.074	9.590
0.8	2.610	11.298
1.0	2.249	13.109
1.2	1.966	14.998

Table 12. Assumed branching fraction of $\Upsilon(5S)$ to neutral B-pairs for the DESY asymmetric B-factory study.

Decay	Fraction	Mixing	C parity
$B_d^{0*}\bar{B}_d^{0*}$	0.436	x_d	1
$B_s^{0*}\bar{B}_s^{0*}$	0.292	x_s	1
$B_d^0\bar{B}_d^{0*}$	0.179	x_d	+1
$B_s^0\bar{B}_s^{0*}$	0.078	x_s	+1
$B_d^0\bar{B}_d^0$	0.013	x_d	1
$B_s^0\bar{B}_s^0$	0.002	x_s	1

values, it should not overly compromise the accuracy of the calculations. With a luminosity of 20 fb^{-1}, one expects 5.4×10^6 $\Upsilon(5S)$ decays, which, with the assumed decay branching ratios and acceptance, have been estimated to lead to $\sim$ 5000 dilepton events from the $B_s^0\bar{B}_s^0$ decays. An analysis of the same-sign dilepton data sample for $\beta\gamma = 1.0$, $x_s = 15$ and 20 fb^{-1} integrated luminosity is shown in figure 20, together with the background. The fit result giving $x_s = 14.91 \pm 1.55$ is also shown, in agreement with the input value. The DESY study is more optimistic than the one by the KEK group, where the value $x_s = 6$ was found to be at the border of measurability. The reason for this markedly improved performance anticipated in the DESY analysis lies in a product of assumed improvements, namely in the vertex resolution, a larger $\beta\gamma$ value implying a more asymmetric machine, and a data sample based on 20 fb^{-1} compared with 10 fb^{-1}, used in the KEK analysis.

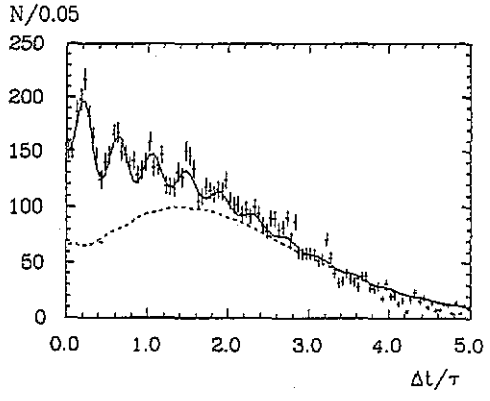

Figure 20. $\delta t/\tau_B$ distribution of same-sign leptons for $x_s = 15$ and a data set of 20 fb^{-1} from $\Upsilon(5S)$ decays in an asymmetric B-factory. The full curve represents the fit result, whereas the broken curve is the background not coming from B_s^0–$\bar{B}_s^0$ mixing (from [88]).

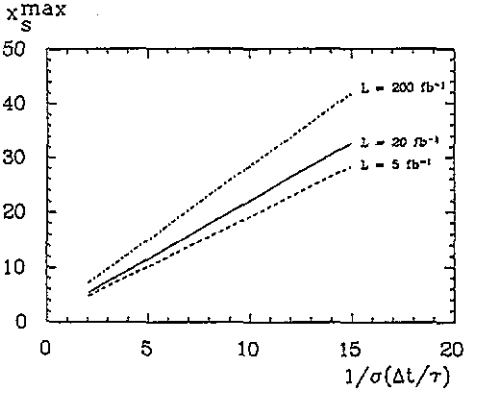

Figure 21. Maximum reachable value of x_s at three standard deviation statistical accuracy as a function of the inverse proper-time resolution at an asymmetric B-factory. The assumed values of the integrated luminosity at the $\Upsilon(5S)$ are indicated (from [88]).

In the DESY simulation to determine x_s^{max}, the luminosity of the machine, the resolution of the vertex detector, and the beam energies ($\beta\gamma$) were varied. The three assumed values for the luminosity and the $\beta\gamma$ factor have already been given above. The criterion of measurability was set at the 3σ level, and this was used to determine x_s^{max} by the χ^2 fit. As in the SLAC study, the maximum reachable x_s followed a straight line when plotted as a function of the resolution $\Delta(\delta t)/\tau_B$, with other parameters fixed. This is shown in figure 21 for the three set of assumed luminosities. This states that, with a data set of 20 fb^{-1}, a resolution of $\Delta(\delta z) = 40$ μm, and a boost of $\beta\gamma = 1.0$, one can reach an x_s value as high as 20 at 3σ level. From this figure one can work out a relation between the integrated luminosity and resolution for a fixed value of x_s. The resulting distributions for $x_s = 10, 15, 20, 25$ are shown in figure 22. This figure underlines the importance of improving the resolution in reaching out for large x_s values. Finally, the spatial resolution $\Delta(\delta z)$ was found not to change significantly for the four assumed values of $\beta\gamma = 0.6, 0.8, 1.0, 1.2$. Hence, the resolution $\Delta(\delta t)/\tau_B$ decreases as the inverse of $\beta\gamma$. Putting all these factors together one arrives at figure 23, where the relative luminosity needed to measure $x_s = 15$ at 3σ as a function of the boost factor $\beta\gamma$ is shown.

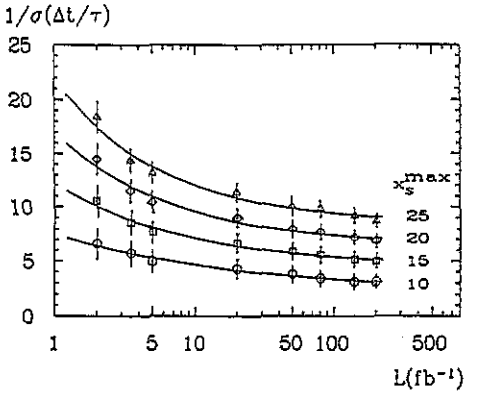

Figure 22. Inverse proper-time resolution as a function of the integrated luminosity for the indicated values of x_s^{max} reachable in an asymmetric B-factory at the $\Upsilon(5S)$ (from [88]).

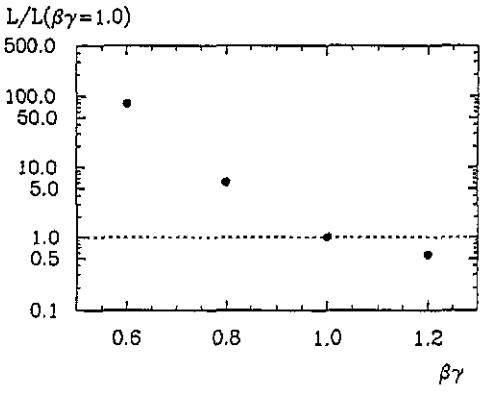

Figure 23. Relative luminosity needed to measure $x_s = 15$ with three standard deviation accuracy as a function of the boost $\beta\gamma$ for an asymmetric B-factory at the $\Upsilon(5S)$. The luminosity for $\beta\gamma = 1.0$ is normalized to 1 (from [88]).

The role of the proper-time resolution, and hence the luminosity requirements, in determining Δx_s has also been quantified by Le Diberder [102]. For a good vertex resolution $\Delta(\delta t)/\tau_B$ (say, $\Delta(\delta t)/\tau_B \leqslant 0.2$) and the presently allowed x_s values, his approach gives the following behaviour for the x_s resolution

$$\Delta x_s \propto \exp(1/2(\Delta(\delta t)/\tau_B)^2(x_s^2 + 1/2)). \tag{100}$$

In the intermediate range, $0.2 < \Delta(\delta t)/\tau_B < 0.3$, Δx_s has the form $\Delta x_s \sim \exp(\Delta(\delta t)/\tau_B x_s)$. In any case, the product $(\Delta(\delta t)/\tau_B)x_s$ determines the x_s resolution, as also discussed in the previous section. The correlation between Δx_s and $\Delta(\delta t)/\tau_B$ in this study is rather close to those in the SLAC and DESY studies. Because of the indicated dependence of Δx_s on $\Delta(\delta t)/\tau_B$ and x_s, the Δx_s dependence on x_s more or less mimics the dependence of $\Delta(\delta t)/\tau_B$.

For an experimental setup geared to the goal of an x_s measurement in $\Upsilon(5S)$ decays, it is preferable to have a larger asymmetry in the beam energies, E_{low} and E_{high}. This large asymmetry in the beam energies is not required for an $\Upsilon(4S)$ machine, built with the principal focus on *CP* violation measurements. In particular, it has been shown in a detector Monte Carlo simulation by the SLAC group [86] that the precision with which one can measure *CP* violation in the B_d system, exemplified by the precision on the phase angle $\sin 2\beta$, does not vary significantly for boosts in the range $\beta\gamma = 0.43$ and $\beta\gamma = 1.0$, with a beampipe radius in the range of 1 to 2 cm. So, as far as *CP* violation studies at the $\Upsilon(4S)$ are concerned, there is no overriding interest in having very asymmetric beams. Whether the requirements of *CP* violation and x_s measurements represent two distinct new machines or whether it will be possible to compensate a smaller value for the $\beta\gamma$ factor at $\Upsilon(5S)$ by significantly improving the vertex resolution, and hence be within the desired range of the $\beta\gamma$ values for the $\Upsilon(4S)$ machine, is an important issue in this field. It deserves further research and development work.

We conclude this section by reiterating the conclusions of all of the above studies, put succinctly in the DESY proposal: *Only a high boost value ($\beta\gamma \geqslant 1.0$) and good vertex resolution ($\Delta(\delta z) \leqslant 40\ \mu m$) can guarantee significant measurements, if x_s is large* [88].

8. Prospects for x_s measurements in ep collisions at HERA

8.1. Charm and bottom physics at HERA

The charm and bottom quark cross sections at the ep collider HERA have been estimated to be O(1 μb) and O(10 nb), respectively. With an integrated luminosity of $\sim 100\ pb^{-1}$ per year, one would have $O(10^6)$ $ep \rightarrow b\bar{b}X$ and $O(10^8)$ $ep \rightarrow c\bar{c}X$ events. This puts the bottom cross section at HERA comparable with the corresponding cross section at the Z^0 peak at LEP and SLC. The charm cross section at HERA is, however, a factor of ~ 200 higher than at LEP/SLC. This provides both an opportunity to undertake precision charm physics at HERA, as well as a substantially more difficult background to deal with in precision studies of bottom physics.

A few remarks about the heavy-quark event topology at HERA are in order. We note that the cross sections for charm- and bottom-quark production at HERA are dominated by the NC process $\gamma g \rightarrow Q\bar{Q}$ at $Q^2 \simeq 0$ (real photoproduction). As a consequence the scattered electron in $ep \rightarrow eQ\bar{Q}X$ is usually lost in the beam pipe. It is not too difficult to imagine that the most energetic heavy hadrons are in the proton direction ($\theta_Q = \pi$ ($Q = c, b$)) due to the obviously larger Lorentz boost in this direction. However, there is also a (less enhanced) peak near $\theta_Q = 0$, i.e. when the heavy hadron is close to the electron beam direction. The simulated energy–angle profiles of the bottom hadron, the decay lepton from the semileptonic process $b \rightarrow c\ell^-\nu_\ell$, and the kaon from both the semileptonic and non-leptonic decays at HERA are shown in figure 24. In order to illustrate the effect of losses through the beam pipe, we also show the energy distributions with a beam pipe cut of 100 mrad. The resulting energy distributions are shown as shaded areas in figure 24. Note that the effect of the beam pipe cut is rather drastic on the energetic hadrons and leptons. We emphasize, in particular, the energetic nature of the bottom hadrons in figure 24, which shows that measurable cross sections at HERA are expected for the bottom hadrons having Lorentz boosts up to $\beta\gamma = 10$. Consequently, with a good vertex detector of the type being installed at the two HERA experiments, H1 and ZEUS, one can make use of the long decay lengths of the B hadrons.

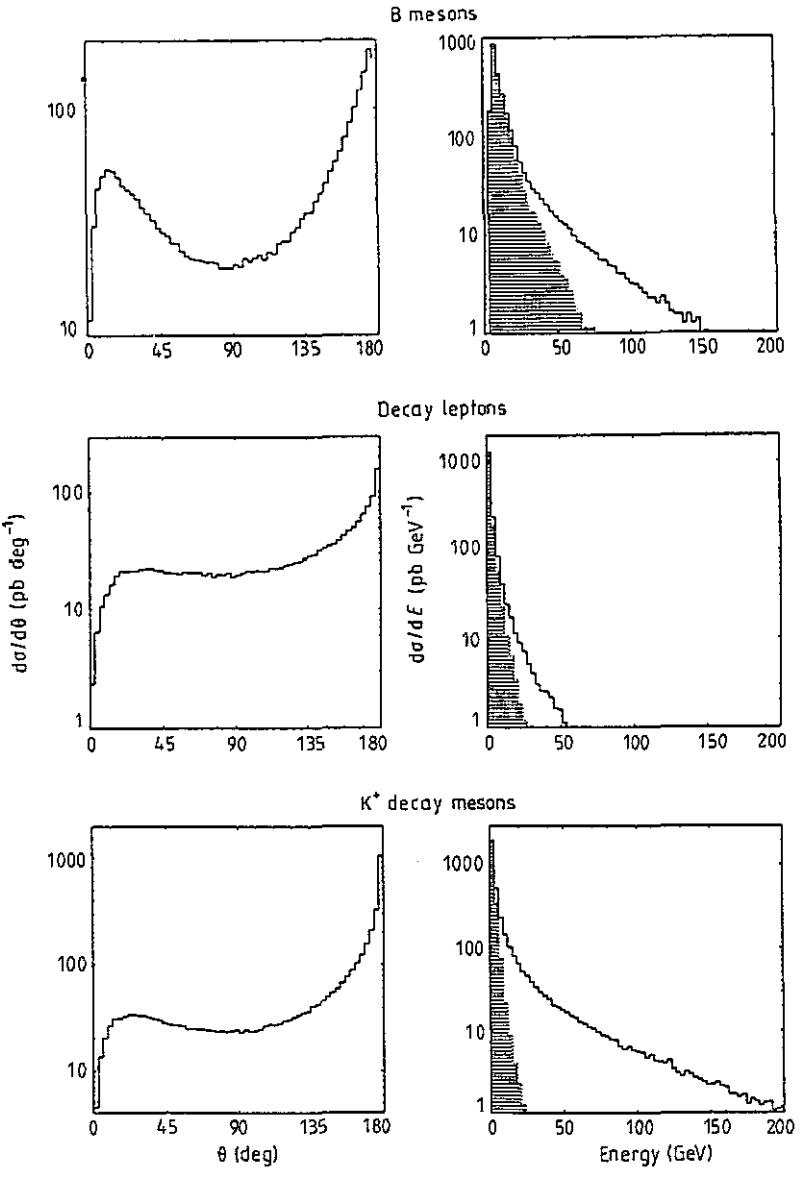

Figure 24. Energy and polar angle distributions for B mesons, the decay kaons and leptons produced in the process ep → $b\bar{b}X$ and subsequent decays of the bottom hadrons, calculated at HERA with $\sqrt{s} = 314$ GeV. The energy distributions resulting after imposing a beam pipe cut of 100 mrad are represented by the shaded areas (from [106]).

8.2. The dilepton final states in ep collisions at HERA

It has been shown in a number of Monte Carlo studies for HERA physics [103–105] that, by demanding a charged lepton in the final state (other than the scattered electron from the NC processes in ep collisions) and/or secondary vertices, the background from the usual DIS processes involving light quarks, ep → $q\bar{q}X$, can be very much reduced. However, since the charm cross section is approximately 100 times larger than the bottom cross

section at HERA, this background will survive the charged lepton and/or secondary vertices requirements. The dilepton final state is of interest for measuring both χ_s and x_s through the time-dependent yield of dileptons. Because of this we also concentrate on the inclusive dilepton final state at HERA

$$\begin{aligned} ep &\to e+ \underbrace{Q\bar{Q}}\, X \\ &\to \ell^{\pm}\ell^{\mp}X, \ell^{\pm}\ell^{\pm}X \qquad (Q = c, b, t; \ell = e, \mu) \end{aligned} \tag{101}$$

which formally has three leptons, but will be measured as a dilepton final state since the scattered e will be lost in most of the cases. In figure 25, we plot the cross sections at HERA for the dilepton events from the charm and bottom quarks as well as from the NC (light quarks) and CC processes, and $W^{\pm}g \to c\bar{s}, \bar{c} \to \ell^- X$. In fact, what is shown is $\sigma(p_T^{\ell} > p_T^{cut})$ where the cut-off p_T^{cut} refers to the p_T of the hardest lepton. It can be easily seen that the dominant background for the NC (light quarks) is already below the $c\bar{c}$ cross section for $p_T^{cut} > 0.4$ GeV and it falls below the $b\bar{b}$ cross section for $p_T^{cut} > 0.8$ GeV. The $b\bar{b}/c\bar{c}$ crossover occurs at around $p_T^{cut} = 1.2$ GeV. We remark that, even with a stringent cut-off $p_T^{cut} = 3$ GeV, one expects an inclusive dilepton sample of $\sim 1.5 \times 10^4$ events (with $b\bar{b}/c\bar{c}$ approximately in the ratio 2:1). Though this number will definitely be decreased by the hardware cut on the second lepton, we expect that it will still leave a sizeable number of dilepton events. Thus, for example, for $p_T^{\ell_1} \geqslant 3$ GeV, $p_T^{\ell_2} \geqslant 1$ GeV, one has ~ 10 pb and ~ 30 pb for the dilepton cross section from charm and bottom, respectively. This would give about ~ 1000 dileptons from the $c\bar{c}$ and ~ 3000 dileptons from the $b\bar{b}$ sample for an integrated luminosity of 100 pb^{-1}. The inclusive dilepton sample can be enriched in the prompt leptons ($b \to c\ell\nu_\ell$) from the $b\bar{b}$ production and decays by imposing an stringent cut-off p_T^{cut} on both leptons, the choice of which will be determined by the experimental conditions.

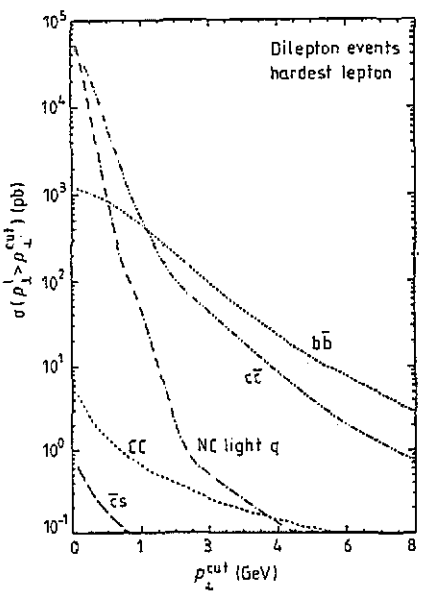

Figure 25. Integrated cross section for the process $ep \to (e, \nu_e)\ell\ell X$ as a function of a cut on the $p_\perp$ of the second hardest lepton for the neutral current processes $ep \to b\bar{b}X$ and $ep \to c\bar{c}X$, light quark + gluon and the charged-current (CC) processes at HERA, with $\sqrt{s} = 314$ GeV. The beam pipe cut is 100 mrad *(from [106])*.

Let us make a score card for the dileptons passing the above cuts at HERA. With the stated cuts this number is estimated to be ~ 4000 for an integrated luminosity of 100 pb^{-1}.

With the present world average of the mixing parameter: $\chi = 0.148 \pm 0.018$, we expect that a fraction $2\chi(1-\chi) \simeq 0.25$ of the dileptons from the $ep \to b\bar{b}X$ sample will consist of same-sign dileptons. This would then yield $750\ell^{\pm}\ell^{\pm}X$ and $2250\ell^{+}\ell^{-}X$ events per 100 pb^{-1} luminosity. We estimate that roughly half of the same-sign dileptons will be due to B_s^0–$\bar{B}_s^0$ mixing and the other half due to B_d^0–$\bar{B}_d^0$ mixing. On the other hand, the $\sim$ (1000) dileptons from the process $ep \to c\bar{c}X$ surviving the cuts are expected to be all of the opposite-sign variety. These can be efficiently discriminated against by using the isolation criterion discussed in [106], for example, resulting in a b-enriched opposite-sign dilepton data sample. This should allow an independent measurement of the time-integrated measure χ at HERA. It has been estimated in [106] that, for a 200 pb^{-1} data sample at HERA, it should be possible to measure χ with an accuracy $\Delta\chi/\chi = 0.07$, which compares favourably with the present measurements, $\chi = 0.148 \pm 0.018$. However, the theoretical uncertainty on χ_s is bigger since, as we have pointed out earlier, the ratio $R(\pm\pm/+-)$ is a measure of $\chi = P_d\chi_d + P_s\chi_s$. Extracting χ_s from a measurement of χ requires the values of P_d and P_s. The uncertainty on P_s is at least 25%. So, the error on χ_s will be dominated by theoretical uncertainty on P_s.

8.3. Time-dependent measurements of B^0–$\bar{B}^0$ mixing at HERA

The oscillation lengths due to B_d^0–$\bar{B}_d^0$ and B_s^0–$\bar{B}_s^0$ mixings can be obtained by convoluting the time-dependent mixing probabilities defined earlier with the energy distribution of the B-hadrons. These were calculated in [106] for the process $ep \to eb\bar{b}X$ using the Monte Carlo programme AROMA [104] at $\sqrt{s} = 314$ GeV. The decay length distributions $d\sigma(ep \to eb\bar{b}X \to B_sX)/dl$ are shown in figure 26 for ($B_s^0 \to B_s^0$, $x_s = 10.0$), and in figure 27 for ($B_s^0 \to \bar{B}_s^0$, $x_s = 10.0$). They have been obtained by fixing the flavour of the other $\bar{b}$-quark in the Monte Carlo event generator. This can be done in an experiment, for example, by demanding $\bar{b} \to l^+X$ in the jet recoiling against the B hadron whose track lengths are being measured. The oscillation lengths are obtained by projecting out the B hadrons in the assumed energy bins indicated on the figures. This projection is essential, since otherwise the oscillations (which depend linearly on E_B) will be smeared by the E_B distributions and will not be discernible. It should be stated here that the cross sections shown in figures 28 and 29 do not take any tagging efficiencies into account.

We note that, as far as the 'right-sign' distributions $d\sigma(ep \to BX)/dl$ with $B \to B$ are concerned, all of them, with the exception of the $B_s \to B_s$ case, are almost exponential in the visible cross section region. Thus, one could parametrize the background in the limit case $x = 0$ and subtract it from the inclusive distribution $d\sigma(ep \to BX)/dl$ for the 'right-sign' transition $B \to B$. The resulting signals showing clear oscillations for the $B_s \to B_s$ case are given in figure 28 for $x_s = 10$. It is shown in figure 29 that these oscillations are not washed out if one convolutes the decay length distribution with a vertex detector resolution of, say, $\sigma_V \sim 100$ μm, and furthermore takes into account the beam pipe acceptance cut of 100 mrad. Similar oscillation patterns can be calculated for the 'wrong-sign meson' $B_s^0 \to \bar{B}_s^0$.

The Monte Carlo studies shown in figures 26–29 give a fairly descriptive picture of a possible strategy for measuring x_s at HERA. The problems in x_s measurements at HERA are very similar to the ones encountered in the corresponding analysis at LEP. It is difficult at present to assess the accessible x_s^{max} at HERA as a function of the luminosity, since, as argued in the preceding sections, this depends very sensitively on the resolution in the proper time, $\Delta t/\tau_B$. This, in turn, cannot be ascertained unless one has a reliable estimator of the B-meson energy, for which a detailed detector-based Monte Carlo study is needed. If one insists on a complete reconstruction of a B_s meson, then one needs a prohibitively large

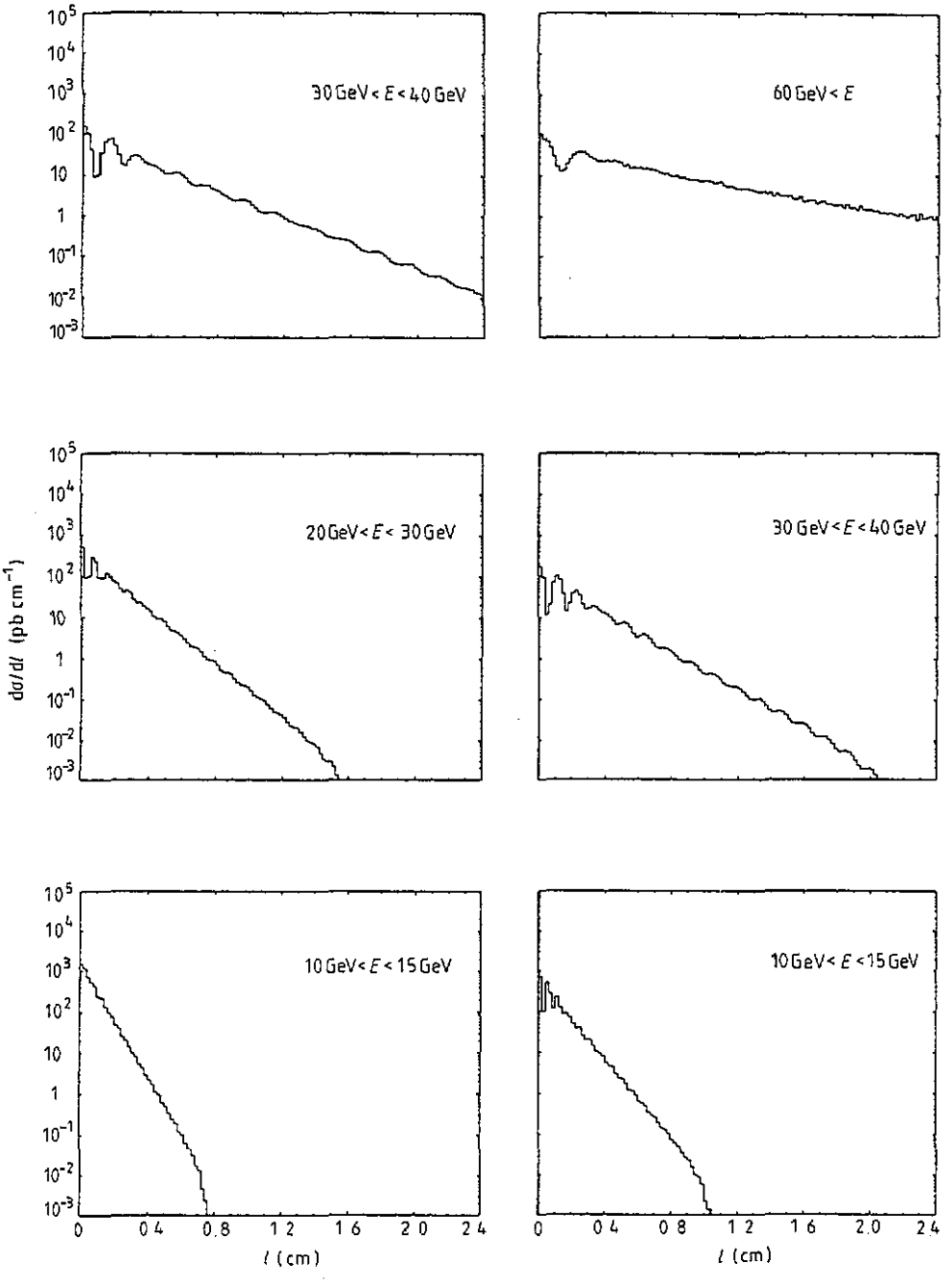

Figure 26. A Monte Carlo study of the decay length distributions, $d\sigma/dl$, for the 'right-sign B_s^0 meson' ($B_s^0 \to B_s^0$) at HERA with $x_s = 10$. The assumed B_s energy bins are indicated on the figures. Note that the B_s tagging efficiency is not included in the estimates of the cross sections (from [106]).

B hadron sample. Again, very likely, the b-quarks produced in the process $ep \to b\bar{b}X$ at HERA will show up most of the time as jets, and the b-jet axis can be used as a good measure

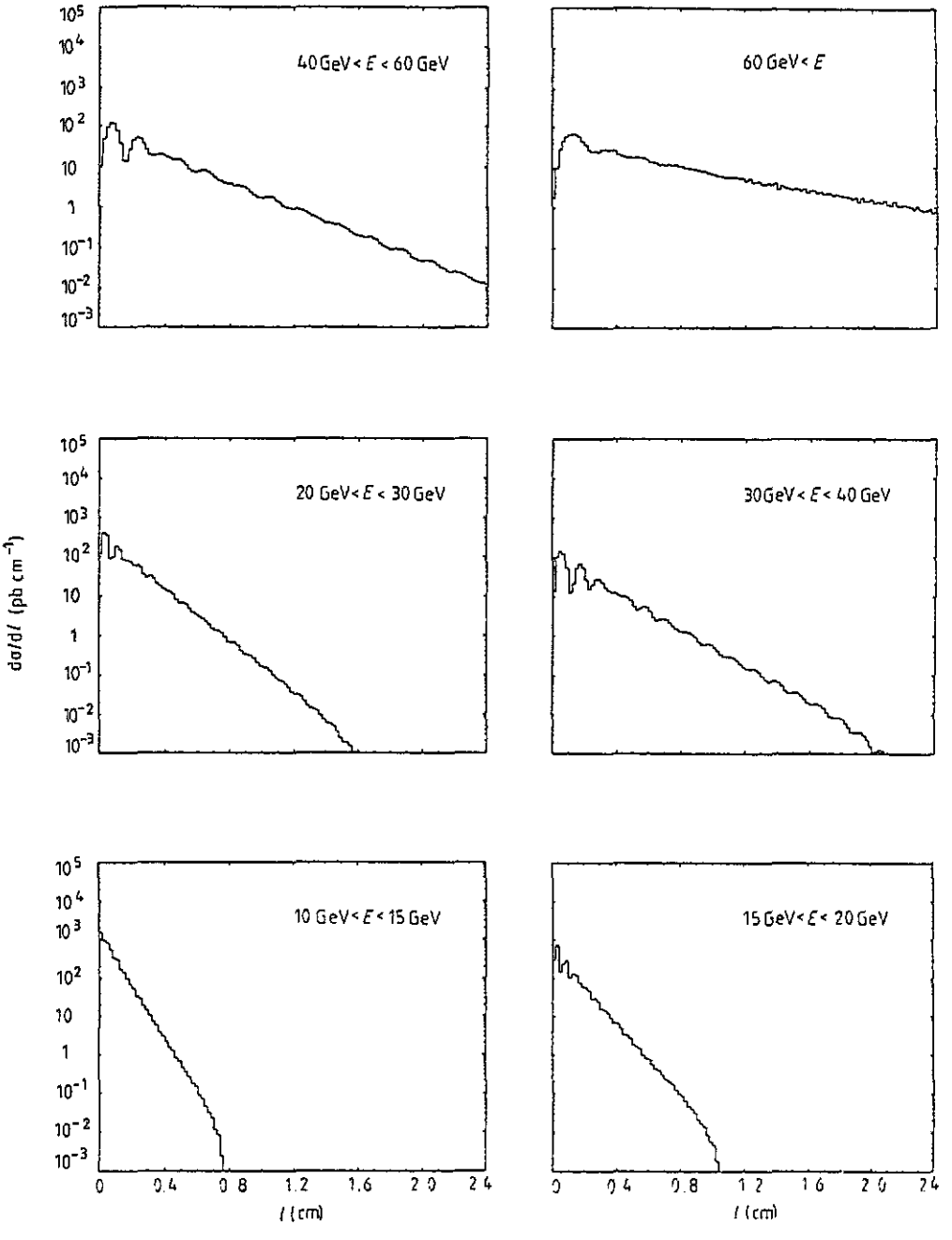

Figure 27. Same as figure 26 but for the 'wrong-sign B_s^0 meson', $B_s^0 \to \bar{B}_s^0$ (from [106]).

of the B hadron direction. One may use the azimuthal angular distribution to separate the b- and $\bar{b}$-jets. Assuming that the D_s meson could be reconstructed with a reasonable efficiency, one could tag on events satisfying a certain cut on the visible B-mass, from the charged lepton and the D_s decay products. Judging from similar efforts in the context of LEP, we

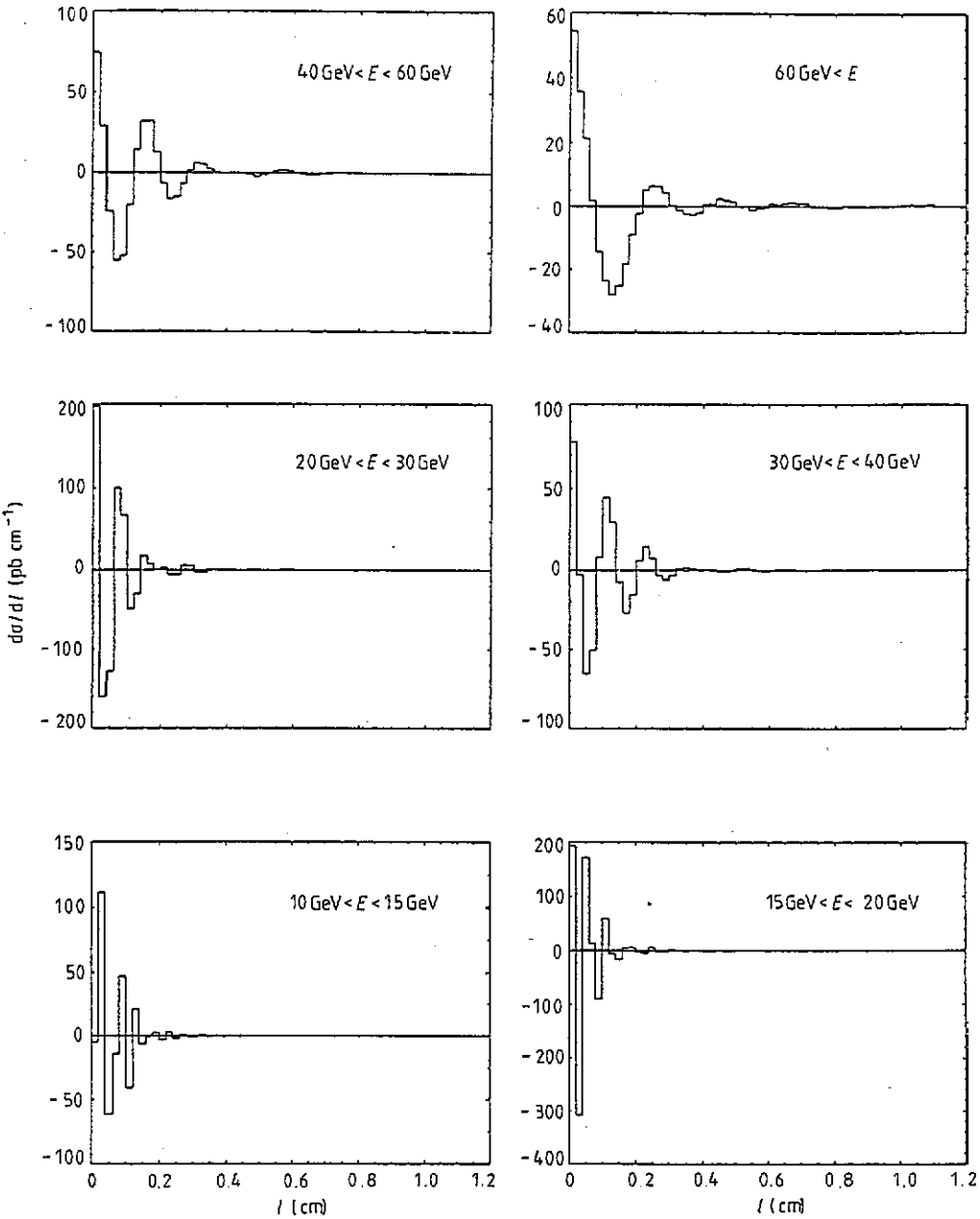

Figure 28. A Monte Carlo study of the B meson decay length distributions, $d\sigma/dl$, for the 'right-sign B_s^0 meson' ($B_s^0 \to B_s^0$) at HERA with $x_s = 10$, after subtracting an exponential background. The assumed B_s energy bins are indicated on the figures. Note that the B_s tagging efficiency is not included in the estimates of the cross sections (from [106]).

expect that, at the end of the day, one would come up with luminosity estimates at HERA very similar to those at LEP, namely that one would need $O(10^4)$ dilepton events to measure x_s with 10% accuracy if $x_s \leqslant 10$. This may require an integrated luminosity $\sim O(1\ \text{fb}^{-1})$

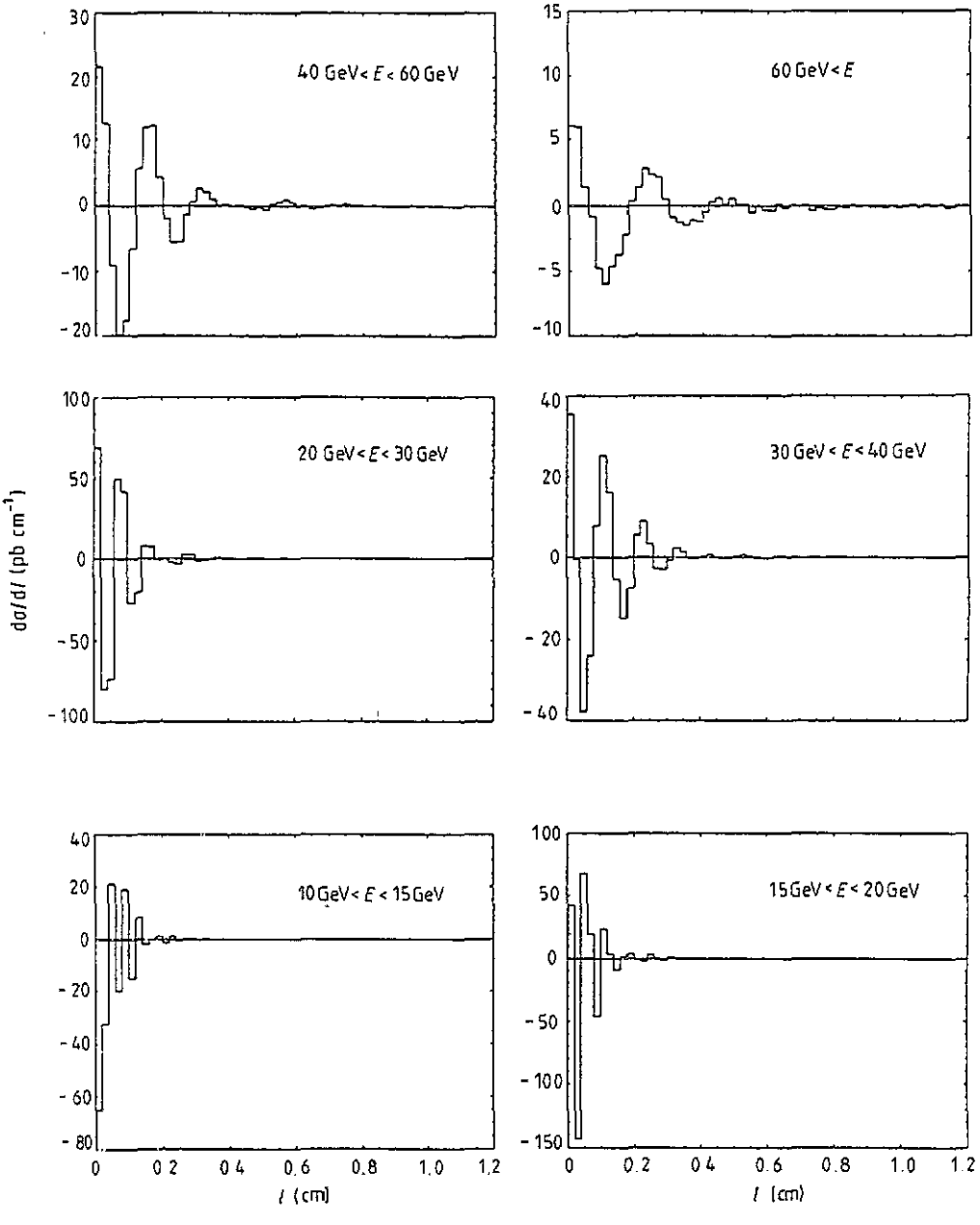

Figure 29. Same as figure 28 but taking additionally into account the vertex detector resolution, assumed to have a Gaussian form with $\sigma_V = 100$ μm (from [106]).

at HERA, vertex detectors having a good resolution, and a good detection efficiency for the D_s mesons to efficiently tag on the B_s meson. In our opinion, measuring x_s at HERA in the ep mode is a long-term goal!

However, one could attempt a fixed target experiment with the incident (800–1000 GeV) proton beam at HERA. In this mode, getting to an integrated luminosity of O(1 fb^{-1}) will be faster; furthermore the cross section/nucleon $\sigma(p + A \rightarrow BX)$ is expected to be a factor

O(3–5) larger, depending on the proton beam energy, than the corresponding cross section $\sigma(e+p \to BX)$. We understand that such a fixed target study with the HERA proton beams is being contemplated at DESY [107].

9. Prospects for x_s measurements in pp($\bar{p}$) collisions

Proton–antiproton collisions at the CERN SP$\bar{P}$S and the Fermilab Tevatron colliders have turned out to be very copious sources of B hadrons, with cross sections $\sigma(p\bar{p} \to B\bar{B}X)$ measured at around (10–20) and (50–100) μb, respectively. The large cross sections have enabled the determination of the time-integrated mixing parameter χ [79, 80], as already discussed in a preceding section. Since the CERN $p\bar{p}$ collider programme has been phased out, the only remaining possibility for doing B-physics with the currently available proton beams is at the Tevatron collider. However, as far as the measurement of x_s is concerned, the present experimental facilities at the Tevatron are not adequate. We note that a fixed-target B-physics proposal using the HERA proton beam (E_p = (800–1000) GeV) on a thin-tungsten target is in the offing [107]. In the future, both the large hadron collider (LHC) at CERN and the Superconducting Super Collider (SSC) in Texas will be very promising environments for doing precision B-physics due to the very large $b\bar{b}$ cross sections. There exists an expression of interest for a bottom collider detector at the SSC [108] and a proposal to do research and development for collider beauty physics at the LHC [109] (see also [110]). Likewise, a number of proposals for doing fixed target B-physics experiments using the LHC Carboni and the SSC proton beams [112, 113] are at hand. The primary interest of these experiments lies in studying *CP* violation in B decays. However, along the way one could also measure rare B decays and x_s, both of which constrain the CKM parameters and the unitarity triangle. In measuring x_s, as well as *CP* violation, it is imperative to have a micro-vertex detector to be able to discriminate between the primary (production) and secondary (decay) vertices. In addition, good lepton (electron and muon) identification, particle identification (for example, using RICH counters), and magnetic fields for charged-track analysis are all essential for B flavour-tagging. We shall assume that all the dedicated B experiments will have these capabilities and review the salient features of some proposals for measuring x_s with proton beams.

9.1. B hadron production cross section in hadron machines

The inclusive cross section $pp \to b + X$ as a function of the beam energy for the collider mode, and the cross section for $p + W \to B + X$ in the fixed-target mode using a tungsten target W (A = 184), estimated using the PYTHIA 5.3 Monte Carlo [114], are shown in figure 30. The fixed-target cross section has been calculated using a linear dependence on A. It is well appreciated that the heavy flavour hadro-production cross sections, in particular for charm and bottom hadrons, depend rather sensitively on the input gluon distribution, particularly the small-x behaviour. Since the gluon density is not known in this region, one has a substantial uncertainty in the rates. Also, due to the resummed higher-order QCD effects [115–117], the cross sections increase at higher energies, compared to the fixed-order perturbative QCD estimates. This can be seen in figure 31 due to Collins and Ellis, where the B hadron production cross section is calculated as a function of the CM energy, assuming an input gluon density with a small-x behaviour $G(x) \propto 1/x$. The three curves refer to the lowest-order, next-to-leading order, and resummed QCD calculations. Using the resummed

cross section, one gets

$$\sigma(pp \to b\bar{b}X) \simeq 400\ \mu b \qquad (LHC(\sqrt{s} = 16\ TeV))$$
$$\sigma(pp \to b\bar{b}X) \simeq 1000\ \mu b \qquad (SSC(\sqrt{s} = 40\ TeV)). \tag{102}$$

Typical cross sections per nucleon for the fixed-target mode are:

$$\sigma(pp \to b\bar{b}X) \simeq 20\ nb \qquad (HERA(E_p = 1\ TeV))$$
$$\sigma(pp \to b\bar{b}X) \simeq 1\ \mu b \qquad (LHC(E_p = 8\ TeV)) \tag{103}$$
$$\sigma(pp \to b\bar{b}X) \simeq 3\ \mu b \qquad (SSC(E_p = 20\ TeV)).$$

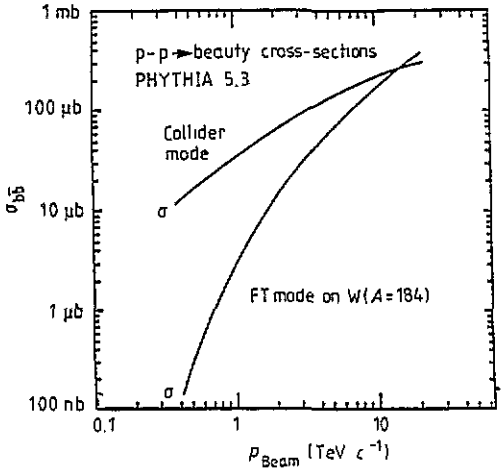

Figure 30. The cross section $pp \to B + X$ as a function of the beam energy for the collider mode (upper curve) and $p + W \to B + X$, in the fixed-target mode, calculated using the PYTHIA Monte Carlo.

There is at least a factor two uncertainty in these cross sections. In what follows, we show some representative estimates concerning B production and detection at these colliders. The characteristic features of beauty production at the LHC in the fixed-target mode (for the external beam option with a 5 mm W-target, as well as the 2 mm H_2 jet target option) and the collider mode are given in table 13. These estimates yield $N_{B\bar{B}}/\text{year} = O(1\text{–}4) \times 10^{10}$ with the indicated luminosities for the LHC. Under similar operating conditions, the yield at the SSC is expected to be a factor of 3 higher, due to larger cross sections. The corresponding yield at HERA (fixed-target mode) is estimated to be $N_{B\bar{B}}/\text{year} = O(3 \times 10^9)$ [107]. So, there will be plenty of B hadrons at all these facilities to undertake measurements concerning *CP* violation, rare B decays and x_s.

9.2. Simulation of x_s measurements in hadron machines

The issues concerning x_s measurements at hadron machines are very similar to those which we discussed in the context of time-dependent measurements at LEP, with the obvious differences in the trigger rates, efficiencies and background. Recapitulating, the ability to

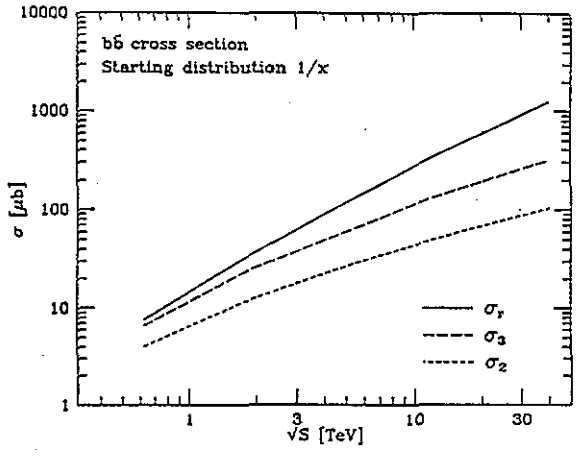

Figure 31. The B-production cross section in pp($\bar{p}$-collisions using a $1/x$ input gluon distribution as a function of the CM energy, $\sqrt{s}$. The three curves σ_2, σ_3 and σ_r correspond to the cross sections calculated with the lowest-order approximation, with the $O(\alpha_s^3)$ approximation, and with the full resummation, respectively (from [116]).

Table 13. Characteristic features of dedicated B-physics experiments at the LHC in the fixed target mode (using an extracted beam and gas jet target) and in the collider mode (from [111]).

	8 TeV Ext. beam $2 < \theta < 75$ mrad	8 TeV Jet target $2 < \theta < 75$ mrad	16 TeV Collider mode $2 < \theta < 600$ mrad
$\sigma(B\bar{B})$ (μb)	$\simeq 1$	$\simeq 1$	$\simeq 200$
$L(cm^{-2}\ s^{-1})$	1×10^{33} (5 mm W)	2×10^{33} (2 mm H_2)	2×10^{31}
$\langle N_{overlap} \rangle$	0.15	1.5	0.02
$N(B\bar{B})$/year	1×10^{10}	2×10^{10}	4×10^{10}
$\langle \beta\gamma c\tau \rangle$ (mm)	29	29	11
$B\bar{B}$/MBias	1/10000	1/50000	1/500
Primary vertex	± 1.4 mm	± 0.6 mm	± 75 mm

measure x_s depends essentially on three parameters: the resolution on the proper time, characterized by the dilution parameter D defined in equation (82), the B_s tagging quality, defined by the parameter A in equation (84), and the effective branching ratio in a specific non-charge conjugate B_s decay mode. As far as B flavour-tagging at the instant of production is concerned, in the collider mode at the LHC and SSC perhaps only the charged leptons from the semileptonic decays, $B \to X\ell^+\nu_\ell$ and the decay kaons $K^\pm$ are useful. Since one has to make sure that the lepton is not a misidentified hadron or a decay product of the much more abundant charmed hadron, additional constraints (in terms of secondary vertex requirement and p_T^ℓ) have to be imposed. The typical trigger efficiency using charged leptons is estimated as 0.03 [108, 118]. Using the secondary (decay) charged kaons, this efficiency can probably be doubled. At lower collider energies and for the fixed target mode, since the CM energy is relatively small, one could also use the $K^\pm$ tags from the primary vertex, as discussed earlier. It has been estimated in [119] that at CERN SPPS energy with $\sqrt{s} = 630$ GeV, the tagging with $K^\pm$ is expected to be much more efficient, given good $K^\pm$ identification, than tagging with charged leptons alone. A detailed Monte Carlo study

based on the detector characteristics has to be performed to determine the overall trigger efficiency.

As far as complete reconstruction of the B_s is concerned, the decay mode which would ideally present itself is the channel $B_s \to J/\psi + \phi$, whose $SU(3)$ analogues $(B_d, B_u) \to J/\psi(K^{*0}, K^{*+})$ have been measured [43] and could be used for calibrating the expected branching ratio. We hope that this and many more decay modes of the B_s will be measured at LEP and HERA, and, of course, at the future proton machines. However, as repeatedly emphasized above, the charge-conjugate $J/\psi\phi$ mode is ill suited for measuring B_s^0 $\bar{B}_s^0$ mixing. The decay mode studied in the present context for the LHC collider study is $B_s \to D_s^* \pi^+\pi^+\pi^-$, $D_s^* \to D_s + \gamma$ with the D_s constructed through its decay modes $D_s^\pm \to K^+K^-\pi^\pm$, $K^+K^-(3\pi)^\pm$, $K^0K^\pm$. The detection efficiency as well as the signal to background ratio depends rather sensitively on the resolution of the electromagnetic calorimeter. With the optimistic choice of the calorimetric resolution $\Delta E/E = 0.5\%/\sqrt{E}$, a reconstruction efficiency of 7×10^{-6} for a completely reconstructed $B_s/\bar{B}_s$ event has been estimated in [110], yielding 4×10^5 reconstructed $B_s/\bar{B}_s$ events. In the BCD estimates [108], the decay modes $B_s \to D_s^-\pi^+$, $D_s^-\pi^+\pi^-\pi^-$, $\bar{D}^0K^{*0}$ have been used to estimate the number of tagged B_s and $\bar{B}_s$ mesons. Recently, a number of two-body B_s decays have been estimated using the $1/N_c$ approximation of the QCD-improved effective Hamiltonian and the Bauer–Stech–Wirbel model in [120]. We draw attention to the CKM-suppressed decay modes $\bar{B}_s \to K^{*+}\rho^-$ and $\bar{B}_s \to K^{*0}J/\psi$, which can be usefully employed to increase the B_s tagging efficiency. The estimated branching ratios are 3×10^{-5} and 1.3×10^{-4}, respectively.

The role of the mis-tagging parameter A, in particular the inverse quadratic dependence of the required number of reconstructed B_s and $\bar{B}_s$ mesons, $N(B\bar{B}) \propto A^{-2}$, has already been noted in an earlier section. The parameter A has been estimated as $A \simeq 0.6$ in the SSC and LHC collider B-studies [108, 110]. Thus, taking into account all these factors, one estimates that 5×10^3 well-tagged events for the oscillation analysis will be available with the LHC collider B detector. Estimates presented in the BCD-EOI are very similar. To quote, starting from 5×10^{11} $B\bar{B}$ pairs at the SSC, it is estimated that a total reconstructed sample of 5.6×10^4 for the oscillation analysis will be available [108]. Assuming perfect time resolution, the numbers above are sufficient to determine x_s up to $x_s = 25$ at the LHC and SSC. To what precision $\Delta x_s/x_s$ can actually be measured depends on the proper-time resolution, characterized by the parameter D discussed earlier. The inverse proportionality of the two can be seen in equation (89). Since, with a good calorimetric resolution, the B_s energy will be measured quite accurately, the error on the proper time will be dominated by the vertex resolution. In a realistic simulation, this resolution must be included to determine the degradation of the signal. The result of a simulated likelihood analysis done with a sample of 5000 tagged $K^+\bar{B}_s^0$, $K^-B_s^0$ and $K^-\bar{B}_s^0$, $K^+B_s^0$, for the LHC collider B detector is shown in figure 32, where an exponential background and perfect proper-time resolution have been assumed. We conclude that there is a good *prima facie* case for attempting to measure x_s in hadron machines, both in the collider and fixed-target modes, if dedicated B detectors could be built.

10. Summary and outlook

One of the most important remaining tests of the SM in the flavour sector is the precision determination of all CKM matrix parameters. The measurement of B_s^0–$\bar{B}_s^0$ mixing is likely to be a very important ingredient in this programme since, combined with the measurement of B_d^0–$\bar{B}_d^0$ mixing, it can be used to give a fairly accurate value of one of the sides of the

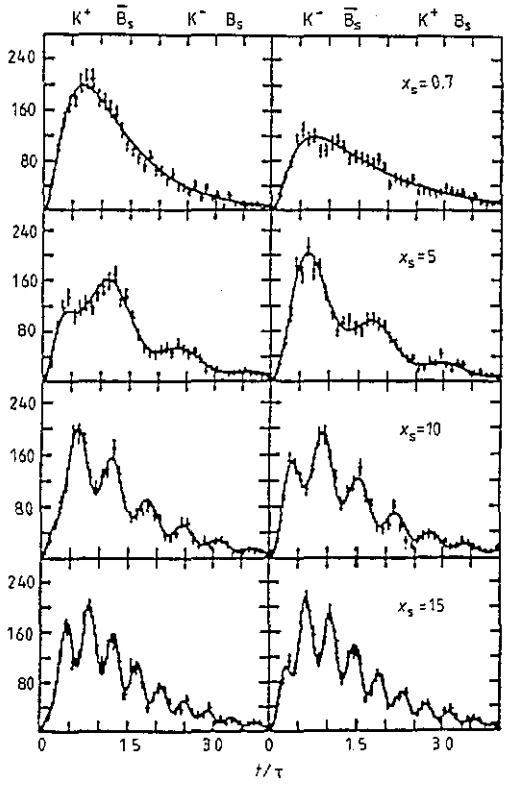

Figure 32. Proper-time measurement for the tagged events $K^+\bar{B}_s$, K^-B_s (LHS) and $K^-\bar{B}_s$, K^+B_s (RHS), for the four assumed values of x_s. The Monte Carlo data points correspond to a total sample of 5000 tagged events and the curve results from the simultaneous maximum likelihood fits to the data (from [110]).

unitarity triangle ($V_{td}/\lambda V_{cb}$). (It must be stressed, however, that this depends on the ratio $f_{B_d}^2 B_{B_d}/f_{B_s}^2 B_{B_s}$, which could deviate significantly from its $SU(3)$ symmetric value = 1.) We have summarized here the present status of B_s^0–$\bar{B}_s^0$ mixing and discussed the outlook for the prospects for x_s measurements in high-energy experimental physics facilities.

First of all, what is the value of x_s expected to be? The calculations of x_s in the SM are uncertain due to the (unknown) top-quark mass and the weak decay matrix elements. However, bounds on the former and model-dependent estimates of the latter are available, and we have used these to estimate x_s in the SM. This exercise gives (at '1σ'):

$$x_s > 3.0 \qquad (f_{B_s}\sqrt{B_{B_s}} = 180 \pm 35 \text{ MeV})$$
$$x_s > 5.2 \qquad (f_{B_s}\sqrt{B_{B_s}} = 225 \pm 25 \text{ MeV}). \tag{104}$$

The corresponding 'central values' (taking $m_t = 150$ GeV) are

$$x_s = 10.0 \qquad (f_{B_s}\sqrt{B_{B_s}} = 180 \pm 35 \text{ MeV})$$
$$x_s = 15.8 \qquad (f_{B_s}\sqrt{B_{B_s}} = 225 \pm 25 \text{ MeV}).$$

All of these values are beyond the reach of time-integrated measurements—time-dependent methods are necessary.

We have reviewed estimates of B_s^0–$\bar{B}_s^0$ mixing in a number of extensions of the SM. Smaller values for x_s than those expected in the SM can be found in several of these—non-minimal supersymmetric models, models with Z-mediated flavour-changing neutral currents, models with four generations, and non-minimal left–right symmetric models. (It should be noted, however, that for the latter two cases a certain amount of fine-tuning is needed.) This underlines the point that experimental searches have to be made with the foresight that $x_s < x_s^{SM}$ is not yet ruled out from experimental constraints.

Present information on the mixing parameters in the B^0–$\bar{B}^0$ complex is available in terms of the time-integrated measures χ_d and the weighted average $\chi = P_d\chi_d + P_s\chi_s$: $\chi_d = 0.155 \pm 0.031$, $\chi = 0.133 \pm 0.01$. An extraction of χ_s from these numbers requires prior knowledge of the $b \to B_d$ and $b \to B_s$ probabilities P_d and P_s. With $P_d = 0.35 \pm 0.05$ and $P_s = 0.20 \pm 0.07$, one obtains $\chi_s = 0.43 \pm 0.17$. This implies $\chi_s > 0.37$ at 90% CL, in agreement with the SM expectation $\chi_s \simeq 0.5$. The first order of business in this area is to reduce the measurement errors on χ_d and χ and infer χ_s in a less model-dependent fashion. This demands measurements of flavour correlations through characteristic features of B_s^0 production and decays. One possibility is to use characteristic charged lepton–kaon states in the decays of the B_s meson, $B_s \to \ell^+K^-\nu_\ell X$, and measure the final state $\ell^+K^-K^-X$ as a reliable estimator of the state $B_s^0K^-X$, giving

$$\frac{P(b \to \ell^+K^-K^-)}{P(b \to \ell^+K^-K^-) + P(b \to \ell^-K^+K^-)} = \chi_s. \tag{106}$$

We expect that with the present and forthcoming statistics at the four LEP experiments, such flavour correlation measurements will be undertaken to determine χ_s. This would allow a determination of x_s if $x_s < 4.0$, beyond which the time-integrated measurements become insensitive to x_s. Even if it turns out that, as expected, x_s cannot be extracted in this way, this kind of technique will be important for B_s tagging in time-dependent measurements.

We now summarize experimental proposals using time-dependent methods to measure x_s. We have given an exhaustive review of the existing and forthcoming experimental facilities involving electron and/or proton beams. Among the ongoing experiments, in our opinion, the best chance of measuring x_s is provided by the experiments at LEP. Since particle identification and momentum measurements are available in (almost) all LEP experiments, the limiting factor at LEP is the integrated luminosity. The required number of Z^0s needed to measure x_s with an assumed precision depends crucially on the resolution on proper time $\Delta t/\tau$, which depends both on the vertex resolution and the B hadron momentum resolution. In a number of Monte Carlo studies at LEP it has been estimated that to measure $x_s \leqslant 10$ with a precision $\Delta x_s/x_s = 0.1$, a proper-time resolution $\Delta t/\tau = 0.1$ and $N_{Z^0} \geqslant 10^7$ would be required. Given the various objective and subjective constraints, $x_s = 10$ defines the reach of LEP experiments. Since this lies comfortably above the estimated SM lower bound on x_s, it is imperative to push at LEP in this direction. The possibility of determining x_s in a range significantly above the sensitivity obtainable through the time-integrated measurements is one good reason to go for the high luminosity LEP option. The same remarks also apply to the impending experiments at HERA, where one would also need $O(10^7)$ B hadron events to reach $x_s = 10$.

Asymmetric B-factory experiments are constrained by somewhat different considerations. Here, the required luminosity is not only determined by the resolution on the decay length difference, $\Delta(\delta z)$, measured, for example, through the decay vertices of the dileptons, but also by the beam energies and the decay branching ratios of the $\Upsilon(5S)$ resonance. Since the time modulation due to mixing is most pronounced in the same-sign final state

with charge conjugation $C = -1$, the decay branching ratio $\Upsilon(5S) \to B_s^* \bar{B}_s^*$ is a crucial parameter. Given a comfortably large branching ratio (say $\geqslant 10\%$) and excellent δz resolution, say $\Delta(\delta z)/\langle z \rangle = 0.1$, the remaining constraining parameter for $x_s^{\max}$ is the machine boost factor $\beta\gamma$. The larger the $\beta\gamma$ (i.e. the more asymmetric the two beams), the smaller is the luminosity required to measure a given x_s. The maximum value of x_s reachable in an asymmetric B factory depend on the assumptions about the mentioned parameters. Using $\Delta(\delta z) = 40\ \mu$m, a boost factor $\beta\gamma = 1$, and a data set of 20–30 fb^{-1}, the SLAC and DESY studies lead to the optimistic conclusion that one would be able to reach as high a value of x_s as 20 at 3σ level. On the other hand, the KEK and Cornell studies, using somewhat more conservative parameters, came to the conclusion that a maximum value for x_s of only 5–7 is measurable. While the upper range of x_s is probably more vulnerable to the systematic errors, such as the non-Gaussian tail in the resolution, the asymmetric B-factories may allow a measurement of x_s in a range significantly beyond those of the LEP experiments.

Finally, we summarize the conclusions for the proton machines. Here the constraining feature is not the number of B hadrons which would be produced in sufficient abundance at the forthcoming hadron colliders (LHC and SSC) and fixed-target proton machines. Rather, it is more the trigger rates, the B_s tagging quality, the vertex resolution and background which pose the real challenge. The dilution factor and mistaggings at hadron machines are much larger compared with those at electron machines. Since the B rates are very high in hadron machines, one can afford to reconstruct completely the B_s mesons in a number of non-leptonic decay modes. The typical efficiency for such a reconstruction is $O(10^{-6})$. This would yield typically $O[10^3(10^4)]$ B_s mesons for the oscillation analysis for an integrated production of $O[10^{10}(10^{11})]$ B hadrons at the LHC and SSC. Such a large B_s data sample would allow, in principle, a measurement of x_s up to $x_s = 25$, assuming an exponentially falling background and perfect resolution. The precision $\Delta x_s/x_s$ depends on the vertex resolution. A realistic Monte Carlo simulation to take that into account has yet to be carried out, and, in the absence of such studies, one has to regard the present claims of measuring x_s values as high as 25 as somewhat idealized. In our opinion, just as in other experimental facilities, in hadronic machines one will also have to work extremely hard to go beyond $x_s = 15$. However, a relatively light top-quark (say $m_t = 130$ GeV) and a moderate value for the product $\left(f_{B_s}^2 B_{B_s}\right) \eta_{B_s}$ may reduce x_s sufficiently and consequently one may not require the experimental capabilities of measuring x_s beyond 15.

In conclusion, it appears that future experiments are well placed to measure x_s. Hopefully this will be done in the not-too-distant future and another part of the CKM puzzle will fall into place.

Acknowledgments

We would like to thank our colleagues active in B physics studies for illuminating discussions. In particular, we are grateful to Daniel Denegri, David Hitlin, Francois Le Diberder, Walter Schmidt-Parzefall, Henning Schröder, Sheldon Stone and Hans-Dietrich Schulz for many discussions and valuable input. This work was supported in part by the Natural Sciences and Engineering Research Council of Canada, and by FCAR, Québec.

Note added in proof. Since the submission of the manuscript a number of new measurements have been reported in B-physics from experiments at LEP and CESR. We have incorporated these results by updating the numbers in the text as far as possible. Concerning the mass of the B_s-meson, it has now been measured at LEP by the ALEPH and DELPHI collaborations using the decay modes $B_s \to \psi'\phi$ and $B_s \to D_s^+\pi^-$. In particular, ALEPH quotes a value

$m(B_s) = 5.3746 \pm 0.0075(\text{stat.}) \pm 0.005(\text{syst.})$ GeV (San Lau Wu (private communication)). This gives a mass difference $m(B_s) - m(B_d) \simeq 96$ MeV, for which we had assumed 100 MeV in the text. Likewise, the lifetime of the B_s^0-meson has now been measured, giving $\tau(B_s) = 1.05 \pm 0.32$ ps, which is nominally smaller than the lifetime for the other B-mesons, $\tau(B_d^0) = 1.46 \pm 0.19$ ps and $\tau(B^-) = 1.34 \pm 0.21$ ps (Drell and Patterson 1992 *Cornell University Report* CLNS 92/1177). We remark that the present measurements are certainly compatible with all three B-meson lifetimes being equal, an assumption that has been made in the various numerical estimates presented in the text.

References

[1] Glashow S L 1961 *Nucl. Phys.* **22** 579
Salam A 1968 *Elementary Particle Theory* ed N Svartholm (Stockholm: Almqvist and Wiksell)
Weinberg S 1967 *Phys. Rev. Lett.* **19** 1264
[2] Cabibbo N 1963 *Phys. Rev. Lett.* **10** 531
Kobayashi M and Maskawa T 1973 *Prog. Theor. Phys.* **49** 652
[3] Wolfenstein L 1945 *Phys. Rev. Lett.* **51** 1945
[4] Aguilar-Benitez M *et al* (Particle Data Group) 1990 *Phys. Lett.* **239B** 1
[5] Altarelli G, Cabibbo M, Corbo G, Maiani L and Martinelli G 1982 *Nucl. Phys.* B **208** 365
[6] Isgur N, Scora D, Grinstein B and Wise M 1989 *Phys. Rev.* D **39** 799
[7] Wirbel M, Stech B and Bauer M 1985 *Z. Phys.* C **29** 637
[8] Körner J G and Schuler G A 1988 *Z. Phys.* C **38** 511
[9] Isgur N and Wise M 1990 *Phys. Lett.* **232B** 113; 1990 *Phys. Lett.* **237B** 527
[10] Luke M E 1990 *Phys. Lett.* **252B** 447
[11] Boyd C G and Brahm D E 1991 *Phys. Lett.* **257B** 393
[12] Neubert M and Rieckert V 1991 *Preprint* Heidelberg HD-THEP-91-6
Neubert M 1991 *Phys. Lett.* **264B** 455; 1991 *Preprint* Heidelberg HD-THEP-91-30
[13] Albrecht H *et al* (ARGUS Collaboration) 1989 *Phys. Lett.* **229B** 175
[14] Roudeau P 1991 *Proc. Int. Lepton–Photon Symp. and Europhysics Conf. on High Energy Physics (Geneva, 1991)* ed S Hegerty, K Potter and E Quercigh to appear
[15] E653 Collaboration 1991 *Proc. Int. Lepton–Photon Symp. and Europhysics Conf. on High Energy Physics (Geneva, 1991)* ed S Hegerty, K Potter and E Quercigh to appear
[16] Fulton R *et al* (CLEO Collaboration) 1991 *Phys. Rev.* D **43** 651
[17] Albrecht H *et al* (ARGUS Collaboration) 1992 *Report* DESY 92-029
[18] Mannel T 1992 *Report* Technische Hochschule Darmstadt Report IKDA 92/6
[19] Rosner J 1990 *Phys. Rev.* D **42** 3732
[20] Ramirez C, Donoghue J and Burdman G 1990 *Phys. Rev.* D **41** 1496
[21] Cassel D 1990 *Proc. 1990 DPF Summer Study on High Energy Physics Research Directions for the Decade (Snowmass, Colorado)* to appear
[22] Schröder H 1991 Invited talk at the ECFA B-Physics Meeting, DESY
[23] Buras A J, Słominski W and Steger H 1984 *Nucl. Phys.* B **238** 529; 1984 **B245** 369
[24] Flynn J 1990 *Mod. Phys. Lett.* A **5** 877
[25] Inami T and Lim C S 1981 *Prog. Theor. Phys.* **65** 297
[26] Carter J 1991 *Proc. Int. Lepton–Photon Symp. and Europhysics Conf. on High Energy Physics (Geneva, 1991)* ed S Hegerty, K Potter and E Quercigh to appear
[27] Abe F *et al* (CDF) 1993 *Phys. Rev.* D
[28] Altarelli G 1991 *Report* CERN-TH.6206/91
[29] Ellis J, Fogli G L and Lisi E 1992 *Phys. Lett.* **274B** 456
[30] Langacker P and Luo M 1991 *Phys. Rev.* D **44** 817
[31] Pich A and de Rafael E 1985 *Phys. Lett.* **158B** 477
[32] Prades J, Dominguez C A, Penarrocha J A, Pich A and de Rafael E 1991 *Z. Phys.* C **51** 287
[33] Donoghue J F, Golowich E and Holstein B R 1982 *Phys. Lett.* **119B** 412
[34] Bilic N, Dominguez C A and Guberina B 1988 *Z. Phys.* C **39** 351
[35] Decker R 1989 *Nucl. Phys.* B *(Proc. Suppl.)* **7A** 180
[36] Reinders L J and Yazaki S 1987 *Nucl. Phys.* B **288** 789
[37] Papadopoulos N A and Vogel H 1991 *Z. Phys.* C **51** 73
[38] Bardeen W A, Buras A J and Gérard J-M 1988 *Phys. Lett.* **211B** 343
[39] Gavela M B *et al* 1988 *Nucl. Phys.* B **206** 113

[40] Bernard C *et al* 1990 *Nucl. Phys.* B *(Proc. Suppl.)* **17** 495
[41] Kilcup G W *et al* 1990 *Phys. Rev. Lett.* **64** 25
[42] Brown F R *et al* (Columbia Collaboration) 1990 *Lattice Workshop (Tallahassee)*
[43] Danilov M 1991 *Proc. Int. Lepton–Photon Symp. and Europhysics Conf. on High Energy Physics (Geneva, 1991)* ed S Hegerty, K Potter and E Quercigh to appear
[44] Buras A J, Jamin M and Weisz P H 1990 *Nucl. Phys.* B **347** 491
[45] Shifman M A and Voloshin M B 1986 *Report* ITEP-54
[46] Narison S 1987 *Phys. Lett.* **198B** 104
[47] Reinders L J 1988 *Phys. Rev.* D **38** 947
[48] Dominguez C A and Paver N 1991 *Phys. Lett.* **269B** 169
[49] Reinders L J and Yazaki S 1988 *Phys. Lett.* **212B** 245
[50] Pich A 1988 *Phys. Lett.* **206B** 322
[51] Capstick S and Godfrey S 1990 *Phys. Rev.* D **41** 2856
[52] Gavela M B *et al* 1988 *Phys. Lett.* **206B** 113
[53] Bernard C, Draper T, Hockney G and Soni A 1988 *Phys. Rev.* D **38** 3540
[54] Allton C R *et al* 1991 *Nucl. Phys.* B **349** 598
[55] Bernard C W, El-Khadra A X and Soni A 1990 *Symp. Lattice '90 (Tallahassee)*
[56] Alexandrou C *et al* 1991 *Preprint* CERN-TH.6113/91
[57] Abada A *et al* *Preprint* Rome-823-1991
[58] Sachrajda C 1992 *Conf.: QCD–20 Years Later (Aachen)*
[59] Barr G D *et al* (NA31) 1992 *Proc. Int. Lepton–Photon Symp. and Europhysics Conf. on High Energy Physics (Geneva, 1991)* ed S Hegerty, K Potter and E Quercigh to appear
[60] Winstein B *et al* (E731) 1992 *Proc. Int. Lepton–Photon Symp. and Europhysics Conf. on High Energy Physics (Geneva, 1991)* ed S Hegerty, K Potter and E Quercigh to appear
[61] Flynn J M and Randall L 1989 *Phys. Lett.* **224B** 221
Buchalla G, Buras A J and Harlander M K 1990 *Nucl. Phys.* B **337** 313
[62] Buras A J 1992 *Proc. Int. Lepton–Photon Symp. and Europhysics Conf. on High Energy Physics (Geneva, 1991)* ed S Hegerty, K Potter and E Quercigh to appear
[63] Schmidtler M and Schubert K R 1992 *Z. Phys.* C **53** 347
Buras A J and Harlander M K 1992 *Report* MPI-PAE/PTh 1/92, TUM-T31-25/92, to appear in *Heavy Flavors* ed A J Buras and M Lindner (Singapore: World Scientific)
[64] Bigi I, Khoze V, Uraltsev N and Sanda A 1989 *CP Violation* ed C Jarlskog (Singapore: World Scientific) p 175; and refs therein
[65] Dunietz I 1992 *B-Decays* ed S Stone (Singapore: World Scientific); and refs therein
[66] Ali A 1991 *Report* DESY 91-080 *Proc. First Int. A D Sakharov Conf. on Physics (Lebedev Inst., Moscow)*
[67] Bertlman R A and Martin A 1980 *Nucl. Phys.* B **168** 111
Byers N and Hwang D S 1987 *Proc. Workshop on High Sensitivity Beauty Physics at Fermilab (Batavia, Illinois)* ed A J Slaughter, N Lockyer and M Schmidt (Batavia: Fermilab) p 199
Martin A and Richard J M 1987 *Phys. Lett.* **185B** 426
Kwong W and Rosner J L 1991 *Phys. Rev.* D **44** 212
[68] London D 1990 *Phys. Lett.* **234B** 354
[69] Bertolini S, Borzumati F and Masiero A 1987 *Phys. Lett.* **194B** 545; 1987 *Phys. Lett.* **198B** 590
Altarelli G and Franzini P 1988 *Z. Phys.* C **37** 271
[70] Bertolini S, Borzumati F and Masiero A 1991 *Report* MPI-Ph/91-71
[71] Bigi I I and F. Gabbiani 1991 *Nucl. Phys.* B **352** 309; and refs therein
[72] Boyd G, Gupta A K, Trivedi S P and Wise M B 1990 *Phys. Lett.* **241B** 584
[73] Abbott L F, Sikivie P and Wise M B 1980 *Phys. Rev.* D **21** 1393
Athanasiu G G, Franzini P J and Gilman F J1985 *Phys. Rev.* D **32** 3010
[74] Beall G, Bander M and Soni A 1982 *Phys. Rev. Lett.* **48** 848
Ecker G, Grimus W and Neufeld H 1983 *Phys. Lett.* **127B** 365
Mohapatra R N, Senjanovic G and Tran M D 1983 *Phys. Rev.* D **28** 546
Gilman F J and Reno M H 1984 *Phys. Rev.* D **29** 937
[75] Ecker G and Grimus W 1985 *Nucl. Phys.* B **258** 328; 1986 *Z. Phys.* C **30** 293; see also Altarelli G and Franzini P 1988 *Z. Phys.* C **37** 271
[76] Langacker P and Sankar S U 1989 *Phys. Rev.* D **40** 1569
[77] London D and Wyler D 1989 *Phys. Lett.* **232B** 503
[78] Nir Y and Silverman S 1990 *Phys. Rev.* D **42** 1477
Silverman D 1992 *Phys. Rev.* D **45** 1800

[79] Albajar C *et al* (UA1) 1991 *Phys. Lett.* **262B** 171
[80] Abe F *et al* (CDF) 1991 *Phys. Rev. Lett.* **24** 3351
[81] Brown D (ALEPH) 1991 Parallel session talk *LP-HEP 91 (Geneva, Switzerland)*
[82] Schröder H 1991 *Report* DESY 91-139; 1992 *B Decays* ed S Stone (Singapore: World Scientific)
[83] Barlow R 1985 *Proc. XX rencontre de Moriond, Heavy Quarks, Flavour Mixing and CP Violation (La Plagne, France)* p 187
Bartel W *et al* (JADE) 1984 *Phys. Lett.* **146B** 437
Bigi I I 1985 *Phys. Lett.* **155B** 125
[84] Ali A and Barreiro F 1986 *Z. Phys.* C **30** 635
[85] Lingel K 1991 *Report* CLNS 91-1043
[86] SLAC 1990 *Reports* SLAC-353, LBL PUB-5245, CALT-68-1588, UC-414
[87] Abe K *et al* 1991 *Report* KEK 90-23
[88] Albrecht H *et al* 1992 *Report* DESY-92-041
[89] Krawczyk P, London D and Steger H 1988 *Nucl. Phys.* B **307** 19
[90] Decamp B *et al* (ALEPH Collaboration) 1991 *Report* CERN-PPE/91-229
[91] Sterman G and Weinberg S 1977 *Phys. Rev. Lett.* **39** 1436
[92] Roudeau P (HLC Study Group) 1990 *Report* LAL 90-47; *Proc. Rencontres de Moriond (Les arcs)* p 521
[93] Albrecht H *et al* 1991 *Dissertation* Lund University; (ARGUS), to be published
[94] Defoix Ch 1990 *Report* LPC 90-08/DELPHI NOTE 90-40/PHYS 67; LPC 90-41
[95] SLAC 1989 *Proc. SLD Physics Week (Kirkwood, CA)* SLAC Report-354
[96] Reeves T W, Panvini R S and Word G B 1989 *Proc. SLD Physics Week (Kirkwood, CA)* SLAC Report-354 p 358
[97] Reeves T W and Panvini R S 1989 *Proc. SLD Physics Week (Kirkwood, CA)* SLAC Report-354 p 370
[98] Peterson C *et al* 1983 *Phys. Rev.* D **27** 105
[99] Pandoulas A 1992 *DPG Meeting (Berlin)* Invited Talk
[100] Byers N and Hwang D S 1987 *Proc. Workshop on High Sensitivity Beauty Physics at Fermilab* ed A J Slaughter, N Lockyer and M P Schmidt (Fermilab) p 199
[101] Lee-Franzini J *et al* 1990 *Phys. Rev. Lett.* **239** 1
[102] Le Diberder F 1990 *Report* SLAC; 1991 ECFA B-Physics Working Group Meeting, CERN, Geneva
[103] Schuler G 1988 *Nucl. Phys.* B **299** 21
[104] Ingelman G and Schuler G 1988 *Report* DESY 88-020; *Report* unpublished
[105] Abbiendi G and Stanco L 1991 *Z. Phys.* C **51** 81; this paper uses the HERWIG Monte Carlo described in Marchesini G and Webber B R 1988 *Nucl. Phys.* B **310** 461
[106] Ali A *et al* 1988 *Proc. HERA Workshop (DESY, Hamburg, FRG)* vol 1, ed R D Peccei, p 393
[107] Schmidt-Parzefall W *et al* 1993 in preparation
[108] Castro H *et al* 1990 *Report* SSC-EOI0008
[109] Ellet J *et al* 1991 *Report* CERN/DRDC 91-18
[110] Ehran S *et al* 1990 *Proc. Large Hadron Collider Workshop (Aachen)* vol 2, ed C Jarlskog and D Rein; CERN-90-10, ECFA 90-133
[111] Carboni G *et al* 1991 *ECFA Working Groups on a B-Meson Factory in Europe (CERN)*
Carboni G *et al* and Fidecaro G 1990 *Proc. Large Hadron Collider Workshop (Aachen)* vol 2, ed C Jarlskog and D Rein; CERN-90-10, ECFA 90-133
[112] Rosen J 1990 *Report* SSC-EOI0013
[113] Cox B *et al* 1990 *Report* SSC-EOI0014
[114] Bengtsson H-U and Sjöstrand T 1987 *Comput. Phys. Commun.* **46** 43
[115] Catani S, Hautmann F and Ciafaloni M 1990 *Phys. Lett.* **242B** 97
[116] Collins J C and Ellis R K 1991 *Nucl. Phys.* B **360** 3
[117] Levin E M *et al* 1991 *Reports* 91-054, 91-065
[118] Stone S 1991 *Preprint* Syracuse University HEPSY 8-91
[119] Brandt A 1989 *Report* CERN-SPSC/89-43
[120] Kramer G and Palmer W F 1992 *Report* DESY 92-043